

מדינת ישראל

משרד התשתיות הלאומיות האנרגיה והמים

אגף מחקר ופיתוח

**NANNOFOSSIL STRATIGRAPHY AND PALEOENVIRONMENTS
OF THE ISRAEL JUDEA GROUP**

דו"ח סיכום

Maria Ovechkina

המכון הגיאולוגי לישראל

האגף לסטרטיגרפיה וחקר תת הקרקע

תמוז תש"פ / June 2020

המחקר ממומן ע"י משרד התשתיות הלאומיות האנרגיה והמים על-פי חוזה מס' 217-17-023

CONTENTS

4.....	תקציר	
Abstract		5
1. Introduction		7
<i>Specific aims of the proposed research</i>		10
2. Material		11
2.1. <i>Geological setting</i>		11
2.2. <i>Lithology</i>		14
2.3. <i>Calcareous nannoplankton</i>		15
3. Methods		16
3.1. <i>Planktic foraminifera and calcareous nannoplankton</i>		16
3.2. <i>Carbon and oxygen stable isotope analyses</i>		20
4. Results		21
<i>Initial results</i>		21
4.1. <i>Biostratigraphy and biochronology</i>		22
4.1.1. <i>Planktic foraminifera biostratigraphy</i>		22
Borehole CT8		22
Borehole CT2		25
4.1.2. <i>The Global Boundary of the Cenomanian Stage, the Stratotype Section</i>		30
4.1.3. <i>Calcareous nannoplankton biostratigraphy</i>		30
Borehole CT8		30
Borehole CT2		36
Borehole Negba 1.....		43
4.2. <i>Calcareous nannoplankton preservation and abundance</i>		47
Borehole CT8		48
Borehole CT2		56
4.3. <i>Calcareous nannoplankton Temperature (TI) and Nutrient (NI) indices</i>		66
Borehole CT8		66
Borehole CT2		67
4.4. <i>Stable isotope analyses</i>		68
Borehole CT8		68
Borehole CT2		70

5. Discussion	73
5.1. <i>Biostratigraphy</i>	73
5.2. <i>Age inferences for the Albian–Cenomanian interval of boreholes CT8 & CT2</i> ...	74
5.3. <i>Integrated stratigraphy</i>	76
5.4. <i>Paleoenvironmental reconstructions</i>	78
5.5. <i>Correlation with the western Tethys record</i>	83
6. Conclusions	87
Expected benefits and potential contribution to goals of the Ministry of Energy and Water Resources	88
Possible applications of the results	89
Acknowledgements	89
Published results	89
References	90
APPENDIX A	101
APPENDIX B	107
APPENDIX C.....	108
APPENDIX D.....	109
APPENDIX E.....	110
PUBLICATION DOCUMENTATION PAGE	111

ננופלנקטון ביוסטרטגרפיה ושיחזור תנאי סביבה של חבורת יהודה בישראל

אובצ'קין מריה

המכון הגיאולוגי לישראל, האגף לסטרטיגרפיה וחקר תת הקרקע

2020

המחקר מציג תוצאות ניתוח של מאספי ננופלנקטון גירי מתוך גלעיני הקידוח של סלעי חבורת יהודה (אלביאן-קנומן) באזור הכרמל (צפון מערב ישראל) ובמישור החוף הדרומי. מאספים עשירים זהו בגלעינים מאזור הכרמל (113 מינים בקידוח CT8 ו-95 מינים בקידוח CT2), כאשר מהגלעין ממישור החוף התקבל מאסף מצומצם (24 מינים בקידוח נגבה-1). על סמך מאספים מאזור הכרמל נערכה חלוקה ביוסטרטגרפית מפורטת. חלוקה ביוסטרטגרפית של ננופלנקטון גירי מאזור הכרמל הושוותה והוקבלה לחלוקה ביוסטרטגרפית של פורמיניפרים פלנקטונים. חלוקה ביוסטרטגרפית של ננופלנקטון ממישור החוף פחות מפורטת, טווחים סטרטיגרפיים שונים שהוגדרו, הוקבלו לטווחים סטרטגרפיים של פורמיניפים פלנקטונים. הנו-מאובנים מראים כי תצורת עספא וטוף טווסים (V2) באזור הכרמל שייכים לאלביאן המאוחר (98.2 מ"ש), כאשר תצורת ערכן תוארכה לאלביאן עליון - קנומן תיכון.

הגבול בין אלביאן לקנומן באזור עובר בשכבה, שנמצאת בחלקו התחתון של תצורת ערכן, ובה לראשונה מופיעים פורמיניפרים פלנקטוניים *Thalmanninella globotruncanoides*. השכבה הזאת נמצאת מעל הגג של טוף טווסים (כ-52 מטרים ב-CT8 וכ-36 מטרים ב-CT2). העדות נתמכת בהופעה של פורמיניפרים של אלביאן *Th. brotzeni* מתחת לשכבת הגבול (כ-26 מטרים ב-CT8 וכ-6.5 מטרים ב-CT2), ובהופעה של נו-פאונה גירית קנומנית *C. kennedyi* מעל השכבה. המידע החדש הזה קורא לבדיקה ועדכון של הטבלה הליטוסטרטגרפית של ישראל, ובפרט – של גילי תצורות עספא וערכן באזור הכרמל. המידע הסטרטיגרפי ממישור החוף פחות מפורט עקב נדירות של נו-מאובנים, אך משייך את תצורת יגור המוגדרת שם לסוף אלביאן – תחילת קנומן, ותצורת נגבה לאלביאן – קנומן עליון.

שיחזור תנאי הסביבה נעשה על סמך אנליזה כמותית של הננופלנקטון הגירי. כך, שכיחות של המין *Watznaueria* spp. בחתך הנבדק מאזור הכרמל משקף טמפרטורות חמימות, סביבת השקעה חופית או של ים פתוח, ותנאים אוליגרופיים. עקב זמינות נוטריינטים נמוכה, נרשמה הפרודקטיביות של הננופלנקטון הגירי הייתה מנוכה גם כן, מלבד שתי אפיזודות של פוריות גבוהה יותר בתת-אזור NC10A ובאזור 11NC. הערכים הנמוכים של Shannon index, וערכים של Evenness ו-Species richness מעידים על תנאי הסביבה הלא יציבים. תצורת עספא (אלביאן מאוחר, לפי ננופלנקטון) הורבדה בתנאים ממוזגים ואוליגוטרופיים. החלק התחתון של תצורת ערכן (סוף אלביאן, לפי ננופלנקטון) הושקע באקלים ממוזג, אך בתנאים מזוטרופיים. החלק העליון של תצורת ערכן (תחילת קנומן) הושקע במים אוליגוטרופיים ובאקלים חם יחסית. גג תצורת ערכן (קנומן תיכון) הושקע במהלך תקופה של קירור הדרגתי, שהתאפיין ברצף של פרקי התחממות וקירור, ובתנאים אוליגוטרופיים.

תוצאות האנליזה הכמותית של הננופלנקטון הגירי תואמת היטב לחלוקה על פי פורמיניפרים פלנקטונים (Lipson-Benitah et al., 1997) מהסביבה הקרובה ולמחזורים של (Haq et al., 1988), ומצביעים על העשרה בחומרי הזנה במהלך עלייה של מפלס הים בין אלביאן העליון לקנומן תחתון.

באזור הכרמל לא אותרו היאטוסים בחתך על סמך הביוסטרטגרפיה, אך ניתוח של הרכב איזוטפי של פחמן מראה תמונה שונה. בגלעין קידוח CT2 (בתצורת עספא, עומקים 169.9-152.6 מ', ובתצורת ערכן, עומקים 74.1-65.0), בהתאמה, האיזוטופים של פחמן מציגים שתי אנומליות חיוביות התואמות היטב לשני אירועים אנוקסיים מוכרים ברקורד הגלובלי: OAE 1D and MCE I (Oceanic Anoxic Event 1d and Middle Cenomanian Event I). בהנחה ששינויים דיאגנטיים לא השפיעו על הרכב האיזוטופי של חמצן ב-CT2, בתקופת אלביאן עליון – קנומן תחתון שוררו טמפרטורות מתונות (~26°C), עם מגמת העלייה בקנומן התחתון, לקראת תקופת התחממות עד ל-32°C בקנומן תיכון. בקידוח CT8, ההרכב האיזוטופי של פחמן ככל הנראה חווה שינויים דיאגנטיים ולא נמצא בו כל עדות לאנומליות איזוטופיות חיוביות, המזוהות עם האירועים האנוקסיים (OAE 1D and MCE I). מאחר וערכים של נוטריינטים וטמפרטורה נמצאים בגבולות הרקורד של אוקיינוס התטיס המערבי, אנחנו מציעים כי ברמה אזורית התקיימו הבדלים הפלאו-אקלימיים.

ABSTRACT

Maria Ovechkina

Geological Survey of Israel, laboratory of Stratigraphy and subsurface exploration

2020

The calcareous nannoplankton from the sediments of the Judea Group (Albian–Cenomanian) of the Carmel area (NW Israel) and the Southern Coastal Plain has been studied. The identified rich assemblages in the Carmel area consist of 113 taxa (borehole CT8) and 95 taxa (borehole CT2). On the Coastal Plain (borehole Negba 1), the impoverished assemblage of 24 taxa is recorded.

The detailed calcareous nannofossil biostratigraphy of the Carmel area has been established and compared with planktic foraminiferal zones. In the Coastal Plain, different stratigraphical intervals are recorded and correlated with planktic foraminiferal zones.

The novel nannofossil data indicate that the Isfiye Formation and the Tavasim Volcanics (V2) calculated as 98.2 Ma in the Carmel area are Late Albian, and the Arqan Fm. is Late Albian–Middle Cenomanian.

The Albian–Cenomanian boundary in the Carmel area is drawn at the level of the first occurrence of *Thalmaninella globotruncanoides* (planktic foraminifera) in the lower part of the Arqan Fm. at ~52 m above the top Tavasim Volcanics in CT8 and at ~35.65 m above the Tavasim Volcanics in CT2. This is supported by the appearance of *Th. brotzeni* (planktic foraminifera) at 26 m (CT8) and 6.55 m (CT2) below, and *C. kennedyi* (nannofossils) above this level. Our novel stratigraphical data prompt a revision of the revision of the litho-stratigraphic table and updating the Arqan Fm. age.

On the Coastal Plain, only wide stratigraphic intervals can be recognized due to rarity of nannofossils: the upper part of the Yagur Fm is Late Albian–Early Cenomanian, the Lower and Upper Members of the Negba Fm is Albian–Late Cenomanian, and the upper part of the Upper Member of the Negba Fm is Late Cenomanian.

The quantitative analysis of the calcareous nannoplankton suggests that the general dominance of *Watznaueria* spp. throughout the whole successions in the Carmel Area reflects the original signal and points to quite warm, open marine or coastal, generally oligotrophic conditions. Due to poor nutrient supply, the productivity of the calcareous

nannoplankton was quite low except for two phases of higher fertility within Subzone NC10a and Zone NC11*. Low values of the Shannon index, Evenness and Species richness can be interpreted as reflecting unstable environment. The Isfiye Formation (Late Albian) accumulated in temperate, oligotrophic conditions. The lower part of the Arqan Formation was deposited under temperate climate but mesotrophic conditions. The higher part of the Arqan Formation (Early Cenomanian) was deposited in oligotrophic waters and relatively warm climate. The uppermost part of the Arqan Formation (Middle–Late Cenomanian) was accumulated during a progressively cooling period, although characterised by alternating warming and cooling phases and oligotrophic conditions.

The calcareous nannoplankton quantitative data correlate very well with those obtained from planktic foraminifera (Lipson-Benitah et al., 1997) from the nearby area, and with cycles and sequences established by Haq et al. (1988), and suggest nutrification during phases of a risen sea level in the Late Albian and Early Cenomanian.

The biostratigraphy in the Carmel Area shows no hiatuses in the studied section, but carbon isotope data reflect different pictures. In the borehole CT2 (Isfiye Fm., depths 169.90–152.60 m), the Oceanic Anoxic Event (OAE) 1d and Middle Cenomanian Event (MCE) I (Arqan Fm., depths 74.10–65.0 m) are detected; these reflect well the globally recorded carbon isotopic anomalies. Considering that the isotopic signal is not diagenetically altered and the $\delta^{18}\text{O}$ signal is not affected in the CT2, the oxygen isotopes suggest temperate conditions during the Late Albian–Early Cenomanian ($\sim 26^\circ\text{C}$) followed by a warming period in the late Early Cenomanian, with temperatures gradually increasing toward the Middle Cenomanian to $\sim 32^\circ\text{C}$.

In the borehole CT8, carbon isotope data seem to be affected by diagenetic alteration showing no evidence of the positive isotopic anomalies, which identify OAE 1d and MCE I worldwide. Temperature and nutrient variations in CT8 correspond to the western Tethys record, thus suggesting that the detected paleoclimatic variations occurred at a supra-regional scale.

1. INTRODUCTION

Cretaceous deposits are widely spread in the Levant basin in general and in Israel in particular. The depositional evolution of the Cretaceous sediments in Israel—subdivided into Stage I – the Yo'av Group (Berriasian–Middle Albian); Stage II – the Kurnub Group (Late Aptian–Early Albian); Stage III – the Judea Group (Late Albian–Turonian); and Stage IV – the Mount Scopus Group (Coniacian–Maastrichtian)—reflects numerous lateral facies-changes and regional unconformities (Derin, 2016). The Yo'av Group shows well-defined facies from the west to east; they generally laterally grade from a shallow to deep water sediments (Derin, 2016). The Kurnub Group consisting of continental sandstones with marine intercalations deposits is overlaid by the Judea Group. The “Judea Limestone Formation” (Wellings, 1944) emended to the Judea Group (Arkin et al., 1965) includes the normal marine limestones, dolomites, interbedded with marls and chalk. The sediments were deposited mostly in a shallow platform regime over a large area of the Arabian Platform (Rosenfeld & Hirsch, 2005). The Judea Group is very diverse lithologically and is composed of numerous formations.

The southern Tethyan margin experienced a large transgression during the Cenomanian, which started at the end of the Albian and extended further to the southeast. The transgression corresponding to the Judea Group started with deposition of dolomites of the Yagur Formation in the Carmel Area, Coastal Plain, and Galilee, whereas in Judea Mountains it is represented by dolomites and limestones of the Kesalon Formation. In the Negev, the transgression is very pronounced and commenced at the very end of the Albian with the deposition of the shallow-marine Judea Gr. on the sandy Kurnub Gr. In the Carmel area, the transgression settings are not so prominent, with the dolomitic Yagur Fm. reflecting the lagoonal environment and ending with deposition of the overlying Isfiye chalk. Offshore and on the westernmost Coastal Plane, the Judea Group corresponds to the Talme Yafe Fm. In the Judea mountains anticlinorium, the Judea Group is represented by several formations, starting with the Albian Kefira Fm. and ending with the Turonian Bina Fm. (Fleischer, 2002).

Four hundred meters of calcareous sediments were deposited on a wide platform in southern Tethyan region (Bein & Weiler, 1976; Sass & Bein, 1982). These rocks are widespread in Israel including the Carmel Region in the northwestern part of the country (Bartov, 1990), and below the coastal plain and offshore (Lipson-Benitah et al., 1995).

For the project, the following two areas have been chosen: the Carmel Region (boreholes CT2 and CT8) and the Coastal Plain (borehole Negba 1) (Fig. 1).

The Albian to Turonian outcrops, consisting of limestones and chalks of Carmel contain a rich macrofaunal assemblage composed of cephalopods, gastropods, bivalves and echinoids (Kashai, 1966; Bein, 1976; Lipson-Benitah et al., 1997), which were used to subdivide and date the succession (Avnimelech, 1965; Lewy & Raab, 1978). The local biostratigraphy of the platform was based mainly on ammonites (Lewy & Raab, 1978). Ostracods were used to establish a detailed biostratigraphy of the Cenomanian and Turonian strata of Carmel (Rosenfeld & Raab, 1974). Microbiostratigraphy of the Cenomanian is based on the planktic foraminifera (Lipson-Benitah et al., 1997); however, planktic foraminifers occur sporadically in these outcrops, and the Cenomanian planktic foraminifera biostratigraphy in Israel has been established on the coastal plain and offshore, where forams occur more frequently (Lipson-Benitah, 1980, 1994; Martinotti, 1993). The Judea Group is the least studied in terms of calcareous nannoplankton, and it is apparent that new paleontological and stratigraphical studies of the Judea Group are much needed. Subsurface (core) material provides an extended record of the depositional history of this part of the Levant Basin and offers a better opportunity to gain a fresh insight into paleoclimates by employing a quantitative analysis of the calcareous nannoplankton.

Despite prolific literature on the sedimentology, micropalaeontology, tectonics and geological mapping of NW Israel (Kafri, 1972; Rosenfeld & Raab, 1974; Bein & Weiler, 1976; Lewy & Raab, 1978; Sass & Bein, 1982; Lipson-Benitah et al., 1995, 1997; Segev, 2009; Karcz & Sneh, 2011), the paleoecology of the region is still poorly investigated. Calcareous nannoplankton of Israel, both fossil and Recent, have been studied for half a century (for review, see Ovechkina et al., 2019), although the coverage of stratigraphic intervals and the selection of research aims are uneven. In particular, calcareous nanofossil assemblages of the mid-Cretaceous remain unstudied, despite broad development of mid-Cretaceous carbonate platforms in the country (Braun & Hirsch, 1994). Calcareous nanofossils have been proved very instrumental in improving the stratigraphic framework of the analogous mid-Cretaceous shallow-marine deposits of the Ajlun Group in Jordan (Schulze et al., 2003) and the Upper Cretaceous–Cenozoic of Lebanon (Müller et al., 2010).

The Albian–Cenomanian succession in the Carmel Region was deposited during four sedimentary cycles separated by phases of maximal regression or transgression (Segev & Sass, 2014). The end of the second cycle is recorded in the Isfyte Fm. recovered in borehole CT8 (Fig. 1). The dolomites of the Yagur Fm., which underlays the aforementioned Isfyte Fm., in the upper part are presented by the miliolid facies (Lipson-Benitah et al., 1995, 1997) in the nearby borehole CT2 and point to a shallow and warm-water environment on the inner platform (Sliter & Baker, 1972). The third cycle, which corresponds to the Arqan Fm., was deposited during a general deepening of the

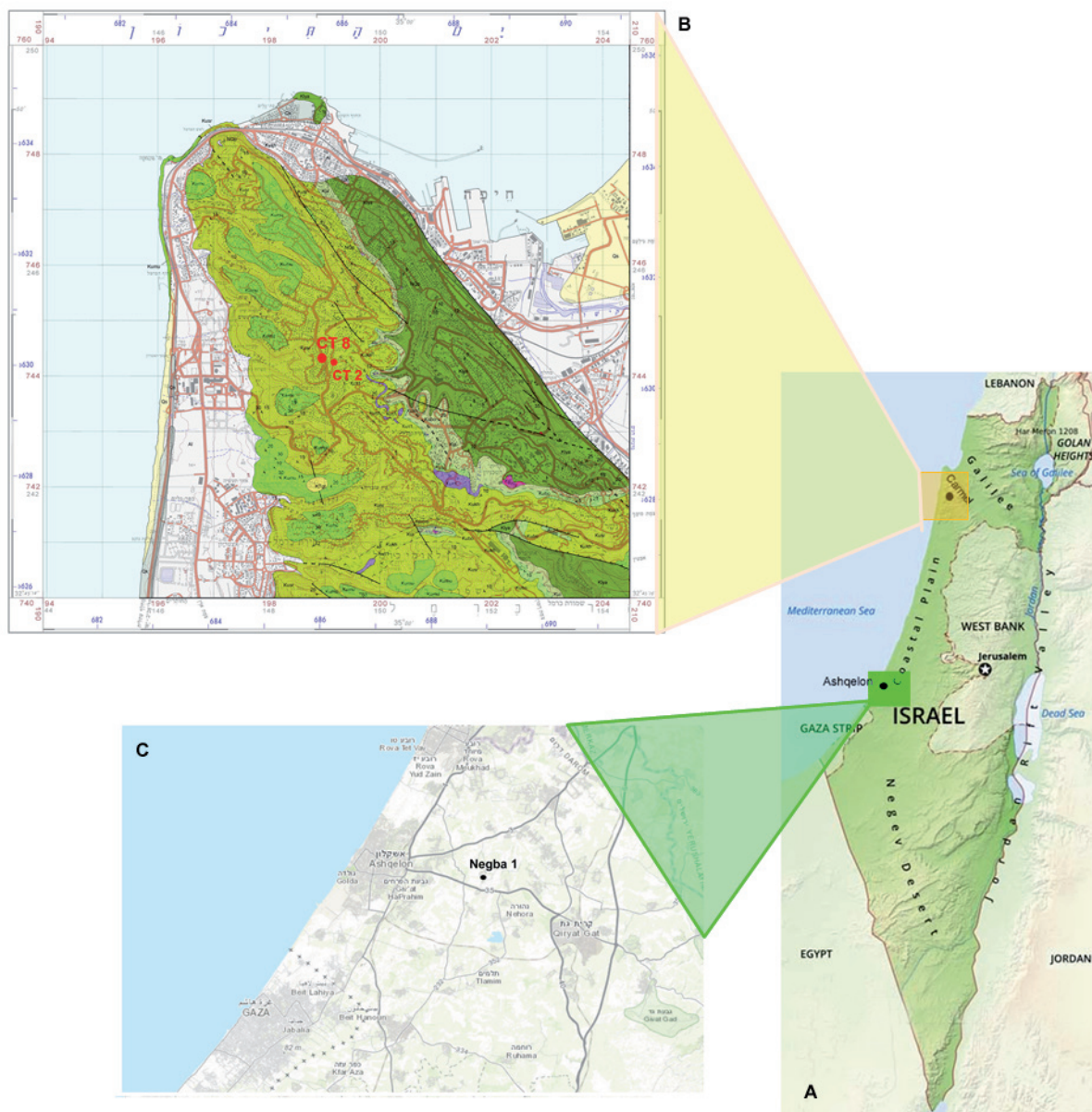


Figure 1. Location map. A – map of Israel, B – Carmel Area, C – Coastal Plain. Red – boreholes CT2 and CT8 in the Carmel Area, black – borehole Negba 1 in the Coastal Plain.

basin, as inferred from the faunistic and lithologic changes (Lipson-Benitah et al., 1995, 1997). The Lower–Middle Cenomanian chinks from the northwestern Carmel Region were deposited in the outer shelf environment (Lipson-Benitah et al., 1995, 1997).

The first palaeoenvironmental reconstruction of the Carmel area during the Cenomanian was made by Lipson-Benitah et al. (1995, 1997), based on quantitative analyses of planktic foraminifera from boreholes CT2 and CT0 at 1 km distance from borehole CT8 (Fig. 1). According to Lipson-Benitah et al. (1995, 1997) the Cenomanian deposits were accumulated in an outer shelf setting, and five ecostratigraphic intervals of alternating low and high relative abundances of planktic foraminifera were recognised, reflecting sea-level changes that correspond to the third order cycles 2.2–2.4 of the supercycle UZA-2 of Haq et al. (1988) and to sequences 2–5 of Robaszynski et al. (1993).

The present endeavour offers a new regional biostratigraphy based on calcareous nannofossils and supplemented by carbon and oxygen stable isotope data. The main aim of this research is to document quantitative fluctuations of nannofossils during the Albian–Cenomanian to improve our understanding of the depositional environment in the Levant Basin in this interval.

Specific aims of the proposed research

The recent research project is dedicated to the mid-Cretaceous calcareous nannoplankton assemblages within the biostratigraphic and paleoclimatic frameworks in the Levant Basin. The main objective of the research is to understand the depositional environment of the Judea Gr. in the Levant Basin using traditional methods of biostratigraphy supplemented by novel techniques of extracting calcareous nannofossils and by an interdisciplinary approach to paleoclimatic reconstructions.

The project emphasizes on

- investigation of the taxonomic composition of the calcareous nannoplankton assemblages from the Judea Gr. in Northern and Central Israel, biostratigraphic sequencing of Albian–Cenomanian deposits in Northern and Central Israel, using existing foraminiferal scheme for comparison;
- reconstruction of relative paleotemperature changes in this part of the Levant Basin during the Albian–Cenomanian using the quantitative analysis of the calcareous nannoplankton assemblages;

- approximation of absolute paleotemperatures using $\delta^{13}\text{C}$ and $\delta^{18}\text{O}$ and testing predictions obtained from the calcareous nannoplankton quantitative analysis against the geochemical data.

2. MATERIAL

2.1. Geological setting

The “Judea Limestone Formation” (Wellings, 1944) emended to the Judea Group with “the fully marine sedimentation” (Arkin et al., 1965) is subdivided into following levels (Fleischer, 2002; Rosenfeld & Hirsch, 2005) (Fig. 2):

Level 1. The Early Albian Yakhini Fm. represented by the carbonate sediments overlies the Aptian regressive Yavne Shale in the Coastal Plain subsurface. Rosenfeld et al. (1995) also placed the initial lower limit of the fully marine sedimentation of the Judea Group in the Coastal Plain of Israel at the Infra-Albian regional low-stand of the Late Aptian Yavne-Hidra event. The Yakhini Fm. is the oldest unit of the Judea Group (Rosenfeld & Hirsch, 2005) intergrades into the Talme Yafe Fm. offshore and on the westernmost coastal plane. This lower subdivision of the Judea Group is only represented in the Coastal Plain. Its carbonate facies interfinger eastward with the marly facies of the early Albian Rama Fm. of the Galilee Group.

Area Levels	Coastal Plain	Carmel
Early-Middle Cenomanian	Negba Fm.	Arqan Fm. Bet Oren Fm. Isfiye Fm.
Late Albian	Yagur Fm.	Yagur Fm.
Early Albian	Yakhini Fm.	

Figure 2. Judea Group levels (Rosenfeld & Hirsch, 2005).

Level 2. The Late Albian Yagur Fm. has been recovered in boreholes on the Coastal Plain and is exposed in the Carmel Area. The Yagur Fm. continues as Talme Yafe Fm. offshore and in the westernmost coastal area. The Yagur Fm. consists of monotonous dolomites with intercalations of limestones.

Level 3. The Early–Middle Cenomanian Negba Fm. in the subsurface of the Coastal Plain consists of dolomites with marl intercalations (Lower member) or dolomites with limestones interbeds and marls in the upper two-thirds (Upper member). In the Mount Carmel this level subdivides into a complex facies system, which parts are often difficult to correlate due to intensive block faulting (Rosenfeld & Hirsch, 2005) (Fig. 2). In the Carmel area the succession of the Isfiye chalk, Bet Oren limestone and Arqan chinks is bounded by the Carmel Reef Complex, intercalated by different types of volcanic tuffs.

Carmel Area

Boreholes CT2 (32.7°N 34.98°E) and CT8 (32.79°N 34.8°E) (Fig. 1) drilled in the northwestern part of the Carmel area were chosen for analysis due to the completeness of the obtained core, which represents nearly 100 % of the drilled interval (Lipson-Benitah et al., 1995, 1997). Samples for calcareous nannoplankton study were taken at approximately 2-m intervals, at the same levels as for foraminiferal samples. A total of 96 samples were collected along the 237.6 m section of the borehole CT2 and 108 samples were collected along the 225 m section of the borehole CT8.

The Carmel area is an isolated hilly belt composed mainly of the Cretaceous (mostly Albian–Turonian) sequences of the Judea Gr. (Sass & Bein, 1978) (Fig. 1), overlain by latest Cretaceous chinks of the Mount Scopus Gr. Mount Carmel is known for its complex stratigraphy and structure, which have been extensively studied over half a century (Picard & Kashai, 1958; Arkin & Hamaoui, 1967; Bein, 1976; Sass & Bein, 1978, 1982; Sass, 1980; Segev & Sass, 2006; Segev, 2009). In the southern part, an anticlinal structure trending north-east is clearly recognised, other parts of the Carmel area are described as block structures (Sass, 1980). Local occurrences of volcanic material with varying thickness and lithology add to this complexity (Sass, 1980; Segev, 2009).

The sequence forming Mount Carmel consists of dolomites, reefoidal limestones, chinks with some cherts and marlstones. Facies changes that mark many stratigraphic units were attributed to the position of the area close to the edge of a large carbonate platform during the Cretaceous (Sass & Bein, 1978). Sediment supply and distribution

was influenced by a rudist reef along the outer margin of the platform (Bein, 1976). Volcanics are represented by 16 separate volcanic events, some being good time markers (Sass, 1980). Segev (2009) recognised five tectonomagmatic events in the Mount Carmel sequence and four Cenomanian volcanic phases.

In the Mount Carmel sequence, four depositional cycles are recognised, viz. the Albian, Lower Cenomanian, Lower–Middle Cenomanian, and Middle Cenomanian–Turonian (Segev & Sass, 2014). Each cycle, composed of several lithofacies, accumulated under a specific regime of transgression and regression. The northern Carmel retains only one volcanic horizon, but the cycles established in the southern areas can still be recognised, with the exception of the fourth cycle which is missing (Segev & Sass, 2014). In the study area, the Tavasim Volcanics are represented; based on $^{40}\text{Ar}/^{39}\text{Ar}$ and K-Ar ages of fresh amphibole megacrysts and basalt samples the age of the volcanics has been established as 98.2 ± 1.1 Ma (Segev, 2009).

Coastal Plain

Negba 1 borehole (31.39°N 34.41°E) (Fig. 1) drilled in the southern Coastal Plain of Israel, is on a structural trend (NE/SW), more or less parallel to the present coastline (Conway, 1992). The Negba-1 lies northeast of the Gevar'am (abrasion) channel and northeast of the Helez/Kohav oil field (Conway, 1992). This borehole was chosen for analysis due to the completeness of the obtained core, which represents over 50% and in some intervals up to nearly 100 % of the drilled interval (unpublished GSI materials). Samples for calcareous nannoplankton study were taken at different intervals of the core (approx. from 2 to 5 m in 12 levels of the borehole). A total of 52 samples were collected along the 620 m section of the borehole.

The central Israel coastal zone is composed of the Pliocene–Pleistocene to Holocene Kurkar Group, composed primarily of alternating units of calcareous sandstones, the Upper Eocene – Miocene Sagiye Group consists of mainly silty clays (Makovsky et al., 2018) and the Lower–Middle Eocene Avedat Group (Sneh, 2008). In the most of the southern Coastal Plain, four main Lower Cretaceous rock complexes are recognized (Graden et al., 1960). One of the most widespread is the Unit L. Cr. I, consisting of uniform black, calcareous shales with a slight admixture of sand in some parts. The overlying L. Cr. II complex, as defined in the Heletz area, is composed of sandy, shaly and limy sediments. The Unit L. Cr. III is the most easily detected in the entire region by

correlatable electric markers. The lower Unit (L. Cr. Unit IIIa) consists of a thick sequence of oolitic, detritic and shaly limestones with minor intercalations of black calcareous shales. The overlying upper Unit (L. Cr. Unit IIIb) consists predominantly of shales and shaly limestones. The L. Cr. IV rock complex remains for its greater part poorly defined both lithologically and geo-electrically. The detailed investigations (Graden et al., 1960) in the Helez area indicate that the first occurrence of possible incipient tectonic movements can be recognized during deposition of the Hauterivian Unit L. Cr. II. By the end of this time a well-developed hinge line was formed to the east of the Heletz area (Graden et al., 1960). The Telamim Fm. (Barremian – Middle Aptian) lies higher and is represented by dolomites. The carbonatic interval of the Early–Middle Albian Yakhini Fm. is between the Telamim and Yagur Fms. The Yakhini Fm. is represented by slightly dolomitic limestones, limestones, marls and carbonatic shales (Derin, 2016). The Late Albian Yagur Fm. consists of dolomites (Rosenfeld and Hirsh, 2005). The overlying Cenomanian Negba Fm. comprises of dolomites with marl intercalations. Negba 1 borehole recovers an interval from the Upper Jurassic (Tithonian) to the Upper Cretaceous (Early Cenomanian Negba Fm. and Turonian Daliyya or Bina Fms) (Derin, 2016).

2.2. Lithology

Carmel Area

Boreholes CT8 and CT2

Several geological maps have been produced for the Carmel area (Segev & Sass, 2006; Karcz & Sneh, 2011; Segev & Sass, 2014). The Yagur Fm., and the Isfiye and Arqan Fms separated by the Tavasim Volcanics (V2) are recognised in the northwest Carmel boreholes according to the newest map of Segev and Sass (2014). The Cenomanian has not been subdivided into substages on available maps.

A detailed lithological description of the CT2 and CT8 cores was given by Lipson-Benitah et al. (1995, 1997). **Borehole CT2** penetrates the Isfiye and Arqan Fms. The Isfiye Fm. (3 m) is composed of dolomite and dolomitized chalk. The Arqan Fm. starts with the tuffaceous layer Tavasim Volcanics (V2) (56 m) overlain by dolomitized chalk (58 m). There is a 3-m layer of indurated chalk between 120.0–115.0 m. The upper part of the Arqan Fm. (120.6 m) is represented by chalk with an increasing amount of chert nodules.

Borehole CT8 penetrates the Yagur, Isfiye and Arqan Fms. The Yagur Fm. (10 m) is composed of dolomite. The Isfiye Fm. (18 m) is represented by dolomitised chalk. The Arqan Fm. starts with the tuffaceous layer Tavasim Tuff (V2) (16 m) overlain by dolomitised chalk and micritic carbonates (57 m). There is a 1-m layer of indurated chalk between 126.75–124.50 m. The upper part of the Arqan Fm. (127 m) is represented by chalk with an increasing amount of chert nodules.

Coastal Plain

Negba 1

The map of the Qiriat Gat Region, where the Negba 1 borehole is located, reflects the Lower– Middle Eocene Avedat Group, the Upper Eocene – Miocene Sagiye Group and the Pliocene–Pleistocene to Holocene Kurkar Group (Sneh, 2008). Older sediments are not shown on the map. A lithological description of the lower part of the borehole Negba 1 (Yakhini, Telamim, Helez and Kidod Fms) was given by Conway (1992). These sediments are overlain by the Yagur Fm., which is less studied. The upper part of the borehole (Negba Fm.) was studied by Lipson-Benitah et al. (1994). Unpublished materials from the GSI library were used for the lithological description.

The lower part of the Yagur Fm. exposed in the borehole consists of dolomitized limestones with rudists and a fragment of *Hamites?* sp. (Aptian ammonite), followed by limestones (~105 m) and dolomites (~140 m).

The Negba Fm. consists of approximately 360 meters of dolomites, chalks, marls and limestones. The lower member is composed of dolomites, fine grained to microcrystalline or coarser sugar limestones (~140 m). Occasional thin intercalations of rudist lumachelle and marly-chalky beds characterize relatively more fossiliferous levels in the succession. Non-carbonate content consists of scattered fragments of chert. The Upper member (~220 m thick), on the whole, is more fossiliferous and consists of marls, chalks and limestones.

2.3. Calcareous nannoplankton

In the Carmel area calcareous nannofossils have been found in all samples except for the lowermost part of the section (Isfiye Fm., samples 1–3) and sample 15 (Tavasim Tuff). However, nannofossils are quite rare at some levels. Their preservation ranges from poor to good (see Methods for definitions), but on average is moderate throughout the sequence; taxa have been identified under a polarising light microscope since

etching and overgrowth are minimal. On the Coastal Plain nannofossils are extremely rare with poor and moderate preservation. All identified species from both areas are listed in Appendix A.

3. METHODS

3.1 Planktic foraminifera and calcareous nannoplankton

The taxonomy and stratigraphical distribution of the planktic foraminifera from the Carmel area (CT8, CT2 boreholes) were studied by Lipson-Benitah et al. (1995, 1997). Following the suggestion of the Cenomanian Working Group of the Subcommittee on Cretaceous Stratigraphy (Kennedy et al., 2004) to define the base of the Cenomanian as the level of the first occurrence (FO) of *Thalmaninella globotruncanoides* (Fig. 3), foraminifera from boreholes CT2 and CT8 were re-examined. All foraminiferal material is stored on microslides at the Geological Survey of Israel (GSI). A total of 124 microslides

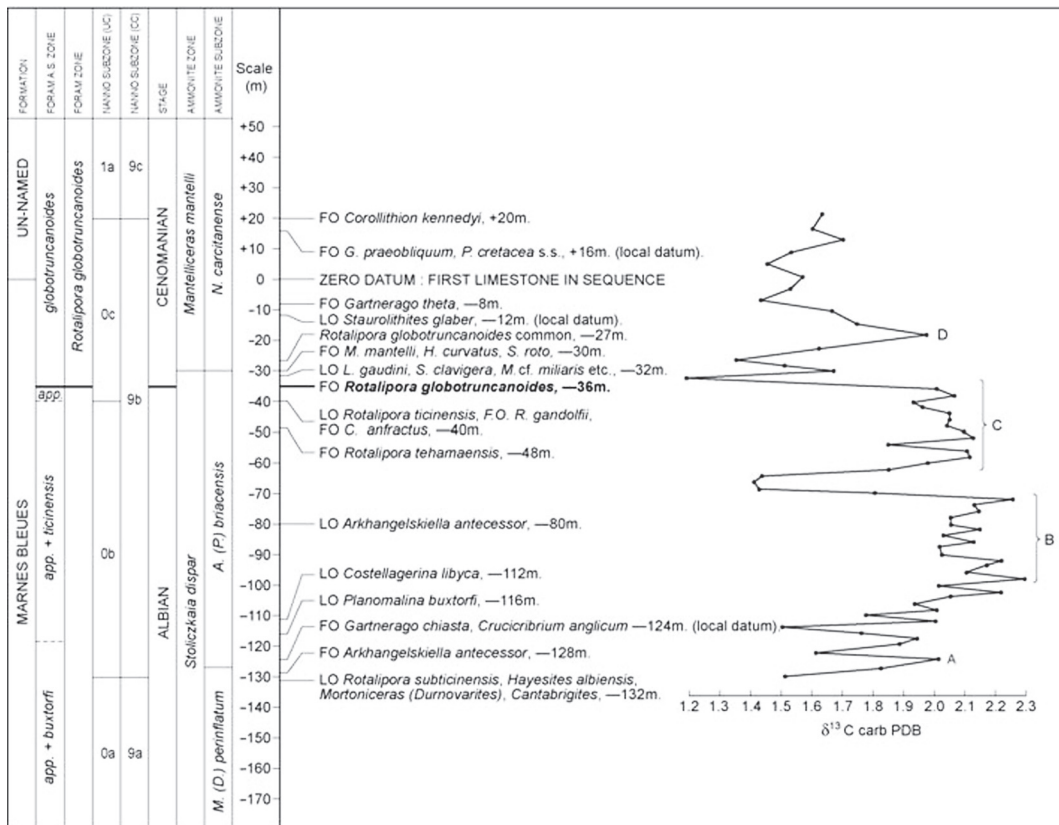


Figure 3. The distribution of key faunal and floral events across the Albian–Cenomanian boundary in the Marnes Bleues succession at the Mont Risou GGSP (Kennedy et al., 2004).

(borehole CT2) and 60 microslides (borehole CT8) were re-checked and stratigraphically important levels of the foraminiferal FOs were confirmed.

For updating the foraminifera biostratigraphy of borehole CT2, the most recent revised Upper Albian – Maastrichtian planktic foraminiferal biostratigraphical zonation of Coccioni and Premoli Silva (2015) for the Tethyan region was used.

The study of the calcareous nannoplankton was done on permanent smear slides prepared using the standard techniques of Bown and Young (1998) and examined under the polarising light microscope Olympus BX53 at 1250× magnification using phase contrast and cross-polarized light. Photographs were taken with a digital camera Olympus SC100.

There are several stratigraphical schemes for the Lower and Upper Cretaceous deposits (Fig. 4). The scheme of Sissingh (1977) with additions by Perch-Nielsen (1985) is accepted as a standard zonation, but is not very detailed one. More thorough zonations are suggested by Roth (1978) for the Tethyan Region (northwestern Atlantic Ocean), and schemes by Bralower et al. (1993, 1995) are most applicable for mid- and low-latitude sites. Burnett’s (1998) zonation provides the best resolution for the Upper Cretaceous—Cenomanian in particular—deposits.

For stratigraphical subdivision of boreholes CT2 and CT8 by calcareous nannoplankton, the integrated stratigraphical zonation of Bralower et al. (1995) for the Tethyan Region

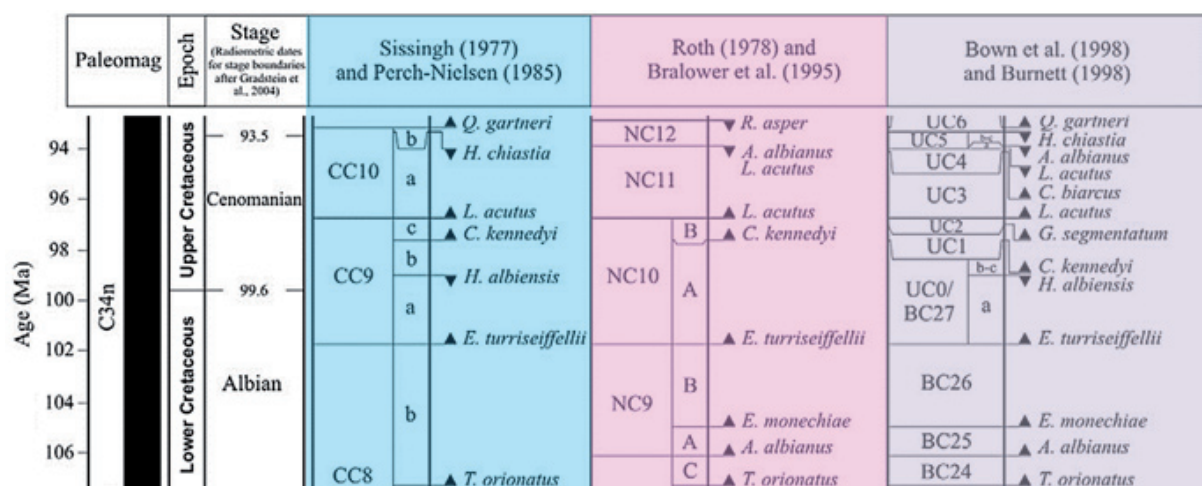


Figure 4. Comparison of the Albian and the Cenomanian nannofossil biostratigraphic zonations of Burnett *et al.* (1998), Bown *et al.* (1998) and with the CC and NC zonation schemes. Radiometric dates for the stage boundaries are from Gradstein *et al.* (2004).

(NC Zones for the Albian) and the zonation by Burnett (1998) for the Tethyan–Intermediate Province (UC Zones for the Cenomanian) were applied. For the biostratigraphical interpretation of the borehole Negba 1 the zonation of Sissingh (1977) with additions of Perch-Nielsen (1985) was used.

The quantitative analysis of nannofloral assemblages was done by counting at least 300 nannofossil specimens in random traverses in each smear slide. In samples with scarce assemblages, counting was done in as many as 350 fields of view. For paleoecological reconstructions, counts were done in 97 samples from borehole CT8 and 81 samples from borehole CT2. To assess the general abundance of the calcareous nannoplankton, the number of coccoliths per field of view was calculated. For borehole Negba 1, the quantitative analyse was not done due to extreme rarity of nannofossils.

Nannofossil preservation was determined based on criteria described in Watkins (1992):

G – good, most specimens exhibit little or no secondary alteration;

M – moderate, all specimens are easily identifiable, but exhibit the effects of some secondary alteration from calcite dissolution and/or overgrowth;

P – poor, identification of species hampered but possible in some cases; specimens exhibit profound effects of secondary alteration from etching and/or overgrowth.

The relation of diversity and abundance of each species was assessed by the Shannon index, Evenness and Species Richness, which was calculated using the software PAST, ver. 3.18 (Hammer et al., 2001). The Species Richness is often used as a measure of a relative stability of ecological conditions (Sanders, 1968; Dodd & Stanton, 1981; Watkins, 1989).

A correlation matrix and a multivariate factor analysis (R-mode) varimax rotation with principal component extraction were run using Statistica 10 (<https://www.tibco.com>). The factor analysis of borehole CT8 was performed on 18 taxa/groups, including species with mean abundances $\geq 1\%$ (11 taxa, Table 1) and taxa with mean abundances $< 1\%$. The latter group (*Z. embergeri*, *P. columnata*, *E. floralis*, *P. cretacea*, *L. carniolensis*, *Lithraphidites* spp. (*L. acutus*, *L. alatus*, *L. eccentricus*, *L. houghtonii*) and *Rh. asper* + *Rh. splendens*) was selected because of their palaeoecological significance. Factor loadings $> \pm 0.5$ were assigned to “dominant taxa”, factor loadings ± 0.3 – 0.5 were assigned to “associated taxa” and loadings ± 0.2 – 0.3 were assigned to “weakly associated taxa”.

Table 1. Descriptive statistics of some nannofossils from 97 samples of borehole CT8.

Species	Mean (%)	Median (%)	Min (%)	Max (%)	SD ¹	Std. error	Skewness	Kurtosis
<i>Watznaueria barnesiae</i>	60.59	61	23.9	84.7	10.34	1.05	-0.66	1.90
<i>Biscutum constans</i>	7.66	6	1.3	35.1	5.46	0.55	2.41	8.05
<i>Watznaueria</i> spp.	3.62	3.3	0.7	9.2	1.58	0.16	1.26	2.35
<i>Zeugrhabdotus bicrescenticus</i>	3.06	2.6	0	8.2	1.63	0.17	0.78	0.20
<i>Cretarhabdus</i> spp./ <i>Retecapsa</i> spp.	2.79	2.6	0.3	6.7	1.28	0.13	0.83	0.87
<i>Zeugrhabdotus diplogrammus</i>	2.10	1.7	0.3	7.4	1.20	0.12	1.53	3.62
<i>Zeugrhabdotus moulladei</i> + <i>Zeugrhabdotus</i> sp. (small)	1.81	1.8	0	3.9	0.74	0.08	0.32	0.76
<i>Tranolithus orionatus</i>	1.65	1	0.3	7.8	1.35	0.14	1.81	4.48
<i>Zeugrhabdotus</i> spp.	1.52	1.3	0	9	1.31	0.13	2.29	10.04
<i>Discorhabdus ignotus</i>	1.37	1.3	0	4.2	0.94	0.10	0.71	0.45
<i>Eiffellithus turriseiffelii</i>	1.24	1	0	4.6	0.94	0.10	1.16	1.61
<i>Zeugrhabdotus embergerii</i>	0.99	0.7	0	4.1	0.86	0.09	1.16	1.31
<i>Prediscosphaera columnata</i>	0.96	1	0	4.6	0.78	0.08	1.70	4.88
<i>Eprolithus floralis</i>	0.83	0.7	0	2.6	0.60	0.06	0.85	0.74
<i>Lithraphidites</i> spp.	0.70	0.3	0	5.4	1.04	0.11	2.45	6.52
<i>Prediscosphaera cretacea</i>	0.67	0.6	0	2.6	0.60	0.06	1.01	0.69
<i>Lithraphidites carniolensis</i>	0.63	0.6	0	2.3	0.59	0.06	1.04	0.73
<i>Rhagodiscus asper</i> / <i>splendens</i>	0.54	0.3	0	2.9	0.52	0.05	1.33	3.31

SD¹ - standart deviation**Table 2.** Descriptive statistics of some nannofossils from 81 samples of borehole CT2.

Species	Mean %	Median %	Min %	Max %	SD ¹	Std. error	Skewness	Kurtosis
<i>Watznaueria barnesiae</i>	55.61	59	27	74.7	10.94	1.22	-0.68	-0.38
<i>Watznaueria</i> spp.	7.21	7.3	2.3	11.3	1.85	0.21	0.02	-0.45
<i>Zeugrhabdotus moulladei</i> + <i>Zeugrhabdotus</i> sp.(small)	5.75	5	0	14.9	3.44	0.38	0.66	-0.42
<i>Biscutum constans</i>	4.14	3.6	0	18.9	2.93	0.33	2.02	7.28
<i>Cretrhabdus</i> spp./ <i>Retecapsa</i> spp.	3.69	3.7	0.7	6.2	0.99	0.11	0.08	0.75
<i>Zeugrhabdotus bicrescenticus</i>	2.80	2.3	1	7	1.34	0.15	1.09	0.48
<i>Zeugrhabdotus diplogrammus</i>	2.49	2.3	1	5.3	1.02	0.11	0.97	0.48
<i>Tranolithus orionatus</i>	1.96	2	0.7	6.3	0.90	0.10	1.80	6.33
<i>Zeugrhabdotus</i> spp.	1.57	1.3	0.3	4.4	0.87	0.10	1.02	0.80
<i>Eiffellithus</i> spp.	1.43	1.3	0	3.7	0.60	0.07	1.60	4.52
<i>Eprolithus floralis</i>	1.21	1	0	4	0.76	0.08	1.81	4.16
<i>Eiffellithus turriseiffelii</i>	1.08	1	0	2.6	0.38	0.04	0.31	3.88
<i>Discorhabdus ignotus</i>	1.03	0.7	0	4	0.79	0.09	1.53	2.68
<i>Prediscosphaera columnata</i>	1.02	0.7	0	3.5	0.61	0.07	2.12	4.99
<i>Lithraphidites carniolensis</i>	0.41	0.3	0	2	0.34	0.04	1.82	5.19
<i>Lithraphidites</i> spp.	0.37	0.3	0	1.6	0.46	0.05	1.05	0.00
<i>Rhagodiscus asper</i> / <i>Rhagodiscus splendens</i>	0.30	0.3	0	2	0.33	0.04	2.15	7.62

SD¹ - standart deviation

The factor analysis of borehole CT2 was performed on 17 taxa/groups, including species with mean abundances $\geq 1\%$ (14 taxa, Table 2) and taxa with mean abundances $< 1\%$. The latter group (*Watznaueria* spp., *Zeugrhabdotus* sp. (small) and *Zeugrhabdotus moulladei*, *Biscutum constans*, *P. columnata*, *Discorhabdus ignotus*, *E. floralis*, *P. cretacea*, *L. carniolensis*, *Lithraphidites* spp. (*L. acutus*, *L. alatus*, *L. eccentricus*, *L. houghtonii*) and *Rh. asper* + *Rh. splendens*) was selected because of their palaeoecological significance. Factor loadings $> \pm 0.5$ were assigned to “dominant taxa”, factor loadings ± 0.3 – 0.5 were assigned to “associated taxa” and loadings ± 0.2 – 0.3 were assigned to “weakly associated taxa”.

For both boreholes (CT2 and CT8) the nannofossil Nutrient Index (NI) was calculated from relative abundances of selected nannofossil taxa following Bottini et al. (2015), with a minor amendment by adding *Zeugrhabdotus* sp. (small) and introducing *Zeugrhabdotus moulladei* Bergen, 1998, which is here assumed to have the same paleoecological affinity as *Z. erectus* (Watkins et al., 2005):

$$NI = [(Z. moulladei + Zeugrhabdotus \text{ sp. (small)} + Biscutum constans + Discorhabdus ignotus) / (Z. moulladei + Z. \text{ sp. (small)} + Biscutum constans + Discorhabdus ignotus + Watznaueria barnesiae)] \times 100,$$

where, *Z. moulladei* + *Z. sp. small* (species with the major axis <3.5 μm), *B. constans* and *D. ignotus* are high productivity indicators, and *W. barnesiae* is a low productivity indicator). High values of the NI specify high productivity and vice versa.

The calculation of the nannofossil Temperature Index (TI) also follows Bottini et al. (2015) and was calculated for both boreholes (CT2 and CT8):

$$TI = [(E. floralis + R. parvidentatum + Staurolithites \text{ sp.}) / (E. floralis + R. parvidentatum + Staurolithites \text{ sp.} + Zeugrhabdotus diplogrammus + Rh. asper)] \times 100,$$

where *E. floralis* + *R. parvidentatum* + *Staurolithites* sp. are cold-water taxa, and *Zeugrhabdotus diplogrammus* + *Rh. asper* are warm water taxa. Low values of the TI specify high temperatures and vice versa.

3.2 Carbon and oxygen stable isotope analyses

For the oxygen and carbon stable isotopes, 81 bulk sediment samples from borehole CT2 and 100 bulk sediment samples from borehole CT8 were analysed. Measurements of $\delta^{13}\text{C}$ and $\delta^{18}\text{O}$ were taken according to the standard technique for bulk sediment samples. Samples were taken from freshly cut rock fragments, crushed and homogenised in an agate mortar. The isotopes were analysed at the Geological Survey of Israel using a Delta Plus mass spectrometer equipped with the gas bench system. All $\delta^{18}\text{O}$ and $\delta^{13}\text{C}$ values were calibrated against the international standard NBS-19, and are reported in ‰ relative to the VPDB standard. The system has an accuracy of $\pm 0.03\text{‰}$ for oxygen and $\pm 0.02\text{‰}$ for carbon isotopes.

4. RESULTS

Initial results

Calcareous nannoplankton from borehole CT8 retrieved in the NW Carmel area was studied. Totally 108 samples were examined for biostratigraphical analysis. The studied sequence composed of the following formations: Isfiye, Tavasim Volcanics and Arqan.

No calcareous nanofossils have been found in the lowest part of the section. The lower part of the Isfiye Fm. (CT8/5–16) is referred to the Upper Albian Subzone NC9b by the presence of *Eiffellithus monechiae*. The upper part of the Isfiye Fm. (CT8/17–47) belongs to the transitional Upper Albian – Lower Cenomanian Zone UC0 (equivalent NC10a) by the presence of *Eiffellithus turriseiffelii* from CT8/17. The interval CT8/48–54 is referred to the Lower Cenomanian Zone UC1 by the presence of *Corollithion kennedyi* from CT8/48. The interval CT8/55–60 belongs to the transitional Lower–Middle Cenomanian Zone UC2 by the presence of *Gartnerago segmentatum* from CT8/55. The upper part (CT8/61–108) is referred to the transitional basal Middle–Upper Cenomanian Zone UC3 by the presence of *Lithraphidites acutus* from CT8/61.

Thus, for the first time the taxonomic composition (over 94 species) and stratigraphic distribution of the calcareous nannoplankton from the Cenomanian of the NW Carmel area have been studied. The detailed calcareous nannoplankton biostratigraphy of this area has been established. For the first time the age of the tuffaceous layer is biostratigraphically identified and is regarded as the Late Albian (lower part) to the Late Albian – Early Cenomanian (upper part). This tuffaceous layer can possibly be correlated with the tectonomagmatic event C.V.–4 established by Segev (2009).

For the quantitative analysis, 300 calcareous nannoplankton specimens were counted in traverses of 80 samples. Fifty-six bulk sediment samples from Borehole CT8 were analyzed for $\delta^{18}\text{O}$. The productivity index (PI) and different ecological indexes were calculated.

The Upper Albian/Cenomanian sediments were deposited in the outer shelf environment. Significantly low Shannon diversity index, Evenness and Species Richness in the assemblage indicate unstable environmental conditions with low fertility. The whole succession was deposited in quite warm (~25–32.5 °C), open marine, oligotrophic conditions with poor nutrient supply. Five paleoecological phases have been recognized

by the quantitative analysis of the calcareous nannoplankton and the PI and $\delta^{18}\text{O}$ values. Warming/cooling events of various scale and fluctuations of eutrophication/oligotrophication have been detected in each phase.

4.1. Biostratigraphy and biochronology

4.1.1. Planktic foraminifera biostratigraphy

Carmel Area

Borehole CT8

The planktic foraminifera biostratigraphy was described in detail elsewhere (Ovechkina et al., 2019).

The following planktic foraminifera zones were established by Lipson-Benitah et al. (1995, 1997) for borehole CT8: *Rotalipora brotzeni* (Lower Cenomanian), *Rotalipora reicheli* (lower Middle Cenomanian), and *Rotalipora cushmani* (Middle Cenomanian) with the *Rotalipora greenhornensis* and the *Pseudotruncana algeriana* subzones (Fig. 5).

According to the revised planktic foraminiferal biostratigraphical zonation for the Upper Albian – Maastrichtian (Coccioni & Premoli Silva, 2015), the following four planktic foraminifera zones have been recognised (Fig. 5).

The planktic foraminifera are first recorded in sample 20 (depth 183.35 m). It is impossible to trace the base of the *Parathalmanninella appenninica* Zone unambiguously. The first occurrence (FO) of *Parathalmanninella appenninica* was observed in sample 26 (depth 169.9 m) by Lipson-Benitah et al. (1995, 1997, as *Rotalipora appenninica*), but the presence of this species at this level has not been verified during the re-examination of the microslides. In the lower part of the Arqan Fm. (samples 32–45), we recognize the Upper Albian *Parathalmanninella appenninica* Zone as the interval from the lowest occurrence of *P. appenninica* to the lowest rare occurrence of *Thalmanninella globotruncanoides*.

The confirmed occurrence of *P. appenninica* has been recorded together with the FO of *Thalmanninella brotzeni* in sample 32 (depth 158.7 m). Thus, the lower boundary of this zone can be drawn at the level of sample 32, as was established by Lipson-Benitah et al. (1995, 1997) for the *R. brotzeni* Zone. The upper boundary of the *P. appenninica* Zone is unambiguously fixed by the FO of *Th. globotruncanoides* in sample 45 (depth 132.5 m). The *P. appenninica* Zone is correlated with the lower part of the

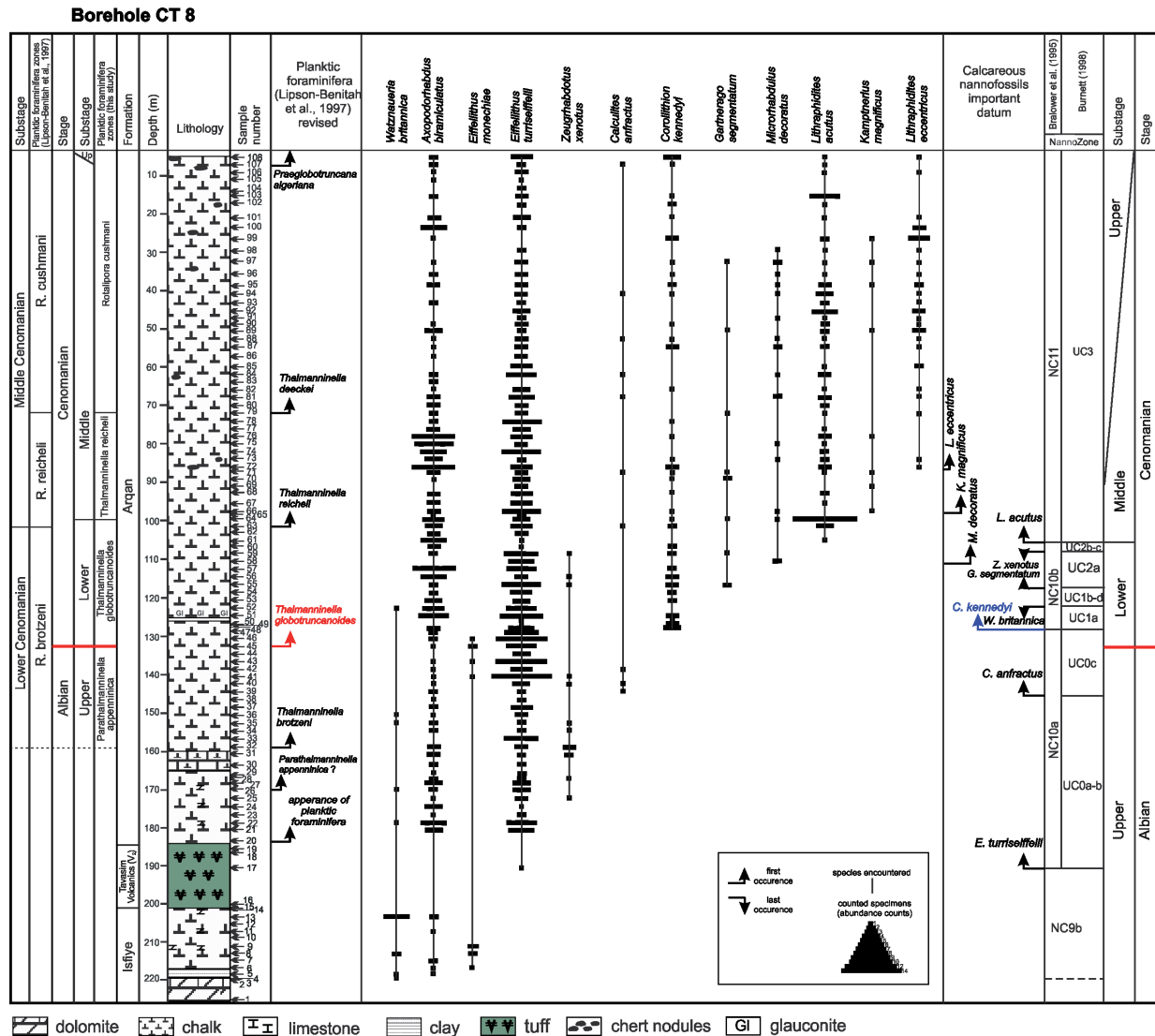


Figure 5. Lithology, vertical distribution of biostratigraphically important nannofossils, and planktic foraminifera events from the borehole CT8 (Carmel Area).

R. brotzeni Zone of Lipson-Benitah et al. (1997), which is considered to be Lower Cenomanian. However, Coccioni and Premoli Silva (2015) accept the Late Albian age of the P. appenninica Zone. Higher, in the interval of samples 45–62, the Lower Cenomanian Thalmanninella globotruncanoides Zone is fixed confidently as the interval from the lowest rare occurrence of *Th. globotruncanoides* to the lowest occurrence of *Thalmanninella reicheli*. The lower boundary of the *Th. globotruncanoides* Zone marks the Albian/Cenomanian boundary (sample 45, depth 132.5 m). The upper boundary of the zone is defined by the last occurrence (LO) of *Th. reicheli* in sample 63 (depth 101.6 m). The interval of this zone is correlated with the upper part of the R. brotzeni Zone of Lipson-Benitah et al. (1997).

In the middle part of the Arqan Fm. (samples 63–78) the Middle Cenomanian *Thalmaninella reicheli* Zone was established as the interval between the first appearance (FA) of *Th. reicheli* to the FA of *Thalmaninella deecke*. The zone is equivalent to the *Th. reicheli* Zone of Coccioni and Premoli Silva (2015), who used the total range of *Th. reicheli*. Because of extremely scarce *Th. reicheli* in our material (the species has been found in sample 63 only), the definition of Lipson-Benitah et al. (1997) is retained. The lower boundary of the zone is established at the depth of 101.6 m (sample 63) and the upper boundary is fixed at the depth of 74 m (sample 78), with the FA of *Th. deecke* in sample 79 (depth 72 m).

The upper part of the Arqan Fm. can be assigned to the upper Middle – uppermost Cenomanian *Rotalipora cushmani* Zone as the interval from the FA of *Th. deecke* to the LO of *Rotalipora cushmani*. The zone is equivalent to the *R. cushmani* Zone of Coccioni and Premoli Silva (2015), who defined this zone as the interval from the highest occurrence of *Th. reicheli* to the highest occurrence of *R. cushmani*. Because *Th. reicheli* is extremely scarce in the studied section, the definition of the *R. cushmani* Zone by Lipson-Benitah et al. (1997) is accepted. The zone is confidently established for the interval of samples 79–108 (depths 72–5 m).

The *R. cushmani* Zone is subdivided into two subzones: *Thalmaninella greenhornensis* Subzone (upper Middle – lower Upper Cenomanian) and *Dicarinella algeriana* Subzone (Upper Cenomanian). The *Th. greenhornensis* Subzone is used as the interval between the FA of *Th. deecke* and the FA of *Dicarinella algeriana* (formerly *Praeglobotruncana algeriana*). The subzone is equivalent to the *Th. greenhornensis* Subzone of Coccioni and Premoli Silva (2015), who defined it as the interval from the highest occurrence of *Th. reicheli* to the lowest occurrence of *D. algeriana*. This subzone is confidently established for the interval of samples 79–106 (depths 72–9 m). Because of extremely scarce *Th. reicheli* in our material, the definition of this subzone by Lipson-Benitah et al. (1997) is followed here. Lipson-Benitah et al. (1997) accepted the Middle Cenomanian age of this subzone, whereas Coccioni and Premoli Silva (2015) suggested a late Middle to early Late Cenomanian age.

The *Dicarinella algeriana* Subzone is used as the interval from the lowest occurrence of *D. algeriana* to the highest occurrence of *R. cushmani*. The subzone is equivalent to the *Praeglobotruncana algeriana* Subzone of Lipson-Benitah et al. (1997) and is recorded

in the uppermost part of the borehole (samples 107–108, depths 7–5 m). The age of this subzone is accepted as Middle–Late Cenomanian (Robaszynsky et al., 1993), but Lipson-Benitah et al. (1995, 1997) suggested a Middle Cenomanian age for this interval, due to the continuous presence of *R. brotzeni* (cf. Grosheny et al., 1992) and *Orbitolina* spp. (Schroeder and Neumann, 1985) in the Junediya Fm. (Lipson-Benitah et al., 1995, 1997).

Borehole CT2

The following planktic foraminiferal zones were established for Borehole CT2: *Rotalipora brotzeni* (Early Cenomanian), *Rotalipora reicheli* (early Middle Cenomanian), and *Rotalipora cushmani* (Middle Cenomanian) with *Rotalipora greenhornensis* and *Pseudotruncana algeriana* subzones (Fig. 6).

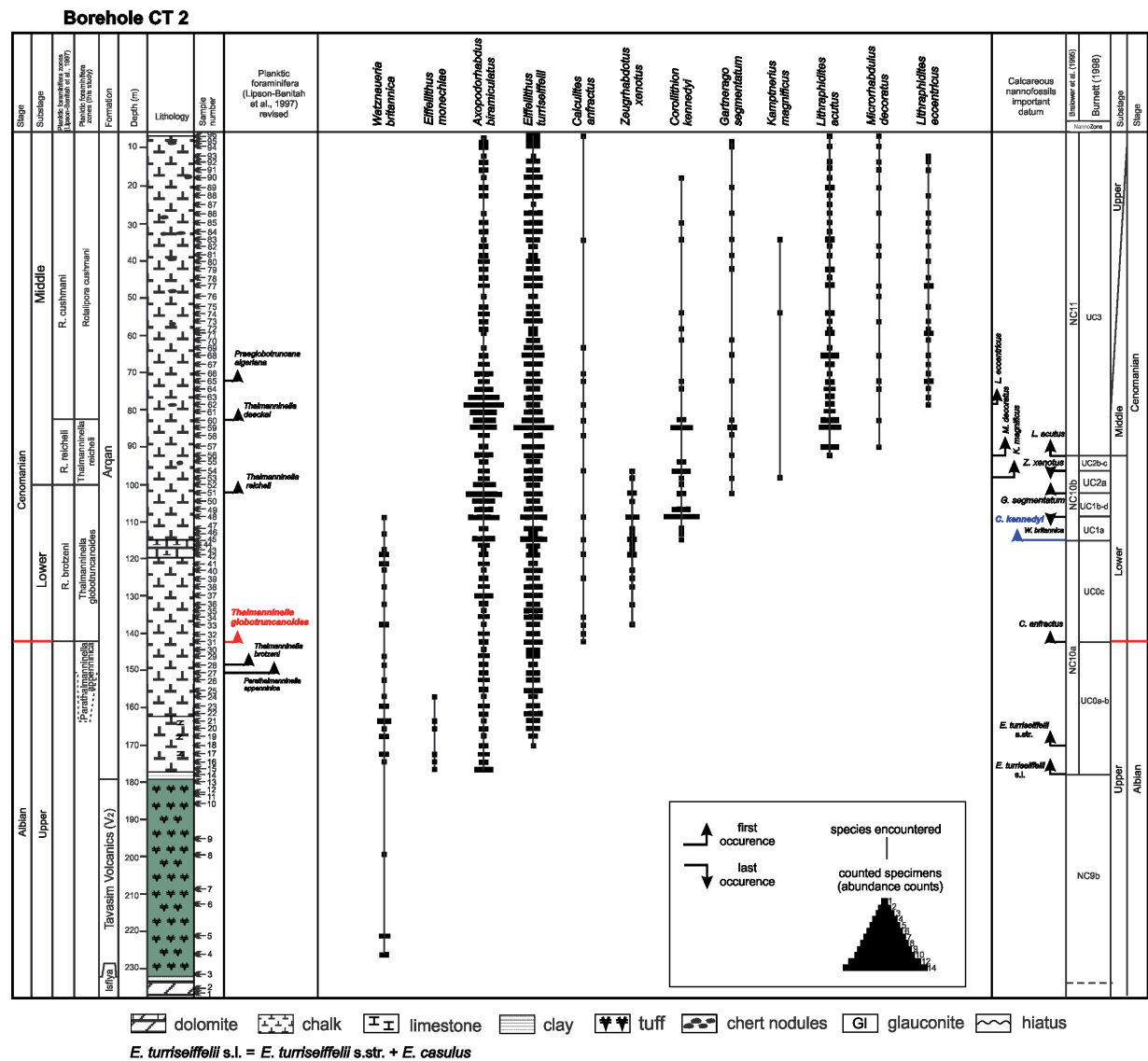


Figure 6. Lithology, vertical distribution of biostratigraphically important nannofossils, and planktic foraminifera events from the borehole CT2 (Carmel Area).

According to the revised planktonic foraminiferal biostratigraphical zonation for the Upper Albian – Maastrichtian (Coccioni & Premoli Silva, 2015), the following four planktonic foraminifera zones have been recognized (Fig. 6).

Parathalmanninella appenninica Zone, Upper Albian

Definition: The interval from the lowest occurrence of *Parathalmanninella appenninica* to the lowest rare occurrence of *Thalmanninella globotruncanoides*.

Authors: Coccioni & Premoli Silva, 2015.

Remarks: *Thalmanninella brotzeni* and *Parathalmanninella gandolfii* appeared in this zone (Coccioni & Premoli Silva, 2015).

The FO of *Parathalmanninella appenninica* is fixed in sample 27 (depth 150.9 m) by Lipson-Benitah et al. (1995, 1997, as *Rotalipora appenninica*), and the presence of this species at this level has been verified during the present re-examination of the microslides. Thus, the lower boundary of this zone has been drawn at the level of sample 27. The upper boundary of the P. appenninica Zone is unambiguously fixed by the FO of *Thalmanninella globotruncanoides* in sample 31 (depth 142.25 m). The confirmed occurrence of *Thalmanninella brotzeni* has been recorded together with the FO of *Parathalmanninella gandolfii* in sample 28 (depth 148.8 m).

The P. appenninica Zone is correlated with the lower part of R. brotzeni Zone of Lipson-Benitah et al. (1997), which is considered to be of the Early Cenomanian age. However, Coccioni and Premoli Silva (2015) accept the Late Albian age of the P. appenninica Zone.

Thalmanninella globotruncanoides Zone, Lower Cenomanian

Definition: The interval from the lowest rare occurrence of *Thalmanninella globotruncanoides* to the lowest occurrence of *Thalmanninella reicheli*.

Authors: Coccioni & Premoli Silva, 2015.

Remarks: This zone is fixed confidently in the interval of samples 31–50. Its lower boundary marks the Albian/Cenomanian boundary (sample 31, depth 142.25 m). The upper boundary of the zone is defined by the lowest occurrence of *Th. reicheli* in sample 51 (depth 102.10 m). The interval of this zone is correlated with the upper part of R. brotzeni Zone of Lipson-Benitah et al. (1997).

Thalmanninella reicheli Zone, Middle Cenomanian

Definition: The interval between the first appearance of *Thalmanninella reicheli* to the

first appearance of *Rotalipora deecke* (now *Thalmaninella deecke*).

Authors: Lipson-Benitah et al. (1997).

Remarks: Lipson-Benitah et al. (1997) named this stratigraphical interval after *Rotalipora reicheli*. Since at present this species belongs to the genus *Thalmaninella*, this zone should be called *Thalmaninella reicheli*.

The zone is equivalent to *Thalmaninella reicheli* Zone of Coccioni and Premoli Silva (2015), who suggested to define this zone by the total range of *Thalmaninella reicheli*. Because of scarce *Th. reicheli* in our material, the definition of Lipson-Benitah et al. (1997) is accepted. The lower boundary of this zone is established at the depth of 102.10 m (sample 51). The upper boundary of this zone is fixed at the depth of 84.45 m (sample 59), with the first appearance of *Thalmaninella deecke* being observed in sample 60 (depth 82.5 m).

A detailed discussion of boundaries and definitions of this zone was published by Lipson-Benitah et al. (1997).

Rotalipora cushmani Zone, upper Middle to uppermost Upper Cenomanian

Definition: The interval from the first appearance of *Thalmaninella deecke* to the last appearance of *Rotalipora cushmani*.

Authors: Lipson-Benitah et al. (1997).

Remarks: The zone is equivalent to the *R. cushmani* Zone of Coccioni and Premoli Silva (2015), who suggested to define this zone as the interval from the highest occurrence of *Thalmaninella reicheli* to the highest occurrence of *Rotalipora cushmani*. Because of extremely scarce *Th. reicheli* in our material, the definition of the *Rotalipora cushmani* Zone of Lipson-Benitah et al. (1997) has been accepted. The zone is confidently established for the interval of samples 60–96 (depths 82.5–6.7 m).

Thalmaninella greenhornensis Subzone, u. Middle – I. Upper Cenomanian

Definition: The interval between the first appearance of *Thalmaninella deecke* and the first appearance of *Dicarinella algeriana* (formerly *Praeglobotruncana algeriana*).

Authors: Lipson-Benitah et al. (1997).

Remarks: The subzone is equivalent to the *Thalmaninella greenhornensis* Subzone of Coccioni and Premoli Silva (2015), who suggested to define this subzone as the interval from the highest occurrence of *Thalmaninella reicheli* to the lowest occurrence of *Dicarinella algeriana*. This subzone is confidently established for the interval of

samples 60–64 (depths 82.50–74.10 m). Because of extremely scarce *Th. reicheli* in our material, the definition of the *Rotalipora greenhornensis* Subzone of Lipson-Benitah et al. (1997) has been accepted here. According to the current taxonomy, this subzone is to be named *Thalmaninella greenhornensis*.

Lipson-Benitah et al. (1997) accepted the Middle Cenomanian age of this subzone, whereas Coccioni and Premoli Silva (2015) suggested the late Middle to early Late Cenomanian age.

Dicarinella algeriana Subzone, lower Upper – uppermost Upper Cenomanian

Definition: The interval from the lowest occurrence of *Dicarinella algeriana* to the highest occurrence of *Rotalipora cushmani*.

Authors: Coccioni & Premoli Silva (2015).

Remarks: The subzone is equivalent to *Praeglobotruncana algeriana* Subzone of Lipson-Benitah et al. (1997) and is detected in the uppermost part of the borehole (samples 65–96, depths 72.0–6.7 m).

Lipson-Benitah et al. (1997) suggested the Middle Cenomanian age for this interval, due to the continuous presence of *R. brotzeni* (cf. Grosheny et al., 1992) and *Orbitolina* spp. (Schroeder & Neumann, 1985) in the Junediya Fm. (Lewy, 1995).

Coastal Plain

Negba 1

The palynological study and stratigraphy of the Jurassic to the Lower Cretaceous (Albian, Yakhini Fm.) of the borehole Negba 1 was done by Conway (1992). Raab (1962) studied ammonites from the sandy shales of the Helez Fm. (Jurassic). The biostratigraphy of the upper part of the Upper member of the Negba Fm. was studied by Reiss during 1955–1964 (unpubl. data, GSI library). The lower samples from the depths of 1725–795 m were studied in detail and the abundant marine predominantly shallow warm water fauna, which includes molluscs, rudists, bryozoans, different algae, echinodermites, corals, annelid tubes, stromatoporoids, benthic foraminifera with calcitic and agglutinated tests, was recorded (unpubl. GSI materials). At the depth of 745 m (core 10) abundant Albian–Cenomanian rudists were recorded. Eleven samples from the studied borehole interval (depths 288–179 m) were analysed and various invertebrates (Stromatoporoidea, Bryozoa, Mollusca, Echinodermata, Corals, Annelida, Rudists) were found (Fig. 7). Microfossils (osracods, calcareous algae, benthic foraminifera) were also

(1994) also mentioned, tests of *Praeglobotruncana*, *Rotalipora*, *Heterohelix* and benthic foraminifera in addition to *Hedbergella* and *Pithonella*, which may be predominant in the micritic matrix. The more indurated levels of limestones, either isolated beds or intercalations of several meters, contain remains of *Orbitolina* and rudists.

4.1.2. The Global Boundary of the Cenomanian Stage, the Stratotype Section

Following recommendations of the Cenomanian Working Group of the Subcommittee on Cretaceous Stratigraphy, a Global boundary Stratotype Section and Point was selected on the western flanks of Mont Risou, Alpes, southeastern France (Kennedy et al., 2004). The base of the Cenomanian stage is defined at the level of 36 m below the top of Marnes Bleues, which corresponds to the FO of the planktic foraminifera *Rotalipora globotruncanoides* (Kennedy et al., 2004), now classified as *Thalmanninella globotruncanoides* (Caron & Premoli Silva, 2007; Coccioni & Premoli Silva, 2015). In the Carmel area, this study places the Albian/Cenomanian boundary at the FO of *Th. globotruncanoides* (borehole CT8 – sample 45, depth 132.5 m; borehole CT2 – sample 31, depth 142.25 m).

4.1.3. Calcareous nannoplankton biostratigraphy

Borehole CT8

The calcareous nannoplankton biostratigraphy was described in detail elsewhere (Ovechkina et al., 2019). The calcareous nannoplankton assemblages of the borehole are fairly rich, consist of 113 taxa (Appendixes A, B; Plates 1–3), and allow the recognition of zones and subzones of the NC (Bralower et al., 1995) and UC (Burnett, 1998) schemes, as follows (Fig. 5).

The lowest part of the Isfiye Fm. is referred to the Upper Albian Subzone NC9b, which lower boundary is defined by the FO of *Eiffellithus monechiae* (sample 5, depth 218.7 m) and upper boundary by the FO of *Eiffellithus turriseiffelii* (sample 6, depth 216.9 m). *Eiffellithus monechiae* is absent from the lowest sample 4, which may be explained by the extreme rarity of the species in the lower part of the section in general. This subzone is characterised by relatively scarce nannofossils, among which rare *Axopodorhabdus biramiculatus* (= *A. albianus*), *Cyclagelosphaera margerelii*, *Eprolithus floralis*, *E. monechiae* and more abundant *Prediscosphaera columnata*, *Manivitella pemmatoidea*, *Retecapsa angustiforata*, *Tranolithus orionatus*, *Watznaueria barnesiae* and *W. fossacincta* have been found.

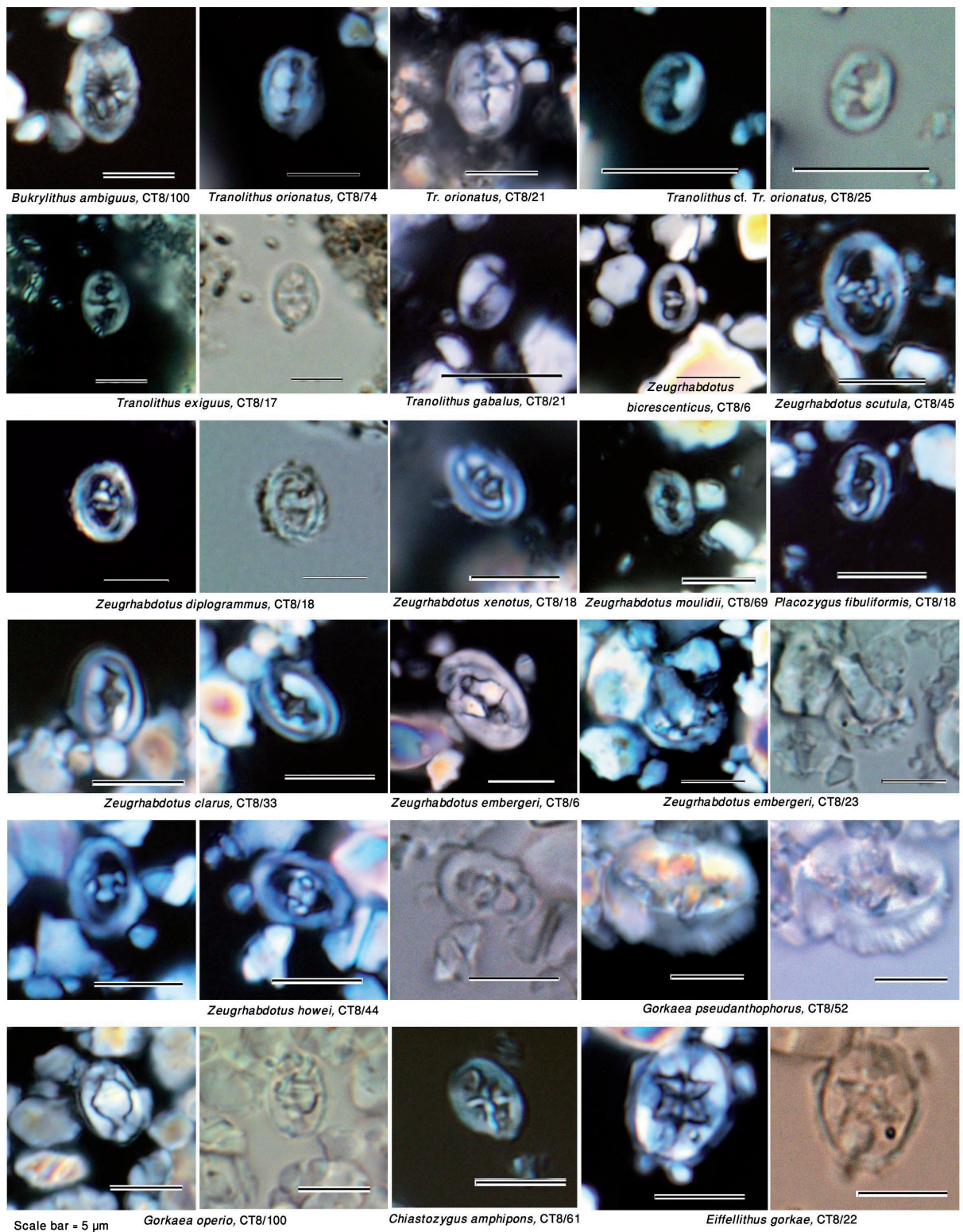


Plate 1. Calcareous nannofossils (LM images) from the Albian–Cenomanian from the Mount Carmel Region (borehole CT8).

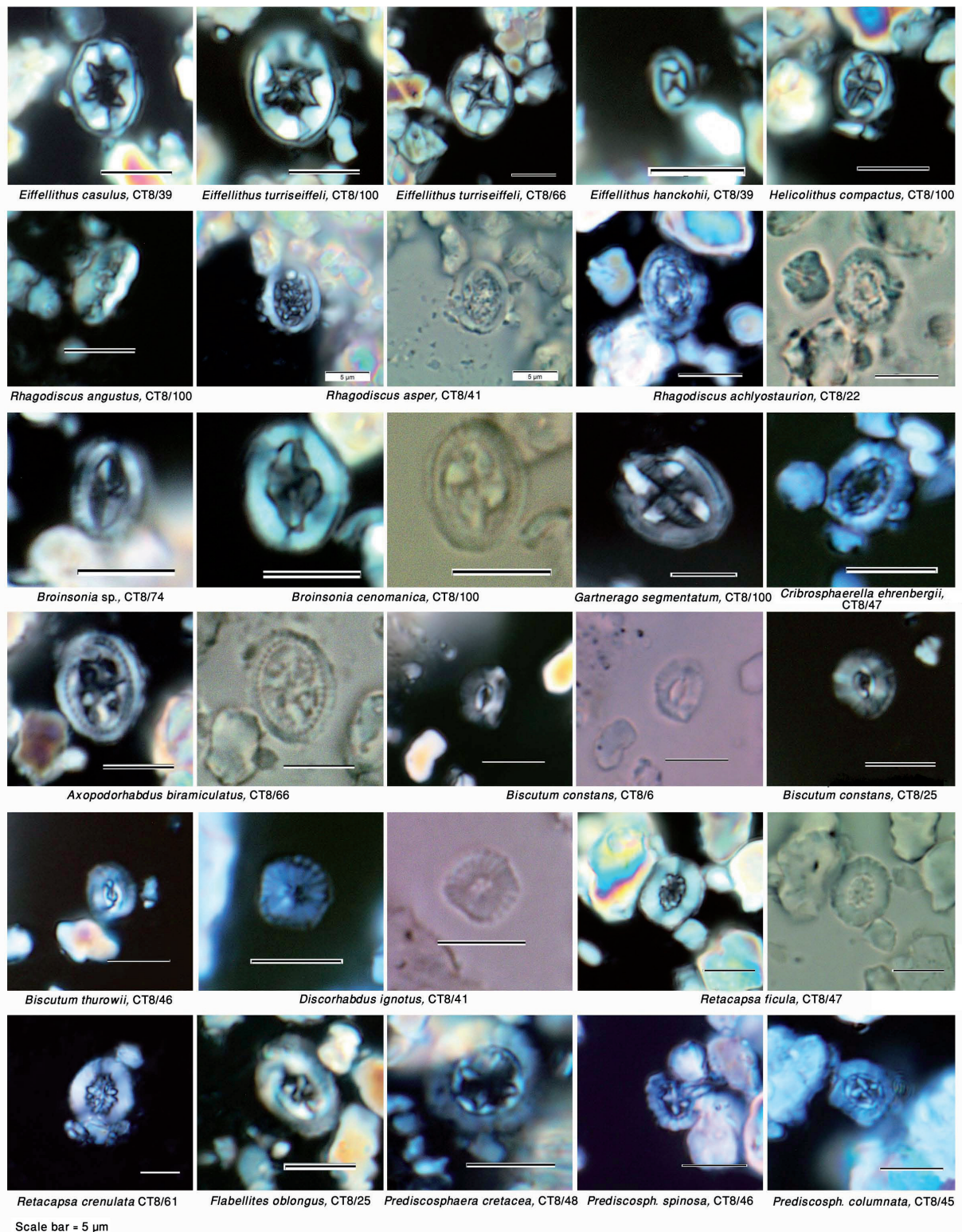


Plate 2. Calcareous nanofossils (LM images) from the Albian–Cenomanian from the Mount Carmel Region (borehole CT8).

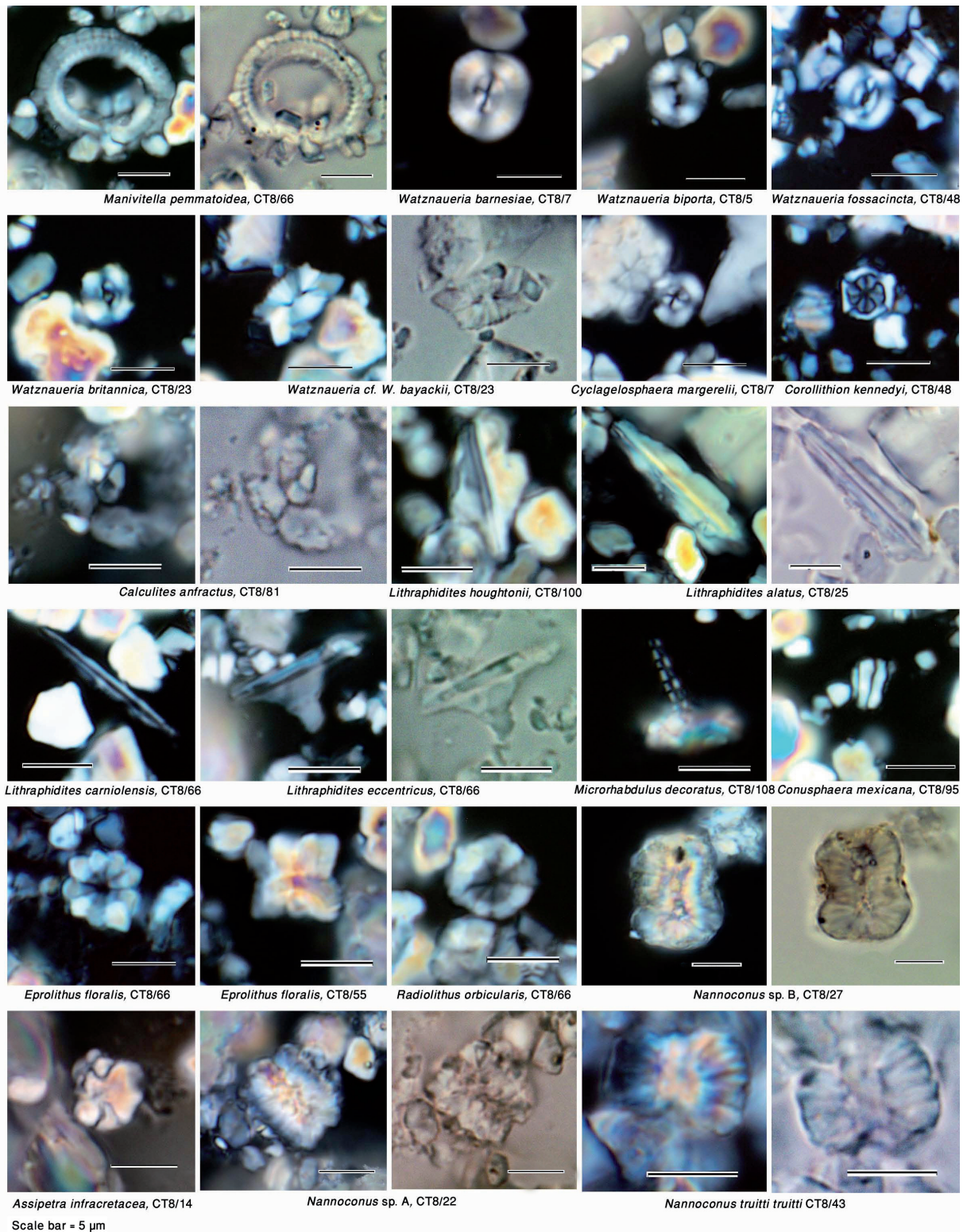


Plate 3. Calcareous nannofossils (LM images) from the Albian–Cenomanian from the Mount Carmel Region (borehole CT8).

The main part of the Isfiye Fm., the Tavasim Tuff and the lower part of the Arqan Fm. (samples 6–47, depths 216.9–128.5 m) belong to UC0 Zone of the Upper Albian – lowermost Cenomanian, a special transitional zone in Burnett’s (1998) Upper Cretaceous scheme. The lower boundary of UC0 Zone is defined by the FO of *Eiffellithus turriseiffelii* s.l. (sample 6, depth 216.9 m) *sensu* Burnett (1998) and Bralower et al. (1993, 1995), or by *Eiffellithus casulus* Shamrock in Shamrock & Watkins 2009 (Ovechkina et al., 2019). The upper boundary of UC0 is marked by the FO of *Corollithion kennedyi* (sample 48, depth 127.15 m). Zone UC0 is equivalent to subzone NC10a of Bralower et al. (1993, 1995). This zone straddles the Lower/Upper Cretaceous boundary and is shared by two discrete biozonations.

Subzones UC0a and UC0b cannot be recognised in the present section due to the absence of the stratigraphically important marker *Hayesites albiensis*, the LO of which defines the top of the UC0a subzone.

Subzone UC0c is identified in the interval of samples 39–47 (depths 144.45–128.50 m) in the studied section. The lower boundary of this subzone is fixed by the FO of *Calculites anfractus* (sample 39, depth 144.45 m) and its upper boundary is marked by the FO of *C. kennedyi* (sample 48, depth 127.15 m).

The interval of samples 48–54 (depths 127.15–118.55 m) is assigned to the Lower Cenomanian UC1 Zone due to the presence of *Corollithion kennedyi*, the FO of which was observed in sample 48 (depth 127.15 m). The upper boundary of this Zone is fixed by the FO of *Gartnerago segmentatum* in sample 55 (depth 116.50 m). Subzone UC1a and undivided subzones UC1b–d are recognised. The FO of *C. kennedyi* is generally used for demarcating the basal Cenomanian (Ando et al., 2015). This level is slightly above the FO of *Th. globotruncanoides* (depth 132.50 m); this pattern of successive FOs of *Th. globotruncanoides* and *C. kennedyi* has been documented elsewhere (e.g., Robaszynski et al., 1993; Watkins et al., 2005; Ando et al., 2015).

The interval of samples 48–52 (depths 127.15–122.50 m) belongs to Subzone UC1a due to the presence of *Watznaueria britannica*, which LO marks the upper boundary of UC1a and is recorded in sample 52 (depth 122.50 m).

Subzones UC1b–d cannot be established because of the absence of *Gartnerago chiasta*, which LO defines the top of UC1b. Subzone UC1c is described as the interval from the LO of *G. chiasta* to the FO of rare and sporadic *Kamptnerius magnificus* or the FO of *Helicolithus anceps*. In our material *H. anceps* is absent, whereas rare and sporadic

K. magnificus has been recorded much higher from sample 66 (depth 97.50 m).

The interval of samples 55–60 (depths 116.50–106.45 m) belongs to the Lower – basal Middle Cenomanian Zone UC2 due to the presence of *Gartnerago segmentatum*, which FO is recorded in sample 55 (depth 116.50 m). Subzone UC2a and undivided subzones UC2b–c are recognised. The interval of samples 55–59 (depths 116.50–108.35 m) belongs to UC2a subzone due to the presence of *Zeugrhabdotus xenotus*, which LO is recorded in sample 59 (depth 108.35 m). The interval between samples 59–61 (depths 108.35–105.15 m, sample 60 at 106.45 m) corresponds to undivided UC2b–c subzones; the marker species *Cylindralithus sculptus*, which FO defines the base of UC2c Subzone, has not been found.

The interval of UC1 and UC2 zones refers to the Lower Cenomanian NC10b Subzone of the Bralower et al. (1995) scheme.

The upper part of the borehole (samples 61–108, depths 105.15–5.00 m) is referred to the transitional Zone UC3 of the basal Middle–Upper Cenomanian due to the presence of *Lithraphidites acutus*, which FO is recorded in sample 61 (depth 105.15 m). *Kamptnerius magnificus* (sample 66, depth 97.50 m) and *Lithraphidites eccentricus* (sample 72, depth 86.05 m) are found in this interval. Another important species is *Microrhabdulus decoratus*, which first appears together with *Lithraphidites acutus* and is an index species for the Upper Cenomanian Zone CC10 (Perch-Nielsen, 1985). In our material the FO of *M. decoratus* has been recorded slightly below the FO of *L. acutus* in sample 58 (depth 110.55 m).

Subzones UC3a–d cannot be subdivided because of the absence of *Gartnerago theta*, *Staurolithites gausorhethium* and *Gartnerago nanum*. The top of subzone UC3d is defined by the LO of *Corollithion kennedyi*. This datum is not reached in the studied section since *C. kennedyi* is still present in the uppermost sample 108 (depth 5.00 m). Burnett (1998) recorded the LO of *C. anfractus* in the upper part of subzone UC3b in the Boreal Realm. In our material, the presence of very rare *C. anfractus* has been fixed in the penultimate sample 107 (depth 7.00 m).

The interval of samples 61–108 (depths 105.15–5.00 m) correlates to the Middle to lower Upper Cenomanian NC11* Zone in the Bralower et al. (1995) scheme as the interval from the FO of *Lithraphidites acutus* to the LO of *Axopodorhabdus albianus* (*A. biramiculatus*), which presents in the uppermost sample 108 (depth 5.00 m).

Borehole CT2

The calcareous nannoplankton assemblage identified in Borehole CT2 is fairly rich (practically the same as in Borehole CT8) and consists of more than 95 species (Appendixes A, C; Plates 4–8). However, nannofossils are quite rare at some levels. Preservation of nannofossils in the present samples ranges from poor to good, but on average is moderate throughout the sequence. Identification of specimens with the light microscope was not hampered by the diagenetic etching and overgrowth of calcite, which have evidently affected some of the assemblages.

No calcareous nannoplankton has been found in the lowermost part of the section (Isfiye Fm., samples 1–2) (Fig. 6).

Axopodorhabdus albianus Zone NC9, Upper Albian

NC9b Nannofossil Subzone, Upper Albian

Definition: The interval from the first occurrence (FO) of *Eiffellithus monechiae* to the FO of *Eiffellithus turriseiffelii*.

Authors: Bralower et al. (1993, 1995).

Remarks: The lower part of the Isfiye Fm. (samples 14–17) is referred to the Upper Albian Subzone NC9b, which lower boundary is defined by the FO of *Eiffellithus monechiae* (sample 15, depth 176.15 m) and upper boundary by the FO of *Eiffellithus turriseiffelii* (sample 18, depth 169.90 m). This subzone is characterized by the presence of *Axopodorhabdus biramiculatus* (= *A. albianus*), *Tranolithus orionatus*, *Eiffellithus casulus*, *E. monechiae* and abundant *Eprolithus floralis*. *Cyclogelosphaera margerelii*, *Gartnerago* sp., *Manivitella pemmatoidea*, *Nannoconus* spp., *Retecapsa angustiforata*, *Retecapsa crenulata*, *Watznaueria barnesae*, *W. biporta* and *W. fossassincta* appear from the lowest sample.

UC0 Nannofossil Zone, Upper Albian – Lower Cenomanian

Definition: The interval from the FO of *Eiffellithus turriseiffelii* to the FO of *Corollithion kennedyi*.

Author: Burnett (1998).

Remarks: Zone UC0 is equivalent to subzone NC10a of Bralower et al. (1993, 1995). This zone straddles the Lower/Upper Cretaceous boundary and is shared by two discrete biozonations. Burnett (1998) named it as a ‘special’ overlapping zone in her Upper Cretaceous scheme.

The succession of the lowest part of the Arqan Fm. (samples 18–44) belongs to this transitional zone; the FO of *E. turrisseiffelii* has been fixed in sample 18 (depth 169.90 m).

This zone corresponds to the foraminiferal *Parathalmanninella appenninica* Zone and lower part of *Th. globotruncanoides* Zone of the Lower Cenomanian.

UC1 Nannofossil Zone, Lower Cenomanian

Definition: The interval from the FO of *Corollithion kennedyi* to the FO of *Gartnerago segmentatum*.

Author: Burnett (1998).

Remarks: The interval of samples 45–50 (foraminiferal *Thalmanninella globotruncanoides* Zone, Lower Cenomanian) is assigned to this zone due to the presence of *Corollithion kennedyi*, which FO has been observed in sample 45 (depth 115.0 m). The FO of *C. kennedyi* is generally used for demarcating the basal Cenomanian (Ando et al., 2015). This level is above the first appearance of *Th. globotruncanoides* (depth 142.25 m). Such a stratigraphical pattern FOs of *Th. globotruncanoides* and *C. kennedyi* has been documented elsewhere (e.g., Robaszynski et al., 1993; Watkins et al., 2005; Ando et al., 2015).

UC1a Nannofossil Subzone, Lower Cenomanian

Definition: The interval from the FO of *Corollithion kennedyi* to the LO of *Watznaueria britannica*.

Author: Burnett (1998).

Remarks: The interval of samples 45–48 (depths 115.0–108.40 m) (foraminiferal *Thalmanninella globotruncanoides* Zone, Lower Cenomanian) belongs to Subzone UC1a due to the presence of *Watznaueria britannica*, which LO is recorded in sample 49 (depth 106.50 m).

UC1b–d Nannofossil subzones, Lower Cenomanian

Remarks: Subzones UC1b, UC1c and UC1d cannot be established because to the absence of stratigraphically important species *Gartnerago chiasta*, which LO marks the top of UC1b. Subzone UC1c is described as the interval from the LO of *G. chiasta* to the FO of rare and sporadic *Kamptnerius magnificus* or the FO of *Helicolithus anceps*. In our material *H. anceps* is absent, whereas rare and sporadic *Kamptnerius magnificus* has been recorded higher from sample 53 (depth 98.0 m).

UC2 Nannofossil Zone, Lower – basal Middle Cenomanian

Definition: The interval from the FO of *Gartnerago segmentatum* to the FO of *Lithraphidites acutus*.

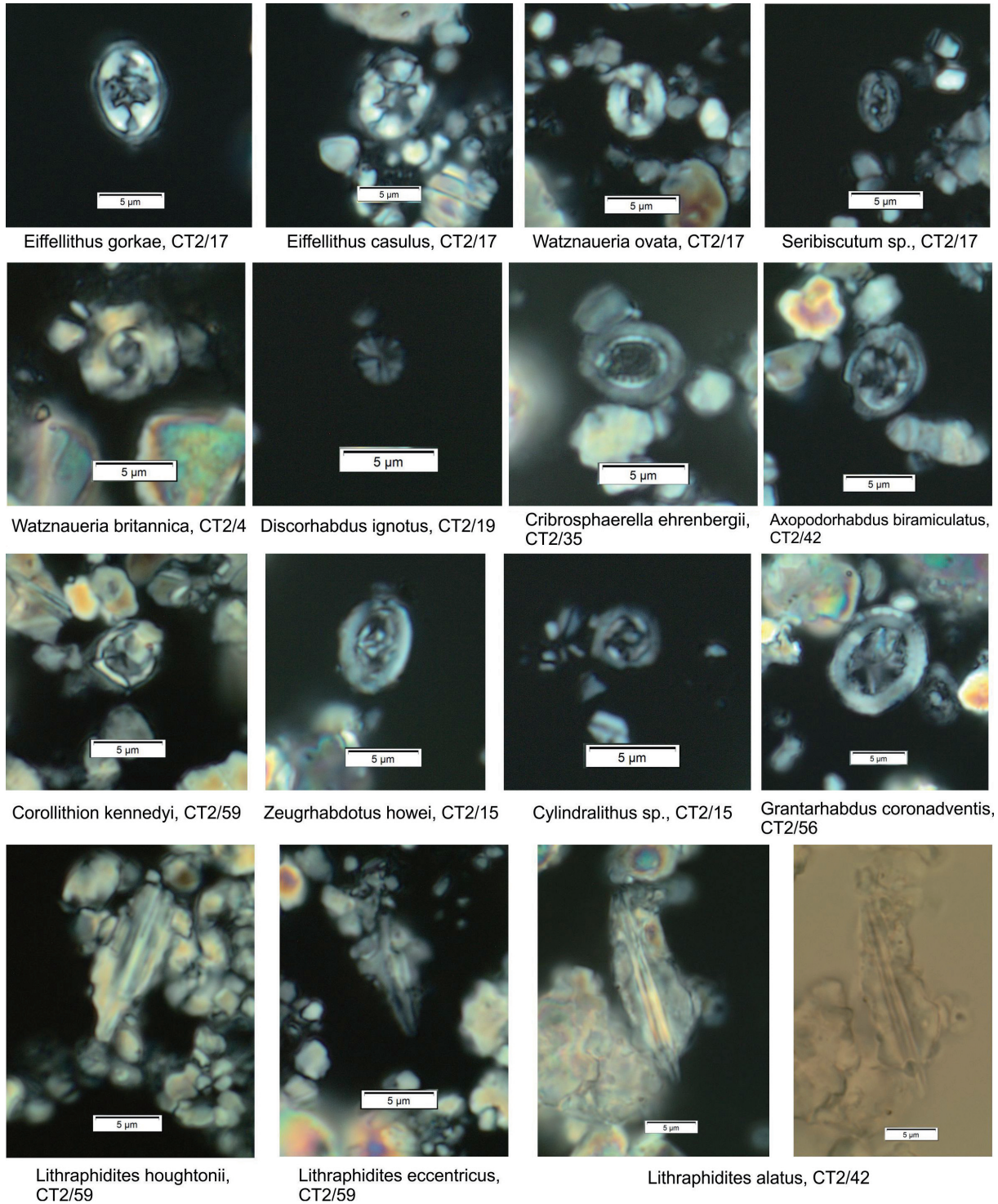
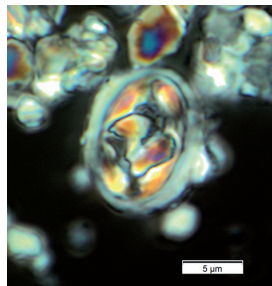


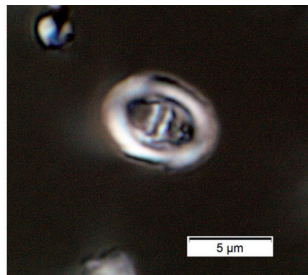
Plate 4. Calcareous nannofossils (LM images) from the Albian–Cenomanian from the Mount Carmel Region (borehole CT2).

Author: Burnett (1998).

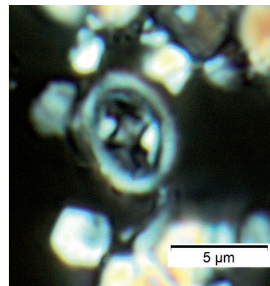
Remarks: The interval of samples 51–55 (uppermost foraminiferal *Thalmanninella globotruncanoides* Zone, Lower Cenomanian, and *Thalmanninella reicheli* Zone, Middle



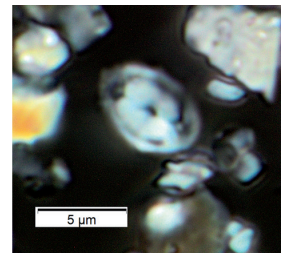
Zeugrhabdodus embergeri,
sample 28



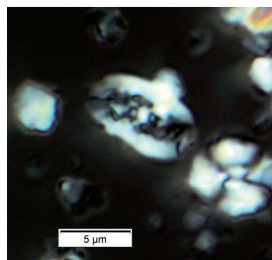
Zeugrhabdodus diplogrammus,
sample 54



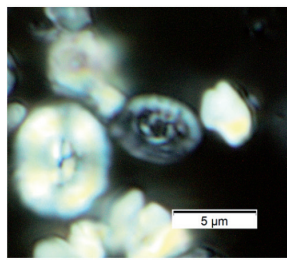
Zeugrhabdodus sp.,
sample 54



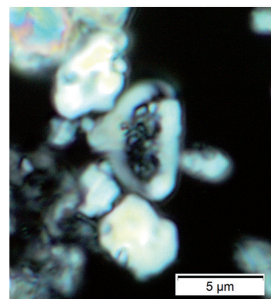
Tranolithus orionatus,
sample 54



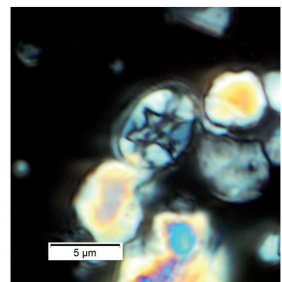
Rhagodiscus angustus,
sample 51



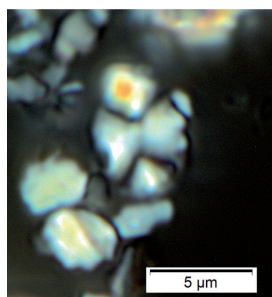
Rhagodiscus asper,
sample 45



Rhagodiscus reniformis,
sample 57



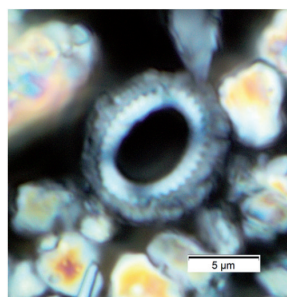
Eiffelithus turriseiffelli,
sample 59



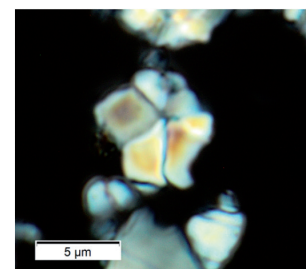
Watznaueria cf.
W. bayackii, sample 56



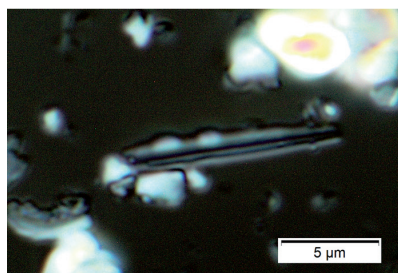
Retecapsa sp.,
sample 18



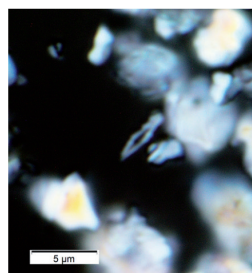
Manivitella pemmatoidea,
sample 45



Braarudosphaera sp.,
sample 59



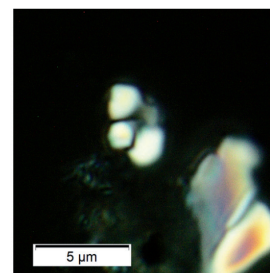
Lithraphidites carniolensis,
sample 50



Calciosolenia fossilis,
sample 45



Corollithion kennedyi,
sample 55



Calculites anfractus,
sample 45

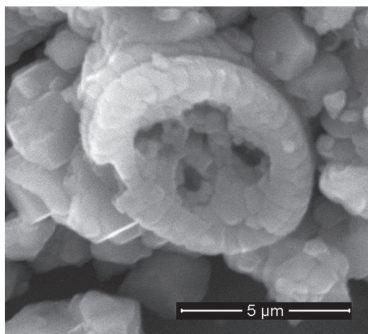
Plate 5. Calcareous nannofossils (LM images) from the Albian–Cenomanian from the Mount Carmel Region (borehole CT2).

Cenomanian) belongs to Zone UC2 due to the presence of *G. segmentatum*, which FO is recorded in sample 51 (depth 102.10 m).

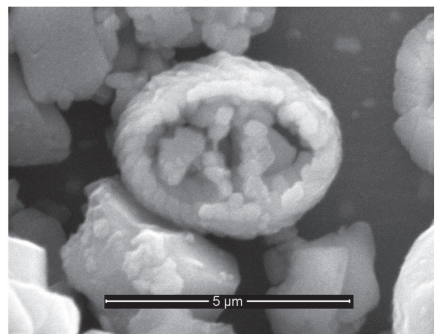
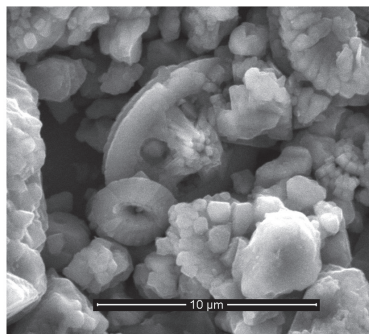
UC2a Nannofossil Subzone, Lower Cenomanian

Definition: The interval from the FO of *Gartnerago segmentatum* to the LO of *Zeugrhabdotus xenotus*.

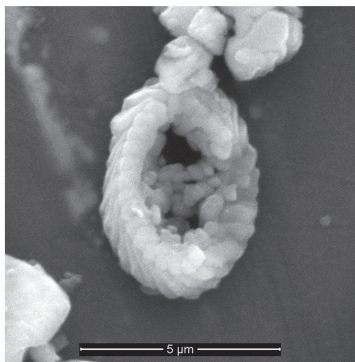
Author: Burnett (1998).



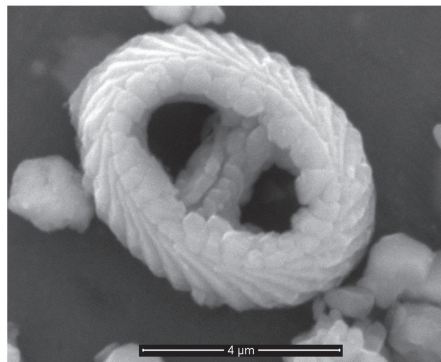
Axopodorhabdus biramiculatus, sample 44



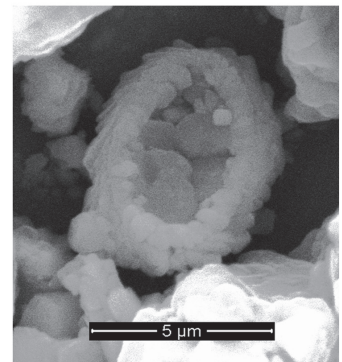
Zeugrhabdotus sp., sample 27



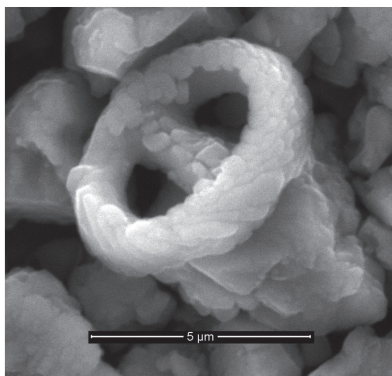
Zeugrhabdotus bicrescenticus, sample 31



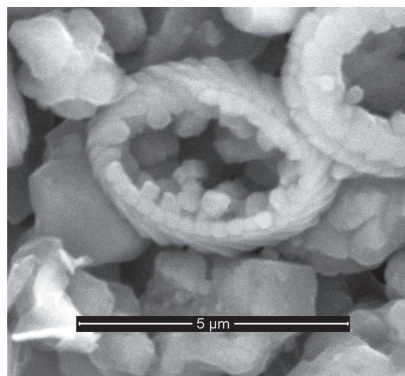
Zeugrhabdotus diplogrammus, sample 31



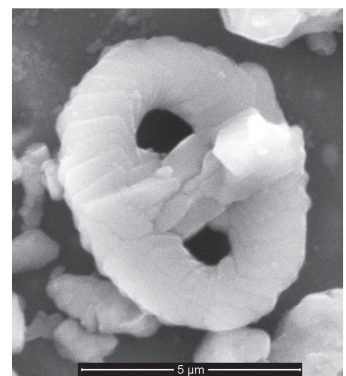
Zeugrhabdotus sp., sample 27



Zeugrhabdotus diplogrammus, sample 40



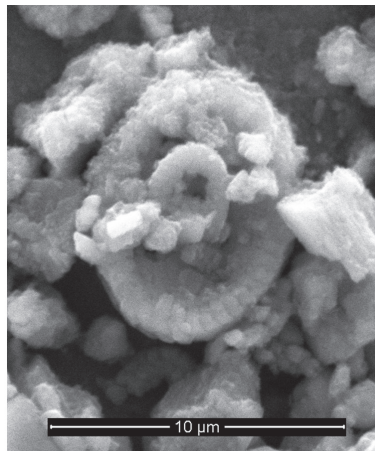
Tranolithus sp., sample 18



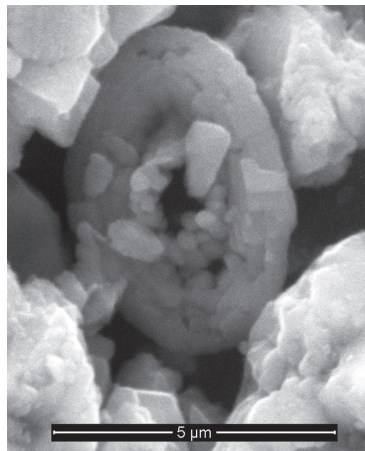
Zeugrhabdotus sp., sample 27

Plate 6. Calcareous nannofossils (SEM images) from the Albian–Cenomanian from the Mount Carmel Region (borehole CT2).

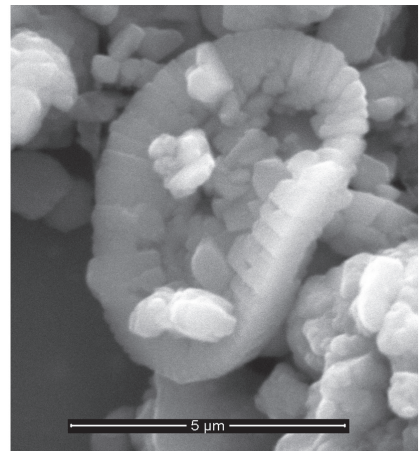
Remarks: The interval of samples 51–54 (depths 102.10–96.15 m) (foraminiferal *Thalmaninella globotruncanoides* Zone, Lower Cenomanian) belongs to this subzone due to the presence of *Z. xenotus*, which LO is recorded in sample 55 (depth 93.90 m).



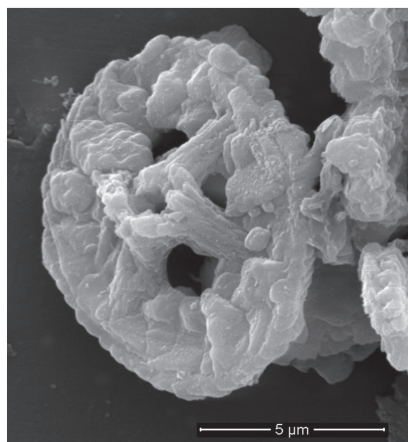
Rhagodiscus amplus, sample 15



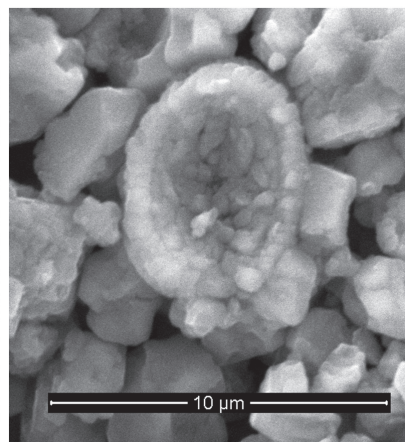
Rh. asper, sample 22



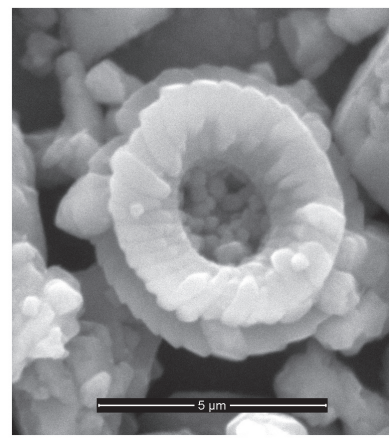
Rhagodiscus asper, sample 22



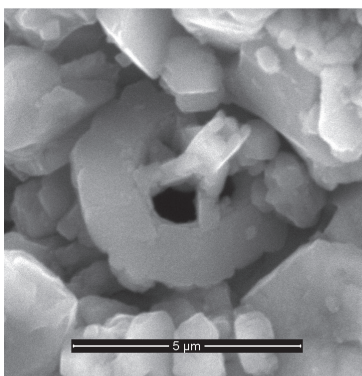
Eiffellithus turriseiffelli, sample 20



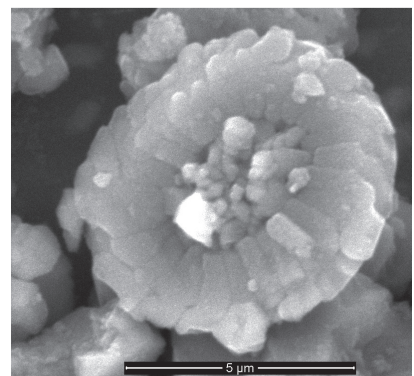
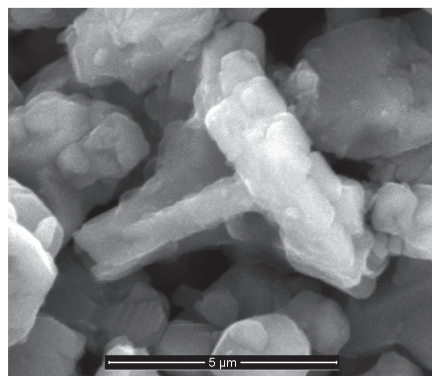
Broinsonia sp., sample 24



Retecapsa sp., sample 18

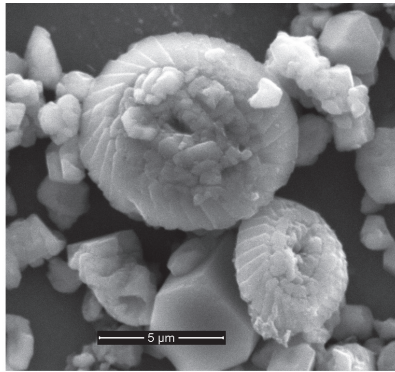


Prediscosphaera columnata, sample 33

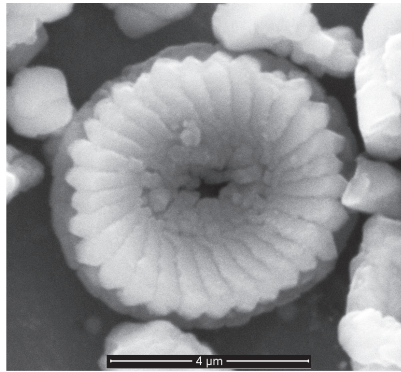


Retecapsa ficula, sample 33

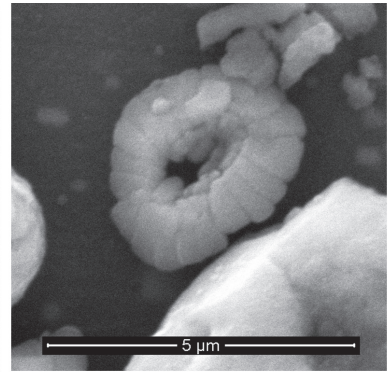
Plate 7. Calcareous nannofossils (SEM images) from the Albian–Cenomanian from the Mount Carmel Region (borehole CT2).



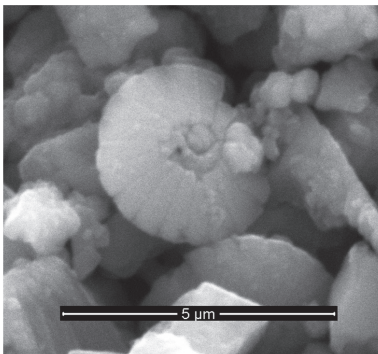
Watznaueria barnesiae, sample 36



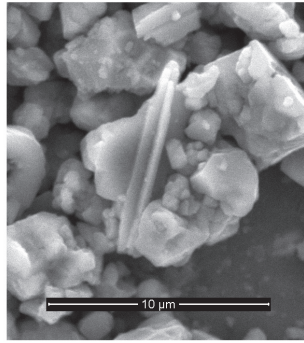
Watznaueria barnesiae, sample 36



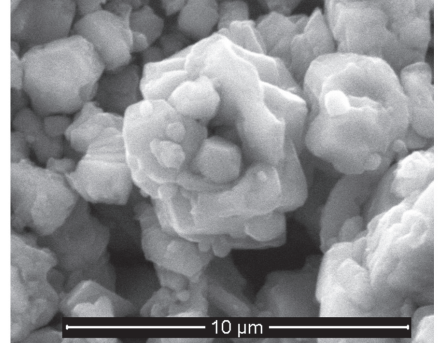
Biscutum constans, sample 45



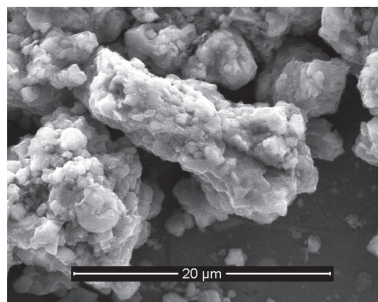
Discorhabdus ignotus, sample 25



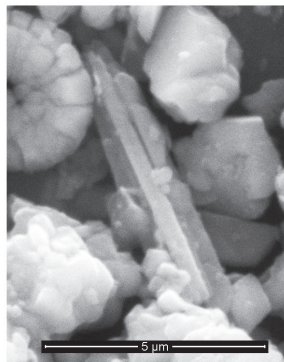
Lithraphidites acutus, sample 57



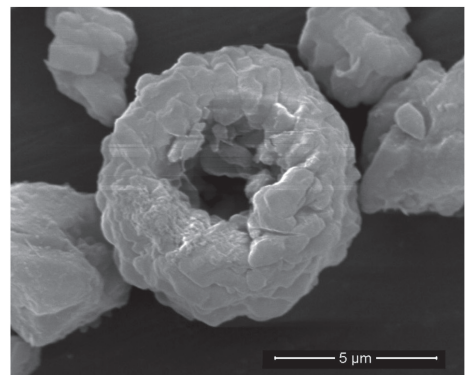
Eprolithus floralis, sample 25



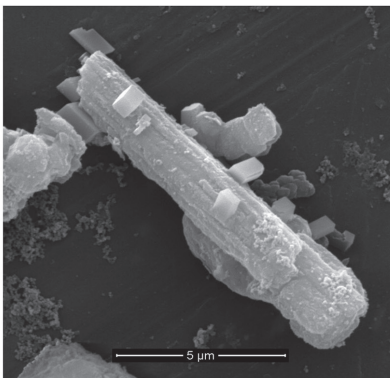
Lithraphidites cf. *L. eccentricus*, s. 65



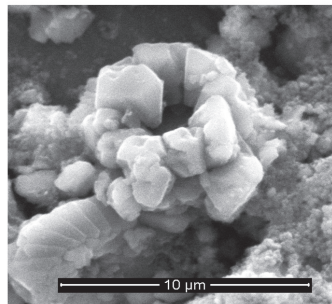
Lithraphidites carniolensis,
sample 25



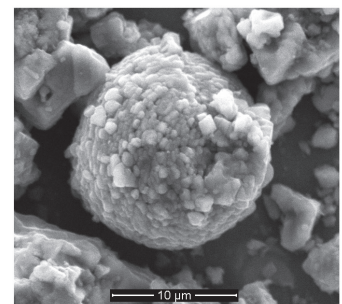
Cylindralithus sp., sample 48



Microrhabdulus decoratus, sample 86



Eprolithus floralis, sample 41



Thoracosphaera sp., sample 65

Plate 8. Calcareous nannofossils (SEM images) from the Albian–Cenomanian from the Mount Carmel Region (borehole CT2).

UC2b–c Nannofossil Subzones, Lower Cenomanian

Remarks: The level of sample 55 (depths 93.90 m) corresponds to undivided UC2b–c subzones; the marker species *Cylindralithus sculptus* has not been found.

UC3 Nannofossil Zone, basal Middle–Upper Cenomanian

Definition: The interval from the FO of *Lithraphidites acutus* to the FO of *Cylindralithus biarcus*.

Author: Burnett (1998).

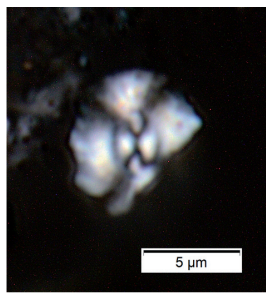
Remarks: The upper part of the borehole (samples 56–96) (foraminiferal zones: the uppermost part of *Thalmaninella reicheli* and *Rotalipora cushmani*, Middle–Upper Cenomanian) is referred to the transitional basal Middle–Upper Cenomanian Zone UC3 due to the presence of *Lithraphidites acutus*, which FO is recorded in sample 56 (depth 92.0 m). The species *Kamptnerius magnificus* (sample 53, depth 98.0 m) and *Lithraphidites eccentricus* (sample 62, depth 78.20 m) are found in this interval. Watkins and Bowdler (1984) described *L. eccentricus* from the Middle Cenomanian interval at DSDP Site 540 (Gulf of Mexico). Ando et al. (2015) suggested that the Early Cenomanian origin of *L. eccentricus* is better justified and the *L. eccentricus* type level cannot be as high as the Middle Cenomanian, which is supported by the position of the first appearance of *L. eccentricus* at the TDP Site 24 in Tanzania. Chin (2016) has recorded the FO of *L. eccentricus* below the FO of *C. kennedyi* in the Lower Cenomanian at DSDP 137 and 547 sites in the North Atlantic. In Borehole CT2 the FO of *L. eccentricus* was fixed higher, in the Middle Cenomanian. Another important species is *Microrhabdulus decoratus*, which according to Perch-Nielsen (1985) first appears together with *L. acutus* and has been reported as the index species for the Upper Cenomanian Zone CC10. In our material, the FO of *M. decoratus* has been recorded together with the FO of *L. acutus* in sample 56 (depth 92.0 m).

Negba 1

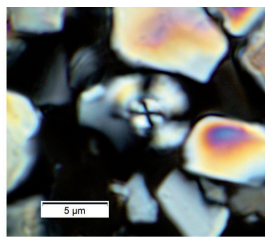
The calcareous nannofossil assemblage in the borehole is extremely impoverished and poorly to moderately preserved. The identified assemblage consists of 24 taxa (Appendixes A, D; Plate 9, Fig. 8).

Watznaueria barnesiae is the only species that occurs more or less consistently but as extremely rare specimens throughout the entire section. All other taxa are found in

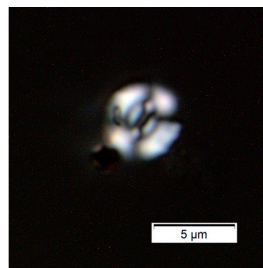
different parts of the section only as single specimens. *Nannoconus* sp. is found as isolated specimens in two samples from the lower part of the section (sample 2, depth 765 m) and in the upper part (sample 45, depth 256 m). *Zeugrhabdotus* sp., *Watznaueria ovata*, *Eiffelithus gorkae* and *Eiffelithus monechiae* are identified in the lower part of the borehole (Yagur Fm., samples 2–20, depths 765–530 m). In the middle part of the section (Lower member of Negba Fm., samples 20–33, depths 530–375 m), *Zeugrhabdotus bicrescenticus*, *Radiolithus orbiculatus*, *Eprolithus floralis*, *Cyclagelosphaera* sp., *Lithraphidites carniolensis* and *Biscutum constans* are found. In the upper part of the studied section (Upper member of Negba Fm., samples 33–50, depths 375–209 m), *Z. moulladei*, *Tranolithus* sp., *Tr. orionatus*, *Axopodorhabdus biramiculatus*,



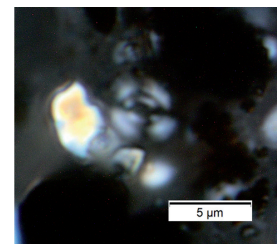
Watznaueria barnesiae,
sample 14



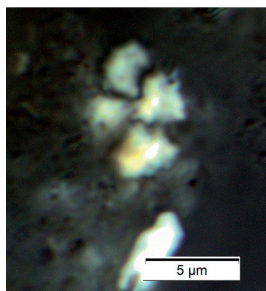
Watznaueria barnesiae,
sample 51



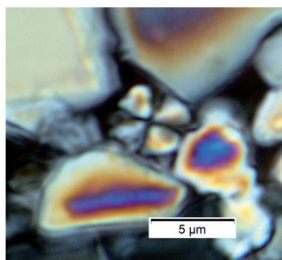
Watznaueria cf.
W. fossacincta, sample 14



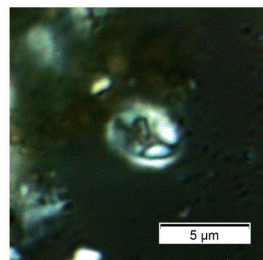
Watznaueria ovata,
sample 14



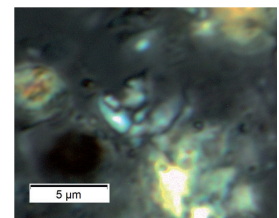
Watznaueria cf.
W. bayackii, sample 14



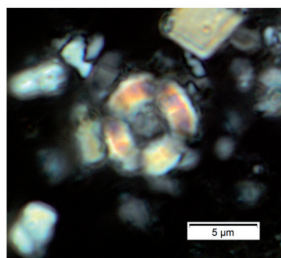
Cyclagelosphaera sp.,
sample 24



Eiffelithus cf.
E. gorkae, sample 1



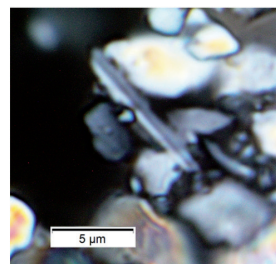
Eiffelithus cf.
E. monechiae, sample 14



Nannoconus sp., sample 2



Lithraphidites carniolensis,
sample 25



Calculites anfractus,
sample 50

Plate 9. Calcareous nannofossils (LM images) from the Albian–Cenomanian from the Coastal Plain (borehole Negba 1).

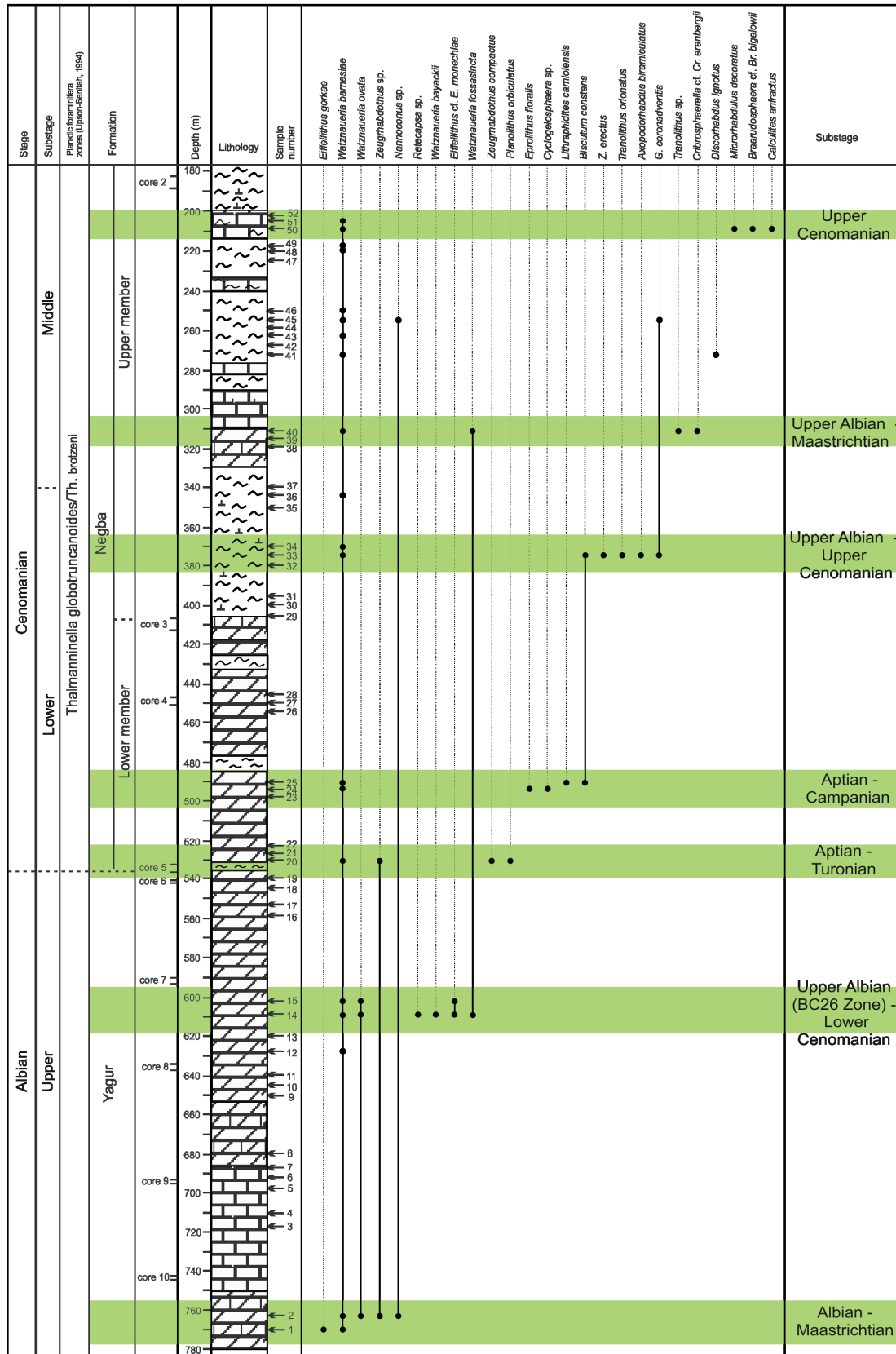


Figure 8. Lithology, vertical distribution of identified calcareous nannoplankton species with planktic foraminifera biostratigraphy from the Coastal Plain (borehole Negba 1).

Grantarhabdus coronadventis, *Watznaueria fossacincta*, *Cribrosphaerella ehrenbergii* and *Discorhabdus ignotus* are identified. In the uppermost part of the borehole (Upper member of Negba Fm., samples 50–52, depths 209–201 m) *Microrhabdulus decoratus*, *Braarudosphaera bigelowii* and *Calculites anfractus* were found.

Many recorded species are distributed in a wide stratigraphic interval: *Biscutum constans* (from the Bathonian (Middle Jurassic) to Late Maastrichtian (Upper Cretaceous), *Braarudosphaera bigelowii* (from the base of the Cenomanian to Recent), *Cribrosphaerella ehrenbergii* (from the Albian NC9a subzone to the Maastrichtian), *Eiffellithus gorkae* (from the Albian to the Maastrichtian), *Discorhabdus ignotus* (from the Oxfordian (Upper Jurassic) to the Maastrichtian (Upper Cretaceous), *Microrhabdulus decoratus* (from the Upper Cenomanian Zone CC10 to the Maastrichtian), *Lithraphidites carniolensis* (from the Lower Berriasian (Lower Cretaceous) to the Maastrichtian (Upper Cretaceous), *Tranolithus orionatus* (from the base of the Albian Zone BC24 to the Maastrichtian), species of *Watznaueria*: *W. barnesiae* (from the Bathonian (Middle Jurassic) to the Maastrichtian), *W. ovata* (from the Callovian (Middle Jurassic) to the Maastrichtian), *W. fossacincta* (from the Bajocian (Middle Jurassic) to the Maastrichtian), *Zeugrhabdotus bicrescenticus* (from the base of the Albian to the Maastrichtian), *Zeugrhabdotus moulladei* (from the base of the Hauterivian (Lower Cretaceous) to the Campanian (Upper Cretaceous).

Species with a narrow stratigraphic distribution are also found: *Axopodorhabdus biramiculatus* (from the Albian BC25 zone to the Cenomanian UC5a subzone), *E. monechiae* (from the Upper Albian BC26 zone to the Lower Cenomanian), *C. anfractus* (from the Albian UC0 / BC27 zone to the Cenomanian UC3b subzone), *E. floralis* (from the base of the Aptian to the Campanian), *Gr. coronadventis* (from the base of the Aptian to the Campanian) and *R. orbiculatus* (from the base of the Aptian to the Turonian).

Since nanofossils are very rare and found in small quantities, it is quite difficult to apply the standart biostratigraphical zonal scheme of Sissingh (1977) with additions of Perch-Nielsen (1985) in full. However, despite the impoverished assemblage, it is still possible to distinguish certain levels and intervals.

The assemblage of the lowermost samples (samples 1–2) consists of species predominantly with a wide stratigraphic distribution, but the sediments cannot be older than the Albian because of the presense of *E. gorkae*.

The interval of samples of 14 and 15 (depths 610–605 m) is confined to the Upper Albian (BC26 Zone) to the Lower Cenomanian based on the presence of *E. monechiae*.

Sample 20 yields the assemblage with *R. orbiculatus*, which first appearance is known to be at the base of the Aptian and last appearance is recorded in the Turonian. Thus, the level of depth 530 m belongs in the interval from the Aptian to Turonian.

The interval of samples of 24–25 consists of the assemblage with *E. floralis* (basal Aptian – Campanian). The co-occurrence of *B. constans*, *Lithraphidites carniolensis*, *Cyclogelosphaera* sp. and *E. floralis* indicates that the deposits (depths 495–490 m) belong to the Aptian–Campanian.

Sample 33 (depth 375 m) yields an assemblage consisting of species with both wide distribution and narrow stratigraphical distribution: *A. biramiculatus* (from the Albian BC25 zone to the Cenomanian UC5a subzone) and *Gr. coronadventis* (from the base of the Aptian to the Campanian). The occurrence of all identified species together in the sample indicates that this level belongs to the Upper Albian to Upper Cenomanian.

Sample 40 (depth 311 m) brings an assemblage with *Tranolithus* sp., *W. fossacincta* and *Cr. ehrenbergii*, which are all distributed in a broad stratigraphical interval. The occurrence these species together indicates that these deposits belong to the Upper Albian – Maastrichtian.

The assemblage of the uppermost sample 50 (depth 209 m) consists of *Microrhabdulus decoratus*, *C. anfractus* and *Br. bigelowii*. The first and second species have a narrow stratigraphical distribution. *Braarudosphaera bigelowii* has a wide stratigraphical distribution but the first appearance of this species was recorded at the base of the Cenomanian. *Microrhabdulus decoratus* is an important zonal marker for the Upper Cenomanian Zone CC10 in Perch-Nielsen (1985) zonation. *Calculites anfractus* is also a zonal marker that defines the base of the Upper Albian subzone UC0c. The last appearance of this species was fixed in the Upper Cenomanian UC3b subzone. The occurrence of these species together is indicating that the deposits at the belong to the Upper Cenomanian.

4.2. Calcareous nannoplankton preservation and abundance

Carmel Area

In our material from the Carmel Region (boreholes CT2 and CT8), calcareous nan-

nofossils are moderately preserved and quite abundant in general, with only a few samples containing poor assemblages or being barren.

In our material, *Watznaueria* is a dominant genus and one of the most resistant to dissolution among Mesozoic calcareous nannofossils (e.g., Thierstein, 1980; Lees et al., 2005). Cretaceous nannofloras with a low species diversity and abundant *W. barnesiae* were considered as poorly-preserved (Lees et al., 2005), and assemblages with *W. barnesiae* exceeding 40% were thought to be diagenetically affected to such an extent that they no longer bear an original palaeoecological signal (Thierstein, 1980; Roth & Bowdler, 1981; Roth, 1984; Roth & Krumbach, 1986; Herrle et al., 2003). However, Williams and Bralower (1995) proposed that a high ratio of *W. barnesiae* is indicative of the assemblage alteration when it reaches higher values (70%). Erba (1992) documented original features preserved in nannofossil assemblages with relative abundance of *W. barnesiae* >40% and suggested that this taxon is typically oceanic and dominant under oligotrophic conditions.

Borehole CT8

In the studied samples of the CT8 core, despite the predominance of *W. barnesiae*, dissolution sensitive taxa (e.g., *B. constans*, *D. ignotus*, *Zeugrhabdotus moulladei* and small *Zeugrhabdotus*) are present and generally common (Figs. 9 and 12). In addition, the abundance or the dissolution-prone taxa is not controlled by the preservation index (Fig. 11). Also, the stable Shannon index (H) (1.8–2.85) indicates a low assemblage alteration. Therefore, we conclude that the abundance of *W. barnesiae* preserves the original palaeoenvironmental signal related to oligotrophy (Mutterlose et al. 2005).

Nannofossil abundance shows relatively high fluctuations, with an average of six specimens per field of view (Fig. 11). The highest values (up to 27 nannofossils/field of view) are recorded in the middle part of the Arqan Fm., which corresponds to the Lower – lower Middle Cenomanian.

In all analysed samples (Figs. 9, 10; Appendix B), the dominant genus is *Watznaueria* (average 64.2%), whereas the genera *Zeugrhabdotus* (avg. 8.5%) and *Biscutum* (avg. 8.0%) exceed 5% of the assemblage (Fig. 9), followed by *Retecapsa/Cretarhabdus* (avg. 2.8%), *Eiffellithus* (avg. 2.5%) and *Tranolithus* (avg. 2.0%), *Prediscosphaera* spp. (1.8%), *Discorhabdus ignotus* (1.4%), *Lithraphidites* spp. (1.3%), *Rhagodiscus* spp. (1.0%), *Manivitella pemmatoidea* (0.9%), *Axopodorhabdus biramiculatus* (0.8%) and

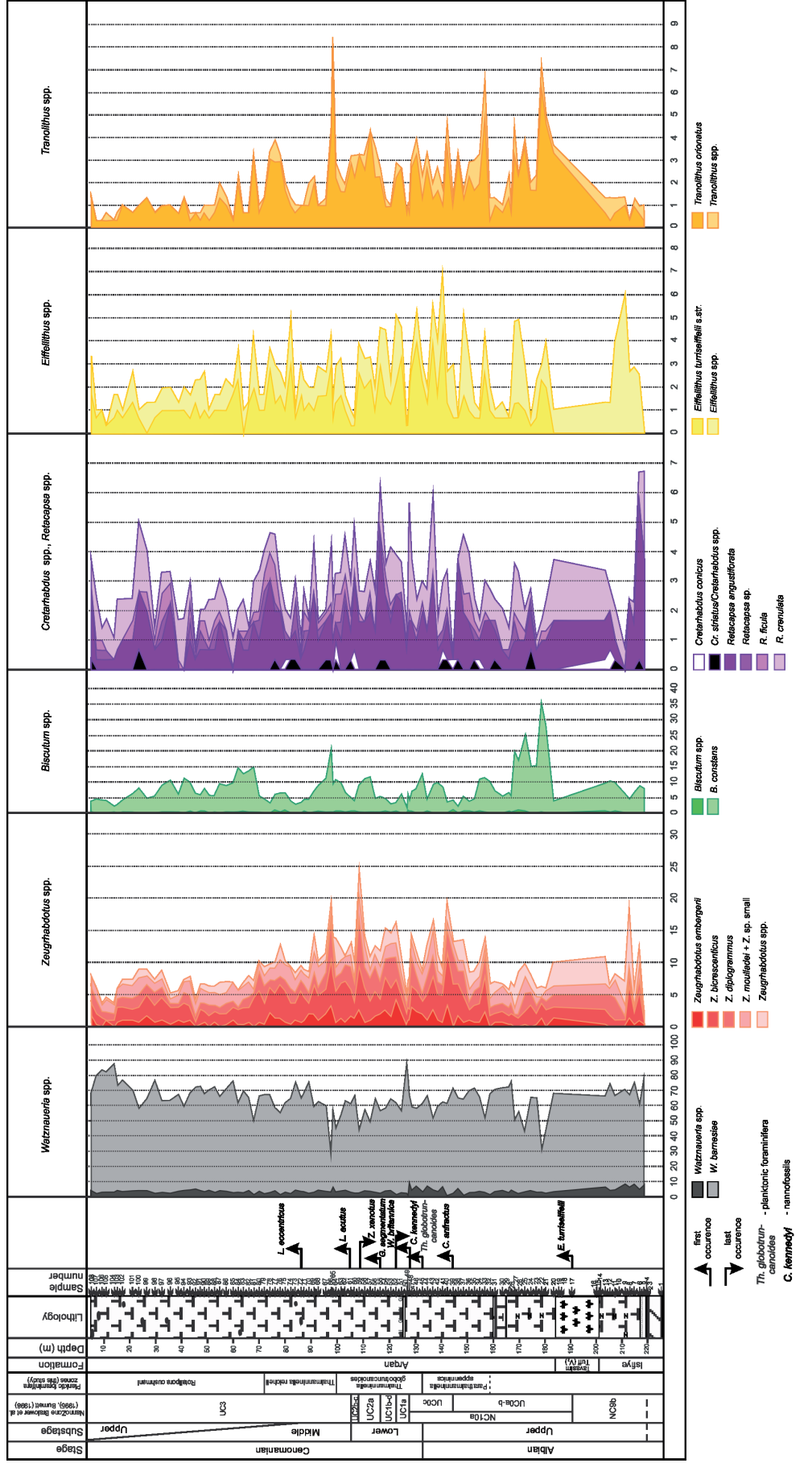


Figure 9. Vertical distribution of relative abundances of dominant and subdominant nannofossil taxa from borehole CT8 (Carmel Region, NW Israel).

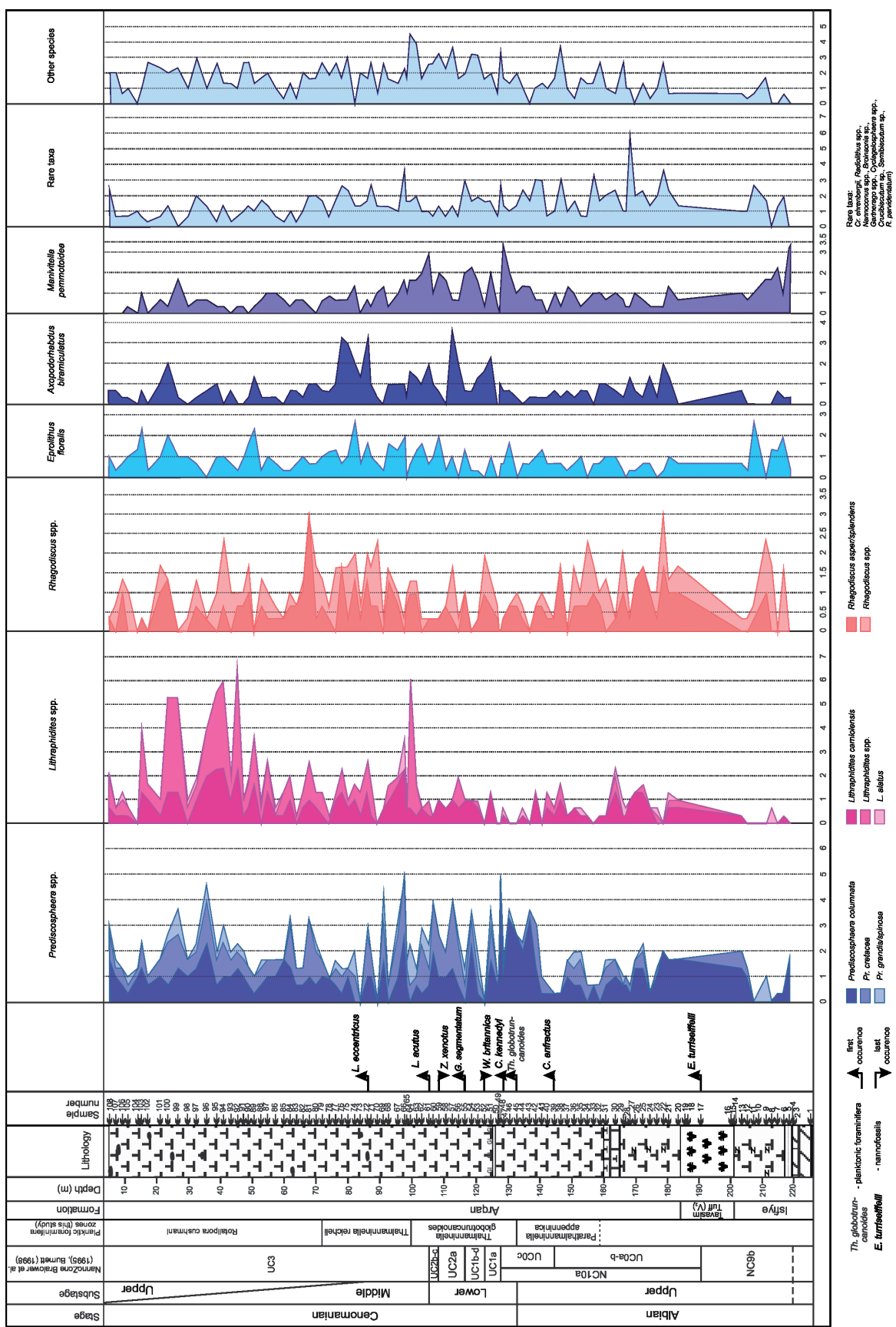


Figure 10. Vertical distribution of relative abundances (<2%) of selected nanofossil taxa from borehole CT8 (Carmel Region).

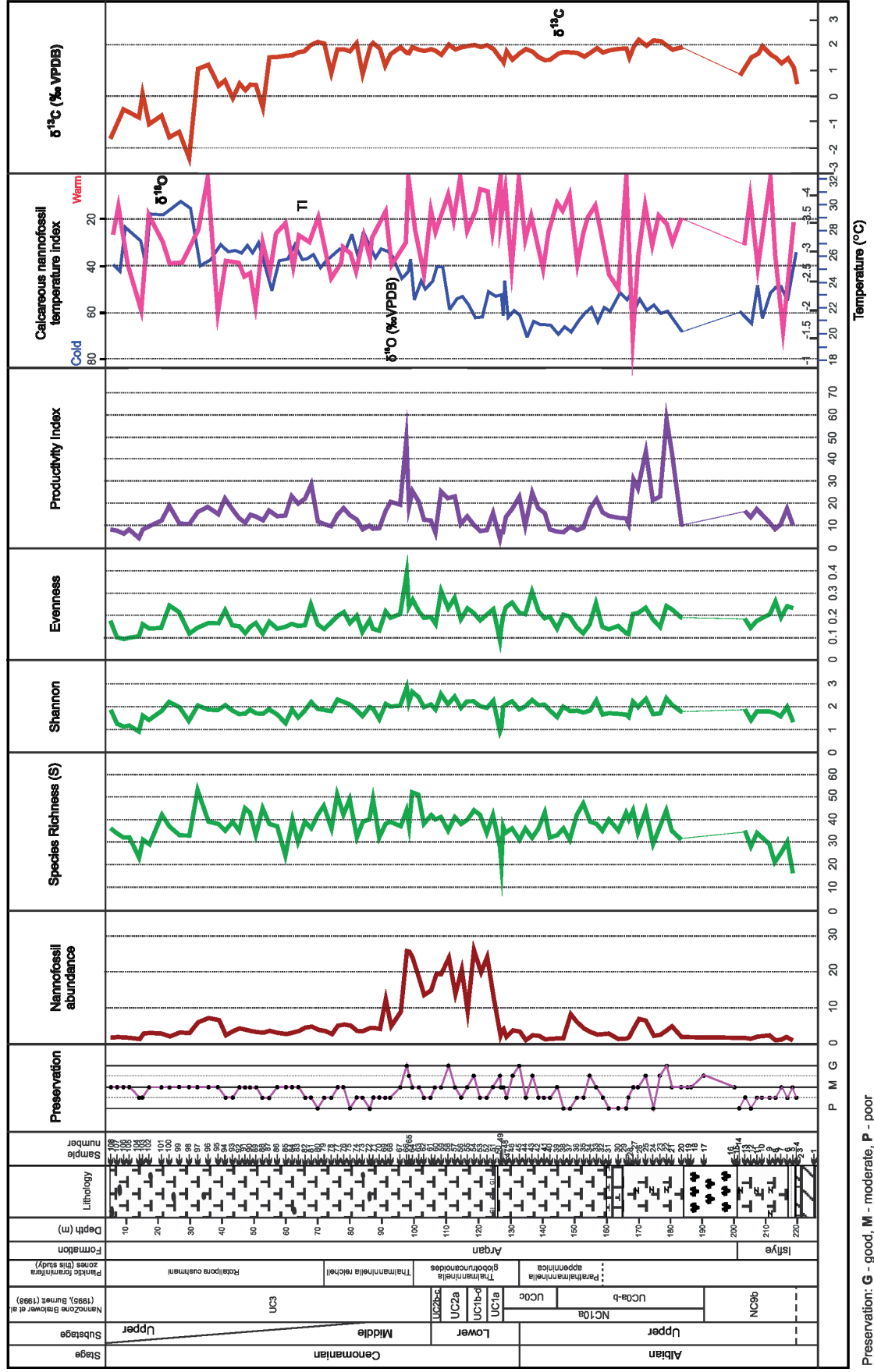


Figure 11. Preservation, vertical distribution of relative nannofossil abundance, Species Richness, Shannon Diversity Index, Evenness, calcareous nannofossil Nutrient and Temperature Indices, carbon and oxygen isotope data from borehole CT8.

Eprolithus floralis (0.8%). Taxa with an average relative abundance <0.5% are grouped as “Rare taxa” (Fig. 10, Appendix E): these include *Cribrosphaerella ehrenbergii* (0.4%), *Radiolithus* spp. (0.3%), *Nannoconus* spp. (0.2%), *Broinsonia/Gartnerago* (0.2%), *Cyclagelosphaera* spp. (0.2%) and *Crucibiscutum* sp./*Seribiscutum* sp./*Repagulum parvidentatum* (0.2%). Very rare species (average relative abundance 0.1–0.5%) are treated as “Other taxa” (1.6%) (Appendix E).

Watznaueria is by far the most common genus (min. 27.1%, max. 87.0%) throughout the CT8 core. The genus is dominated by *W. barnesiae* (avg. 60.6%) (Fig. 9); other six species (*W. britannica*, *W. biporta*, *W. ovata*, *W. fossacincta*, *W. cf. W. bayackii*, *W. manivittiae*) occur rarely throughout the entire succession.

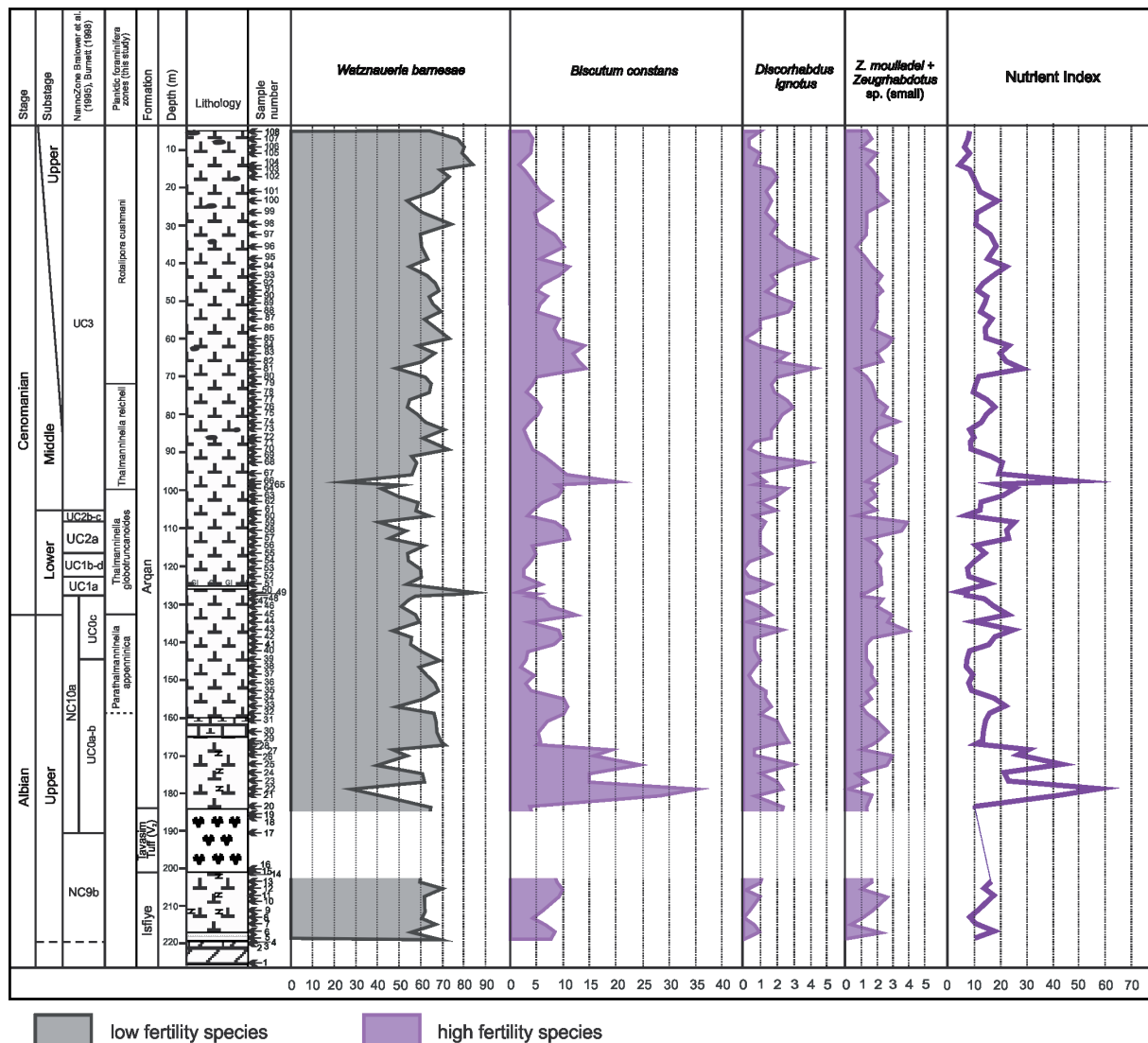


Figure 12. Vertical distribution of relative abundances of calcareous nannofossil productivity indicators, calcareous nannofossil Nutrient and Temperature Indices from bore-hole CT8 (Carmel Region, NW Israel).

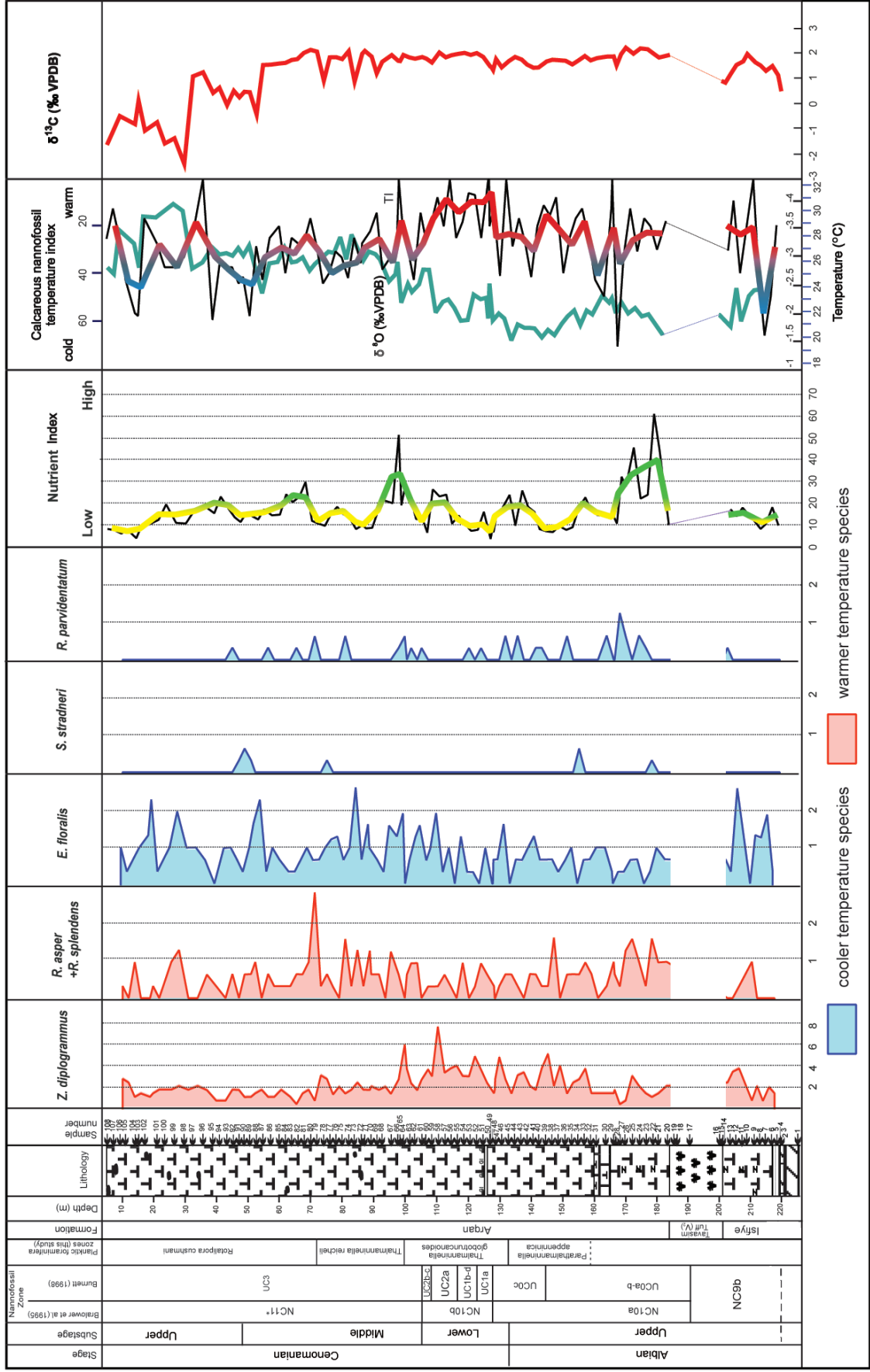


Figure 13. Vertical distribution of relative abundances of calcareous nannofossil temperature indicators, calcareous nannofossil Nutrient and Temperature Indices, oxygen and carbon isotopes data in the borehole CT8 (Carmel region, NW Israel).

The genus *Zeugrhabdotus* (min. 1.7%, max. 21.7%) (Fig. 9) is represented by *Z. diplogrammus*, *Z. bicrescenticus* (common), *Z. embergeri*, *Z. scutula*, *Z. moulladei* (frequent), *Z. howei*, *Z. noeliae*, *Z. clarus*, *Z. xenotus*, and small *Zeugrhabdotus* sp. (rare).

The genus *Biscutum* (avg. 8.0%) (Fig. 9) shows sharp fluctuations from 1.3–35.4% and is represented by abundant *B. constans* (avg. 7.7%) (Fig. 9), with rare *B. thurowii* and *Biscutum* sp.).

The *Retecapsa/Cretarhabdus* group (avg. 2.8%) (Fig. 9) includes *C. conicus*, *C. striatus*, *Cretarhabdus* sp., *R. angustiforata*, *R. sp.*, *R. ficula*, and *R. crenulata*.

The genus *Eiffellithus* (avg. 2.5%) (Fig. 9) is represented by *E. casulus*, *E. gorkae*, *E. hancockii*, *E. monechiae*, and *E. turriseiffelii*.

The genus *Tranolithus* was observed throughout the entire succession (avg. 2.0%) (Fig. 9) and is represented by *T. orionatus* (most abundant, avg. 1.7%) and *T. gabalus*.

The genus *Prediscosphaera* (avg. 1.8%) (Fig. 10) is represented by *P. columnata*, *P. cretacea* (common), *P. grandis* (rare), and *P. spinosa* (very rare).

The genus *Discorhabdus* (Fig. 12) is represented by a single species, *D. ignotus* (0.3–4.2%, avg. 1.4%), which occurs throughout the section.

The genus *Lithraphidites* (0–6.5%, avg. 1.3%) (Fig. 10) is represented by *L. carniolensis*, *L. alatus*, *L. acutus*, *L. eccentricus*, *L. houghtonii*, and *Lithraphidites* sp.

The genus *Rhagodiscus* (0–3%, avg. 1.0%) (Figs. 10 and 13) is represented by *Rh. asper*, *Rh. splendens*, *Rh. achlyostaurion*, *Rh. amphus*, *Rh. angustus*, *Rh. sageri*, and *Rhagodiscus* sp.

The fluctuations of the species richness, Shannon Index, and Evenness throughout the studied interval are summarised in Fig. 11. The species richness (S) is low/moderate (mean 37) and varies from 16 to 53 species per sample; it is often used as a measure of a relative stability of ecological conditions (Sanders, 1968; Dodd & Stanton, 1981; Watkins, 1989). The Shannon diversity Index (H) is moderate (mean 1.8) and varies from 1.8–2.85. Evenness (E) varies from 0.09–0.39 with an average of 0.19.

Pearson's correlation coefficients calculated for the selected nannofossil taxa are summarized in Table 3. *Watznaueria barnesiae* shows the highest negative correlation with *B. constans*, *Z. bicrescenticus*, *T. orionatus* and *E. turriseiffelii*. There is a strong negative correlation between *W. barnesiae* and the group of *Cretarhabdus* spp./*Retecapsa* spp., *Z. diplogrammus*, *Z. embergeri*, *L. carniolensis* and *Rh. asper*+*Rh.*

Table 3. Pearson's correlation matrix of selected calcareous nannofossil taxa from the borehole CT8. Significant coefficients (p<0.01) are in bold.

	<i>W. barnesiae</i>	<i>B. constans</i>	<i>Watznaueria</i> spp.	<i>Z. bicrescenticus</i>	<i>Cretarhabdus</i> spp./ <i>Retecapsa</i> spp.	<i>Z. diplogrammus</i>	<i>Z. moulladei + Zeugrhabdotus</i> spp. (small)	<i>T. orionatus</i>	<i>E. turriseiffelii</i>	<i>Z. embergeri</i>	<i>P. columnata</i>	<i>E. floralis</i>	<i>Lithraphidites</i> spp.	<i>P. cretacea</i>	<i>L. carniolensis</i>	<i>R. asper/R. splendens</i>
<i>W. barnesiae</i>																
<i>B. constans</i>	-0.660															
<i>Watznaueria</i> spp.	-0.063	-0.070														
<i>Z. bicrescenticus</i>	-0.027	-0.124	0.113													
<i>Cretarhabdus</i> spp./ <i>Retecapsa</i> spp.	-0.501	-0.027	-0.124	0.213												
<i>Z. diplogrammus</i>	-0.306	-0.087	0.113	0.213	0.240											
<i>Z. moulladei + Zeugrhabdotus</i> spp. (small)	-0.354	-0.093	-0.056	0.581	0.240	0.193										
<i>T. orionatus</i>	-0.113	-0.094	-0.115	0.123	-0.029	0.193	-0.053									
<i>E. turriseiffelii</i>	-0.689	0.469	-0.109	0.416	0.141	0.319	-0.053									
<i>Z. embergeri</i>	-0.302	0.033	0.173	0.202	0.137	0.053	0.146	0.053								
<i>P. columnata</i>	-0.195	-0.510	-0.144	0.198	-0.086	0.130	-0.185	-0.094	0.182							
<i>E. floralis</i>	-0.260	-0.149	-0.086	0.235	-0.083	0.130	-0.122	-0.157	0.088	0.087						
<i>Lithraphidites</i> spp.	-0.063	-0.292	-0.149	0.138	-0.160	0.107	-0.100	-0.093	0.078	0.087	0.088					
<i>P. cretacea</i>	-0.149	-0.086	0.110	0.142	0.078	0.134	0.170	-0.122	-0.068	0.138	0.223	0.276				
<i>L. carniolensis</i>	-0.315	-0.146	-0.111	0.123	-0.020	-0.022	0.125	0.087	-0.078	0.405	0.093	0.000	0.058	0.238	0.554	0.549
<i>R. asper/R. splendens</i>	-0.307	0.328	-0.203	0.032	-0.186	-0.222	0.058	0.317	0.037	0.362	0.225	-0.103	-0.161	0.002	0.120	0.057

Significant coefficients (P<0.01) are in bold

splendens. *Biscutum constans* has a positive correlation with *T. orionatus* and *Rh. asper+Rh. splendens*. There are positive correlations between *Z. bicrescenticus* and *Z. diplogrammus*, *Z. embergeri*, *T. orionatus* and *E. turriseiffelii*. Positively correlated are the following pairs: *Z. moulladei+Zeugrhabdotus* sp. (small) and *E. turriseiffelii*; *D. ignotus* and *Lithraphidites* spp.; *P. columnata* and *E. turriseiffelii*; and *Lithraphidites* spp.+*P. cretacea* and *L. carniolensis*.

Three significant factors were extracted from the varimax rotation factor analysis, representing 47.24% of the total variance (Table 4).

The PC1 (21.22% of total variance) shows the highest positive loadings for *Z. bicrescenticus*, *T. orionatus*, *E. turriseiffelii*, *Z. embergeri*, *Z. diplogrammus* and *Cretarhabdus* spp./*Retecapsa* spp., and a negative loading for *W. barnesiae*. The associated species *P. cretacea* shows a positive loading, while *Rh. asper+Rh. splendens* and *Lithraphidites* spp. (weakly associated species) present negative loadings. *Zeugrhabdotus moulladei+Zeugrhabdotus* sp. (small) show low positive loadings (associated species).

The PC2 (15.16% of total variance) shows high positive loadings for *D. ignotus*, *E. floralis* and *P. cretacea*, *L. carniolensis*, *Lithraphidites* spp. and, as associated taxa, *Z. moulladei+Zeugrhabdotus* sp. (small). Weakly associated taxa *Zeugrhabdotus* spp. and *Watznaueria* spp. demonstrate low negative loadings.

The PC3 (10.86% of total variance) shows high positive loadings for *B. constans*, *D. ignotus* (associated taxa), and a negative loading for *W. barnesiae*. Associated taxa

Table 4. Factor analysis Varimax normalized Rotation with principal component Extraction based on 18 taxa from borehole CT8, Carmel region. Rotation is R-mode.

	Factor 1	Factor 2	Factor 3
<i>Watznaueria barnesiae</i>	-0.60	-0.19	-0.69
<i>Biscutum constans</i>	-0.02	-0.05	0.85
<i>Watznaueria</i> spp.	0.02	-0.24	-0.16
<i>Zeughrabdotus bicrescenticus</i>	0.72	0.21	0.08
<i>Cretarhabdus</i> spp./ <i>Retacapsa</i> spp.	0.54	-0.07	-0.12
<i>Zeughrabdotus diplogrammus</i>	0.78	0.02	-0.16
<i>Zeughrabdotus moulladei</i> + <i>Zeughrabdotus</i> sp. (small)	0.26	0.29	-0.10
<i>Tranolithus orionatus</i>	0.50	-0.09	0.68
<i>Zeughrabdotus</i> spp.	0.29	-0.26	0.10
<i>Discorhabdus ignotus</i>	-0.26	0.62	0.35
<i>Eiffellithus turriseiffelii</i>	0.56	0.15	0.33
<i>Zeughrabdotus embergerii</i>	0.80	-0.03	-0.03
<i>Prediscosphaera columnata</i>	0.30	-0.08	0.14
<i>Eprolithus floralis</i>	0.15	0.51	-0.19
<i>Lithraphidites</i> spp.	-0.25	0.69	0.01
<i>Prediscosphaera cretacea</i>	0.24	0.66	0.04
<i>Lithraphidites carniolensis</i>	0.02	0.79	0.16
<i>Rhagodiscus asper</i> / <i>Rhagodiscus splendens</i>	-0.20	0.18	0.67
Total Variance percent	21.22	15.16	10.86

Factor Loadings (Varimax normalized) (18 taxa)

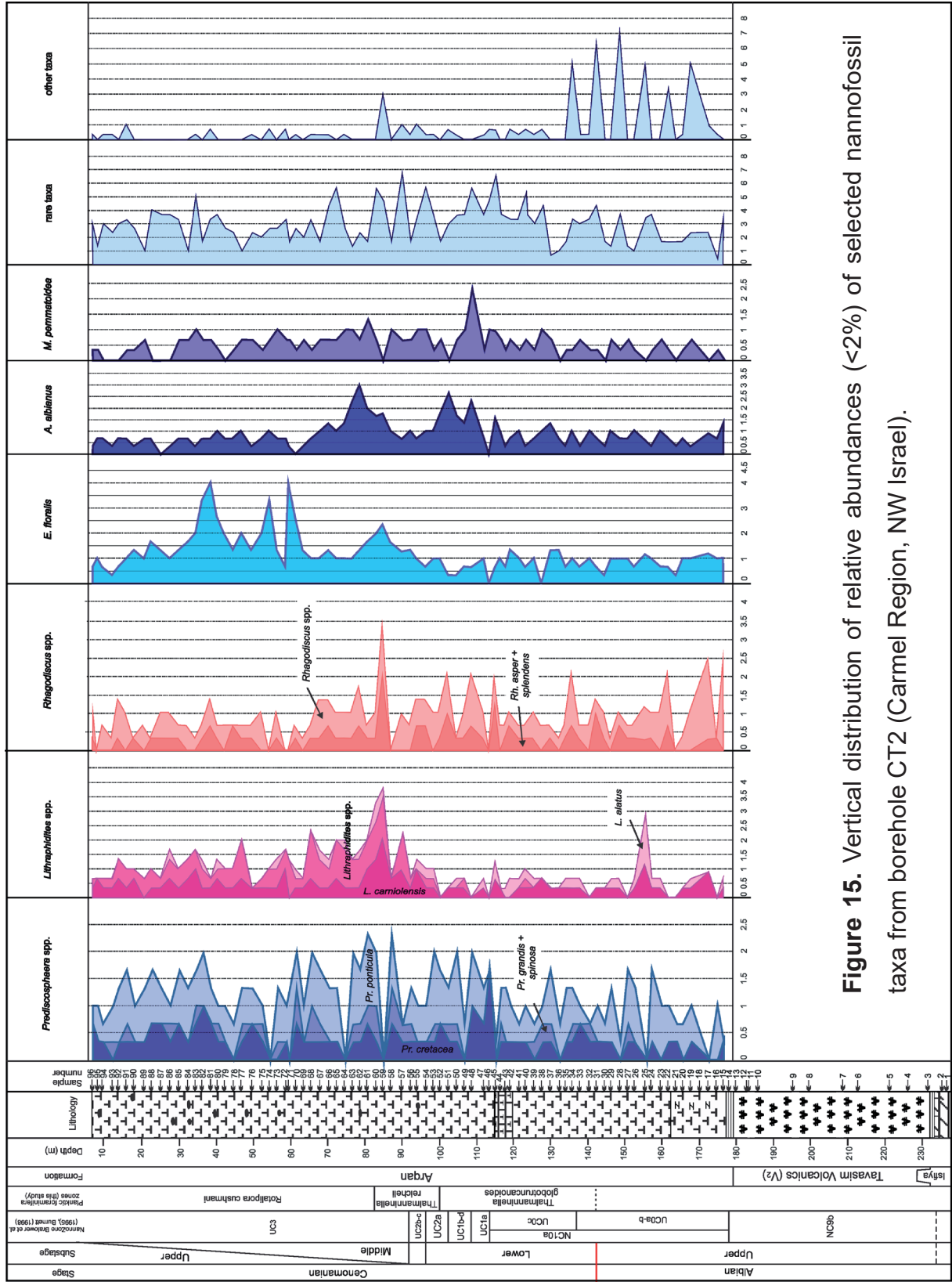
0.67	dominant taxa
0.33	associated and

T. orionatus, *Rh. asper*+*Rh. splendens* and *E. turriseiffelii* demonstrate high positive loadings.

Borehole CT2

In the analysed material from borehole CT2, despite the predominance of *W. barnesiae*, dissolution sensitive taxa (e.g., *B. constans*, *D. ignotus*, *Zeughrabdotus moulladei* and small *Zeughrabdotus*) are present and generally common (Figs. 14 and 17). In addition, the abundance or the dissolution-prone taxa is not controlled by the preservation index (Fig. 16). Also, the stable Shannon index (H) (1.2–2.68) indicates a low assemblage alteration. Therefore, we conclude that the abundance of *W. barnesiae* preserves the original palaeoenvironmental signal related to oligotrophy (Mutterlose et al. 2005).

Nannofossil abundance shows relatively high fluctuations, with an average of six specimens per field of view (Fig. 16). The highest values (up to 18 nannofossils/field of view) are recorded in the middle part of the Arqan Fm., which corresponds to the Lower – lower Middle Cenomanian.



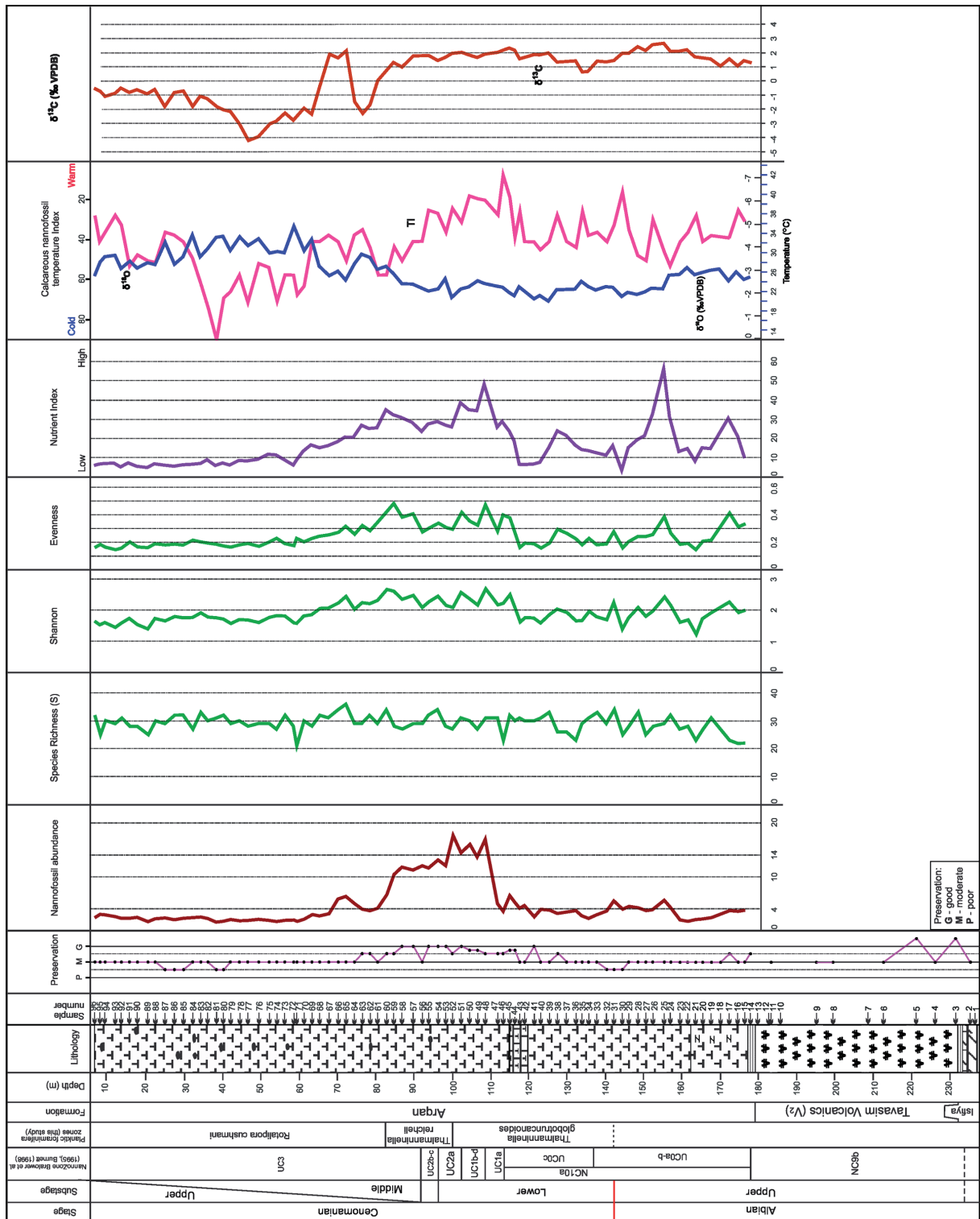


Figure 16. Preservation, vertical distribution of relative nanofossil abundance, Species Richness, Shannon Diversity Index, Evenness, calcareous nanofossil Nutrient and Temperature Indices, carbon and oxygen isotope data from borehole CT2 (Carmel Region, NW Israel).

Discorhabdus ignotus (1.1%), *Lithraphidites* spp. (1.0%), *Rhagodiscus* spp. (0.9%), *Axopodorhabdus biramiculatus* (0.9%) and *Manivitella pemmatoidea* (0.5%). Taxa with an average relative abundance <0.5% are grouped as “Rare taxa” (2.8 %) (Fig. 15, Appendix E): these include *Cribrosphaerella* spp. (0.4%), *Broinsonia/Gartnerago* (0.4%), *Helicolithus* spp. (0.3%), *Chistozygus* spp. (0.3%), *Radiolithus* spp. (0.3%), *Gorkaea operio* (0.2%), *Cyclagelosphaera* spp. (0.2%), *Crucibiscutum* sp./*Seribiscutum* sp./*Repagulum parvidentatum* (0.2%), *Nannoconus* spp. (0.1%) and *Grantarhabdus coronadventis* (0.1%). Very rare species (average relative abundance <0.1%) are treated as “Other taxa” (0.5%) (Appendix E).

The genus *Watznaueria* is by far the commonest element (min. 33.2%, max. 80.0%) throughout the CT2 core. The genus is dominated by *W. barnesiae* (avg. 55.5%) (Fig. 14), other six species (*W. britannica*, *W. biporta*, *W. ovata*, *W. fossacincta*, *W. cf. W. bayackii*, and *W. manivitiae*) occur rarely throughout the entire succession.

The genus *Zeugrhabdotus* (min. 5.6%, max. 26.6%) (Fig. 14) is represented by *Z. diplogrammus*, *Z. bicrescenticus* (common), *Z. embergeri*, *Z. scutula*, *Z. moulladei* (frequent), *Z. howei*, *Z. noeliae*, *Z. clarus*, *Z. xenotus*, small *Zeugrhabdotus* sp. (rare) and *Zeugrhabdotus* sp.

The genus *Biscutum* (avg. 4.7%) (Fig. 14) shows sharp fluctuations from 1.0–20.0% and is represented by abundant *B. constans* (avg. 4.3%), with rare *B. thurowii*.

The *Retecapsa/Cretarhabdus* group (avg. 3.7%) (Fig. 14) shows fluctuations from 0.7–6.2% and includes *C. conicus*, *R. angustiforata*, *R. fenestrata*, *R. ficula*, and *R. crenulata*.

The genus *Eiffellithus* (avg. 2.5%) (Fig. 14) with fluctuations from 0.7–5.3% is represented by *E. casulus*, *E. gorkae*, *E. monechiae*, and *E. turriseiffelii*.

The genus *Tranolithus* was observed throughout the entire succession (avg. 2.4%, min. 0.7%, max. 7.7%) (Fig. 14) and is represented by *T. orionatus* (most abundant, avg. 2.0%) and *T. gabalus*.

The genus *Prediscosphaera* (0–4.9%, avg. 2.2%) (Fig. 15) is represented by *P. columnata*, *P. ponticula*, *P. cretacea* (common), *P. grandis* (rare), and *P. spinosa* (very rare).

The genus *Discorhabdus* (Fig. 17) is represented by a single species, *D. ignotus* (0–4.0%, avg. 1.1%), which occurs practically throughout the entire section.

The genus *Lithraphidites* (0–3.8%, avg. 1.0%) (Fig. 15) is represented by *L. carniolensis*, *L. alatus*, *L. acutus*, *L. eccentricus*, and *L. houghtonii*.

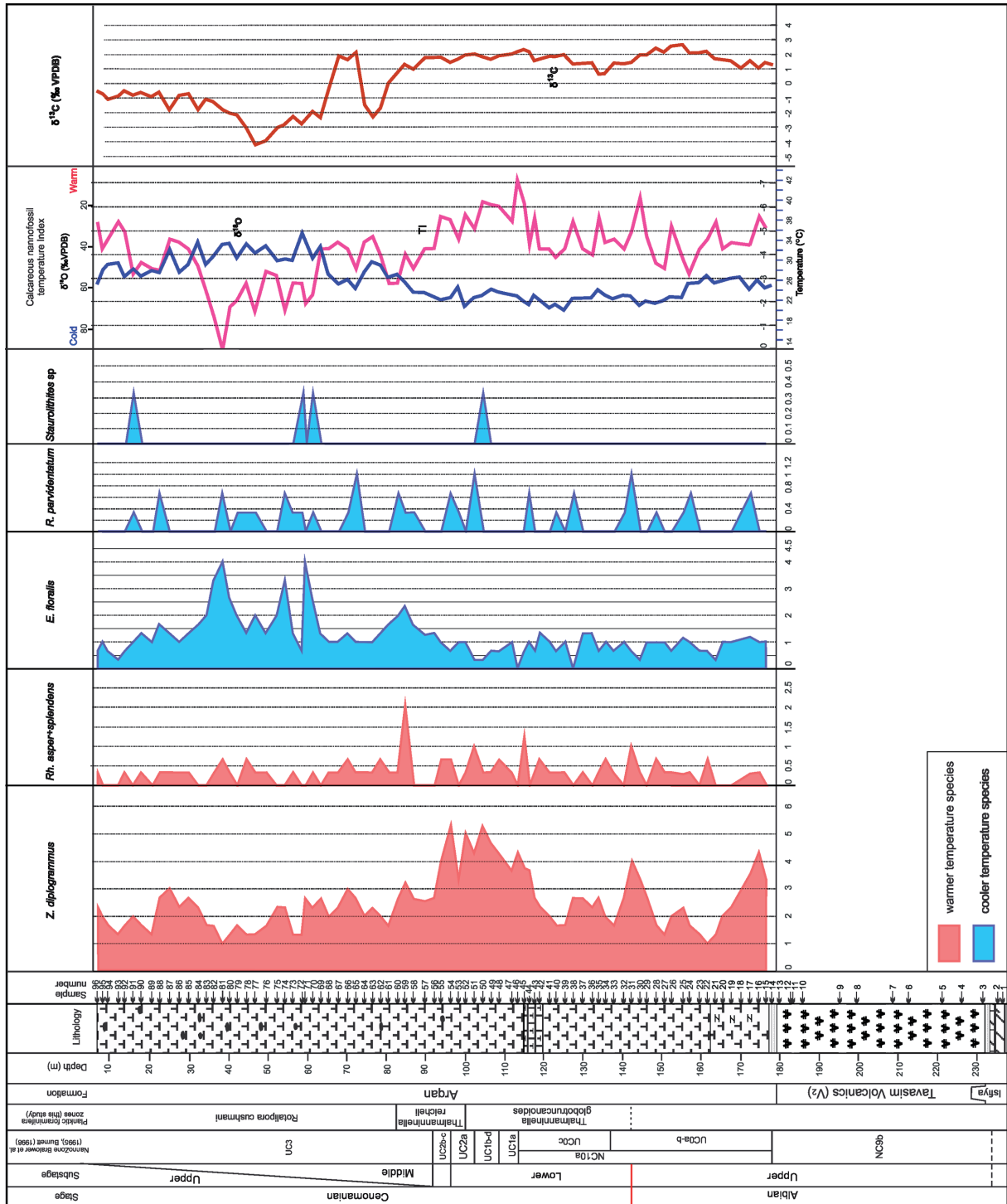


Figure 18. Vertical distribution of relative abundances of calcareous nannofossil temperature indicators, calcareous nannofossil Nutrient and Temperature Indices, oxygen and carbon isotopes data in the borehole CT2 (Carmel region, NW Israel).

The genus *Rhagodiscus* (0–3.2%, avg. 0.9%) (Figs. 15, 18) is represented by *Rh. asper*, *Rh. splendens*, *Rh. achlyostaurion*, *Rh. amphus*, *Rh. angustus*, *Rh. sageri*, and *Rh. reniformis*.

The fluctuations of the species richness, Shannon Index, and Evenness throughout the studied interval are summarised in Fig. 16. The species richness (S) is low/moderate (mean 29.1) and varies from 21 to 36 species per sample; it is often used as a measure of a relative stability of ecological conditions (Sanders, 1968; Dodd & Stanton, 1981; Watkins, 1989). The Shannon diversity Index (H) is moderate (mean 1.92) and varies from 1.2–2.68. Evenness (E) varies from 0.14–0.48 with an average of 0.25.

Pearson's correlation coefficients calculated for the selected nannofossil taxa are summarized in Table 5. *Watznaueria barnesiae* shows the highest negative correlation with *Z. moulladei*+*Zeugrhabdotus* sp. (small), *B. constans*, *Z. bicrescenticus*, *Z. diplogrammus*, *Zeugrhabdotus* spp., *D. ignotus* and *Pr. columnata*. There is a strong negative correlation between *W. barnesiae* with *Eiffellithus* spp., *E. turriseiffelii*, *L. carniolensis* and *Rh. asper*+*Rh. splendens*. The group of *Z. moulladei*+*Zeugrhabdotus* sp. (small) shows the highest positive correlation with *Biscutum constans*, *Z. bicrescenticus*, *Z. diplogrammus* and *D. ignotus*. There is a strong positive correlation between *Z. moulladei*+*Zeugrhabdotus* sp. (small) with *T. orionatus*, *Zeugrhabdotus* spp. and *Pr. columnata*. *Biscutum constans* has a highest positive correlation with *D. ignotus* and a strong positive correlation with *Z. bicrescenticus* and *Z. diplogrammus*. *Biscutum constans* has a high positive correlation with *D. ignotus* and shows a strong positive correlation with *Z. bicrescenticus* and *Z. diplogrammus*. There is a strong negative correlation between *Biscutum constans* with *Watznaueria* spp. The group of *Cretarhabdus* spp./*Retecapsa* spp. has a strong positive correlation with *Watznaueria* spp. There is a highest positive correlation between *Z. bicrescenticus* with *Z. diplogrammus* and *Z. moulladei*+*Zeugrhabdotus* sp. (small). *Zeugrhabdotus bicrescenticus* shows a strong positive correlation with *Biscutum constans*, *T. orionatus*, *Zeugrhabdotus* spp. and *Eiffellithus* spp. *Zeugrhabdotus bicrescenticus* has a strong negative correlation with *E. floralis*. There is a strong positive correlation between *Z. diplogrammus* and *Zeugrhabdotus* spp. and *Eiffellithus* spp. *Zeugrhabdotus* spp. has a strong positive correlation with *T. orionatus*, *D. ignotus* and *Eiffellithus* spp. *Tranolithus orionatus* shows a strong positive correlation with *Eiffellithus* spp. and *Pr. columnata*. *Eiffellithus turriseiffelii* has

a positive correlation with *D. ignotus*, *Pr. columnata*, *L. carniolensis*, *Lithraphidites* spp. and *Rh. asper*+*Rh. splendens*. *D. ignotus* positively correlated with *Pr. columnata* and *L. carniolensis*. *Prediscosphaera columnata* shows positive correlation with *L. carniolensis* and *Rh. asper*+*Rh. splendens*. Positively correlated are the following pairs: *E. floralis* and *Lithraphidites* spp., and *L. carniolensis* with *Lithraphidites* spp.

Three significant factors were extracted from the varimax rotation factor analysis, representing 57.75% of the total variance (Table 6).

The PC1 (31.52% of total variance) shows the highest positive loadings for *Z. bi-crescenticus*, *T. orionatus*, *Zeugrhabdotus* spp., *Eiffellithus* spp., and a negative loading for *W. barnesiae*. The associated species of the group of *Zeugrhabdotus moulladei*+*Zeugrhabdotus* sp. (small) and *Rh. asper*+*Rh. splendens* show a positive loadings, while *E. floralis* (weakly associated species) presents a negative loading.

Table 6. Factor analysis Varimax normalized Rotation with principal component Extraction based on 17 taxa from borehole CT2, Carmel region. Rotation is R-mode.

	Factor 1	Factor 2	Factor 3
<i>Watznaueria barnesiae</i>	-0.59	-0.11	-0.75
<i>Watznaueria</i> spp.	0.03	0.70	-0.23
<i>Zeugrhabdotus moulladei</i> + <i>Zeugrhabdotus</i> sp.(small)	0.36	-0.23	0.76
<i>Biscutum constans</i>	0.12	-0.39	0.81
<i>Cretrhabdus</i> spp./ <i>Retecapsa</i> spp.	0.04	0.46	0.08
<i>Zeugrhabdotus compactus</i>	0.70	-0.37	0.30
<i>Zeugrhabdotus diplogrammus</i>	0.66	-0.24	0.32
<i>Tranolithus orionatus</i>	0.68	-0.19	0.11
<i>Zeugrhabdotus</i> spp.	0.78	0.08	0.14
<i>Eiffellithus</i> spp.	0.74	0.12	0.03
<i>Eprolithus floralis</i>	-0.26	0.51	-0.09
<i>Eiffellithus turriseiffeli</i>	-0.02	0.40	0.59
<i>Discorhabdus ignotus</i>	0.18	0.07	0.81
<i>Prediscosphaera columnata</i>	0.28	0.39	0.50
<i>Lithraphidites carniolensis</i>	0.01	0.62	0.47
<i>Lithraphidites</i> spp.	-0.16	0.75	0.06
<i>Rhagodiscus asper</i> / <i>Rhagodiscus splendens</i>	0.35	0.31	0.32
Total Variance percent	31.52	17.28	8.95

Factor Loadings (Varimax normalized) (17 taxa)

0.78 dominant taxa

0.66

0.47 associated taxa

The PC2 (17.28% of total variance) shows high positive loadings for *Lithraphidites* spp., *Watznaueria* spp., *L. carniolensis* and *E. floralis*. The associated taxa of the group of *Cretarhabdus* spp./*Retecapsa* spp., *E. turriseiffelii*, *Pr. columnata*, *Rh. asper*+*Rh. splendens* have positive loadings, while *B. constans* and *Z. bicrescenticus* show negative loadings. Weakly associated taxa *Z. diplogrammus* and *Zeugrhabdotus moulladei*+*Zeugrhabdotus* sp. (small) demonstrate low negative loadings.

The PC3 (8.95% of total variance) shows highest positive loadings for *B. constans*, *Zeugrhabdotus moulladei*+*Zeugrhabdotus* sp. (small), *D. ignotus*, high positive loadings for *E. turriseiffelii* and *Pr. columnata*, while *W. barnesiae* demonstrates the highest negative loading. The associated taxa *Z. bicrescenticus*, *Z. diplogrammus*, *L. carniolensis* and *Rh. asper*+*Rh. splendens* show positive loadings.

4.3. Calcareous nannoplankton Temperature (TI) and Nutrient (NI) indices

Borehole CT8

Of the three factors extracted from the factor analysis, PC3 represents surface water fertility, since oligotrophic species *W. barnesiae* shows opposite loadings with respect to mesotrophic taxa *B. constans* and *D. ignotus* (Table 4, Fig. 12). On the contrary, the positive and negative loadings of the assemblages, given by PC1 and PC2, cannot be related to temperature. This probably depends on the relatively low abundances of species indicative of temperatures (*Z. diplogrammus*, *Rh. asper*, *E. floralis*, *R. parvidentatum*, and *Staurolithites* spp.), which together constitute ca. 3.6% of the total assemblage being a negligible part of the variability in the whole dataset (Fig. 13). However, although the 'temperature' species are scarce in the section, they show minor fluctuations that are independent from the total abundance variations, and may reflect a primary signal (see Discussion).

The NI is generally low (mean 15.52) and varies from 3.8–57.57 with rapid fluctuations throughout the succession (Figs. 11–13), therefore a relatively suppressed fertility is reconstructed for the studied interval with minor occasional increases as evidenced by NI values above 20 (detected around 180–170, 140–130, 110–90 and 70–60 m). The TI (mean 29.75) shows rapid fluctuations in the interval of 0–83.33 m (Figs. 11–13) pointing to generally warm temperatures, with the lowest values (warmest conditions) displayed

between 120–110 m (Lower Cenomanian). Some decrease in paleotemperatures is estimated from ca. 100 m upwards, where the TI is shifted towards higher values. This phase corresponds to a minor decrease in abundance of *Z. diplogrammus* and a relative increase in *E. floralis*. Cooler interludes (highest TI values) are detected at ca. 215 m and 170 m (Upper Albian).

Borehole CT2

Of the three factors extracted from the factor analysis, PC1 relates to temperature, since warm-water species *Z. diplogrammus* and *Rh. asper/Rh. splendens* show opposite loadings with respect to cold-water *E. floralis* (Table 6, Fig. 18). The ‘temperature’ species are scarce in the section, they show minor fluctuations that are independent from the total abundance variations, and may reflect a primary signal (see Discussion). On the contrary, positive and negative loadings of the assemblages, given by PC2, cannot be clearly related to temperature. PC2 demonstrates opposite loadings of cold-temperature *E. floralis* with respect to warm-temperature *Z. diplogrammus*, however cold-temperature *E. floralis* also positively correlates with warm-temperature *Rh. asper/Rh. splendens*. PC3 represents surface water fertility, since oligotrophic species *W. barnesiae* shows opposite loadings compared to mesotrophic taxa *B. constans* *Zeugrhabdotus moulladei*+*Zeugrhabdotus* sp. (small) and *D. ignotus* (Table 6, Fig. 17).

The NI is generally low (mean 17.0) and varies from 3.6–56.2 with rapid fluctuations throughout the succession (Figs. 16, 17), therefore a relatively suppressed fertility is reconstructed for the studied interval with minor occasional increases as evidenced by NI values above 20 (detected in 174–172, 157–150, 130–127 and 115–72 m intervals). The TI (mean 34.3) shows rapid fluctuations in the interval of 0–82.4 m (Figs. 16, 18) pointing to generally warm temperatures, with the lowest values (warmest conditions) displayed between 146–142 m and 108–98 m (Lower Cenomanian). Some decrease in palaeotemperatures is estimated from ca. 92 m upwards, where the TI is shifted towards higher values. This phase corresponds to a minor decrease in abundance of *Z. diplogrammus* and a relative increase in *E. floralis*. Cooler interludes (highest TI values) are detected at ca. 38 m (Middle Cenomanian).

4.4 Stable isotope analyses

Borehole CT8 (Table 7)

The oxygen isotope profile shows remarkable positive and negative fluctuations throughout the succession (Fig. 11), with two trends: one (below the tuff deposits) reflecting a gradual decrease of the oxygen values, and the other (above the tuff deposits) showing increasing values.

In the Isfiye Fm., a positive shift of ca. +1.06‰ [-2.97 to -1.91‰] is presented below the tuffaceous deposits. Directly above the tuffaceous deposits (samples 20 to 30), a negative shift of ca. -0.68‰ [-1.58 to -2.26‰] is observed. In the interval of samples 31–44, the values of oxygen are practically constant [-1.93 to -1.46‰]. A negative $\delta^{18}\text{O}$ shift of ca. -1.4‰ [-1.85 to -3.25‰] is identified in the interval of samples 45–75. The interval corresponding to samples 76 to 96 is characterised by constant values of $\delta^{18}\text{O}$. A positive $\delta^{18}\text{O}$ anomaly of ca. +0.81‰ [-3.11 to -2.30‰] marks samples 62–54.7 m. In the upper part of the section (samples 98–108), a positive shift of ca. +0.94‰ [-3.70 to -2.76‰] is identified.

The $\delta^{13}\text{C}$ value changes from 0.47–2.00‰ in the Isfiye Fm. below the tuff (Figs. 11, 13). Above the tuffaceous layer, the lower and middle parts of the Arqan Fm. (samples 20–68) are characterised by almost constant $\delta^{13}\text{C}$ values (1.88–1.64‰) with minor fluctuations that include a relative decrease from ca. 2‰ at 180–170 m to ca. 1.5‰ at 170–160 m. The interval of samples 69–87 is characterised by very rapid fluctuations of $\delta^{13}\text{C}$ values from 0.88–2.07‰. Above this interval, a rapid two-step decrease of the $\delta^{13}\text{C}$ values is detected. The first step (samples 89–98) shows an abrupt decrease of the $\delta^{13}\text{C}$ value from 0.43 to -2.41‰. The second one (samples 99–108) displays a gentler decline of the $\delta^{13}\text{C}$ value from -1.39 to -1.66‰.

The $\delta^{13}\text{C}$ curve of the studied section differs significantly from $\delta^{13}\text{C}$ records from other localities (e.g., Jarvis et al., 2006; Gambacorta et al., 2015; Giorgioni et al., 2015; Bornemann et al., 2017): the $\delta^{13}\text{C}$ values detected throughout the Upper Albian to Lower Cenomanian of the CT8 section are relatively uniform, contained within ca. 1–2‰. The Upper Cenomanian is marked instead by rather negative carbon isotopic values which do not find correspondence with any equivalent record worldwide. These differences may result from diagenetic alteration and/or may reflect the presence of

Table 7. Values of $\delta^{18}\text{O}$ and $\delta^{13}\text{C}$ from bulk sediment samples of borehole CT8. Samples 4–64 were analyzed in 2017, samples 65–108 were analyzed during this project.

ID	d13C	d18O
108	-1.66	-2.76
107	-1.10	-2.65
106	-0.52	-3.38
104	-0.85	-3.14
103	0.09	-2.75
102	-1.11	-3.60
101	-0.76	-3.59
100	-1.62	-8.33
99	-1.39	-3.77
98	-2.41	-3.70
97	1.05	-2.73
96	1.21	-2.84
95	0.40	-3.11
94	0.59	-2.98
93	-0.09	-3.00
92	0.50	-2.97
91	0.21	-3.10
90	0.45	-2.96
89	0.43	-3.14
88	-0.46	-5.39
87	1.50	-2.30
86	1.53	-2.81
85	1.58	-2.84
84	1.59	-3.11
83	1.71	-2.84
82	1.74	-2.87
81	1.97	-2.94
80	2.11	-2.70
79	2.03	-2.81
78	0.89	-4.52
77	1.81	-3.03
76	1.82	-3.01
75	1.74	-3.25
74	2.06	-2.87
73	0.88	-3.26
72	1.96	-3.02
71	2.07	-2.88
70	1.84	-3.04
69	1.17	-2.99
68	1.64	-2.90
67	1.91	-2.51
66	1.67	-2.63
65	1.67	-2.86

ID	d13C	d18O
64	1.91	-2.13
63	1.82	-2.46
62	1.75	-2.32
61	1.84	-2.46
60	1.77	-2.71
59	1.62	-2.71
58	2.01	-1.96
57	1.81	-2.16
56	1.90	-2.19
37	1.71	-1.57
36	1.66	-1.76
35	1.54	-1.89
34	1.70	-1.99
33	1.87	-1.75
32	1.69	-2.00
31	1.77	-1.93
30	1.85	-2.26
29	1.85	-2.13
28	1.51	-2.22
27	1.94	-1.96
26	2.19	-2.14
25	1.97	-1.95
24	2.18	-2.04
23	2.14	-1.89
22	1.95	-1.93
21	1.81	-3.27
20	1.88	-1.58
14	0.82	-1.91
13	1.16	-2.86
12	1.51	-1.72
11	1.65	-2.38
10	1.95	-1.81
9	1.61	-2.26
8	1.49	-2.36
7	1.28	-2.37
6	1.47	-2.12
5	1.11	-2.72
4	0.47	-2.97

hiatuses. The $\delta^{13}\text{C}$ curve of the studied section differs significantly from $\delta^{13}\text{C}$ records in other localities (e.g., Jarvis et al., 2006; Gambacorta et al., 2015; Giorgioni et al., 2015; Bornemann et al., 2017). The $\delta^{13}\text{C}$ values detected throughout the Upper Albian to Lower Cenomanian of the CT8 section are relatively uniform, contained within ca. 1–2‰. The Middle Cenomanian is characterised by transitional values of $\delta^{13}\text{C}$ within 1–2 ‰ in the lower part and sharp changes in the upper part. The Upper Cenomanian is marked by rather negative carbon isotopic values that do not match any record worldwide, except, possibly, the Shilaif and Natih basins (United Arab Emirates), where a prominent decrease in $\delta^{13}\text{C}$ values is detected in the Late Cenomanian prior to OAE2 (Vahrenkamp, 2013; Wohlwend et al., 2016; Hennhofer et al., 2019). Such differences may reflect either diagenetic alteration or/and the presence of hiatuses. Noteworthy, the $\delta^{18}\text{O}$ values become more positive with depth (and not negative as expected from a strong impact of the diagenesis), and there is no correlation ($R^2=0.05$) between *W. barnesiae* abundance and the $\delta^{18}\text{O}$ record. The latter may imply the absence of a diagenetic imprint on both chemical and micropaleontological proxies, so the oxygen isotope data from borehole CT8 possibly preserve a primary isotopic signal.

Borehole CT2 (Table 8)

The oxygen isotope profile shows remarkable positive and negative fluctuations across the succession (Fig. 16), with three trends in the the Isfiye Fm. and two trends in the Arqan Fm.

In the lower part of the Isfiye Fm., a negative shift of ca. -0.42‰ [-2.68 to -3.11‰] is observed. The interval corresponding to samples 22–30, a positive shift of ca. +1.27‰ [-3.11 to -1.84‰] is presented. In the interval of samples 31–38, the values of oxygen are practically constant [-2.25 to -2.14‰]. A significant negative anomaly of ca. -3.26‰ [-1.65 to -4.91‰] is recorded in the interval of samples 39–72. In the upper part of the section (samples 73–96), a positive shift of ca. +1.02‰ [-3.76 to -2.74‰] is identified.

The carbon isotope profile also shows notable positive and negative fluctuations throughout the succession (Fig. 16), with two trends in the the Isfiye Fm. and three trends in the Arqan Fm.

The lower part of the Isfiye Fm. (samples 14–17) are characterised by almost constant $\delta^{13}\text{C}$ values (1.28–1.57‰) with minor fluctuations that include a relative decrease from ca. 1.07‰ at 175–172 m. A significant positive anomaly of ca. +1.52‰ (1.05 to -2.57‰)

Table 7. Values of $\delta^{18}\text{O}$ and $\delta^{13}\text{C}$ from bulk sediment samples from borehole CT2.

sample	d13C	d18O	sample	d13C	d18O
CT2-14	1.28	-2.69	CT2-59	1.29	-2.86
CT2-15	1.44	-2.59	CT2-60	0.73	-3.17
CT2-16	1.07	-2.92	CT2-61	0.02	-3.03
CT2-17	1.57	-2.53	CT2-62	-1.68	-3.54
CT2-18	1.05	-3.04	CT2-63	-2.30	-3.70
CT2-19	1.56	-2.99	CT2-64	-1.46	-3.27
CT2-21	1.71	-2.80	CT2-65	2.14	-2.56
CT2-22	2.20	-3.11	CT2-66	1.64	-2.95
CT2-23	2.12	-2.81	CT2-67	1.91	-2.75
CT2-24	2.10	-2.77	CT2-68	-0.39	-3.18
CT2-25	2.66	-2.18	CT2-69	-2.35	-4.34
CT2-26	2.57	-2.21	CT2-70	-1.90	-3.85
CT2-27	2.15	-2.05	CT2-72	-2.78	-4.91
CT2-28	2.42	-1.94	CT2-73	-2.26	-3.76
CT2-29	1.96	-2.02	CT2-74	-2.85	-3.81
CT2-30	1.96	-1.84	CT2-75	-3.02	-3.75
CT2-31	1.46	-2.25	CT2-76	-3.95	-4.37
CT2-32	1.36	-2.27	CT2-77	-4.19	-4.07
CT2-33	1.40	-2.13	CT2-78	-3.02	-4.45
CT2-34	0.68	-2.28	CT2-79	-2.15	-3.86
CT2-35	0.65	-2.51	CT2-80	-2.02	-4.48
CT2-36	1.43	-2.16	CT2-81	-1.82	-4.42
CT2-38	1.34	-2.14	CT2-82	-1.23	-3.93
CT2-39	2.00	-1.65	CT2-83	-1.06	-3.58
CT2-40	1.85	-1.89	CT2-84	-1.78	-4.52
CT2-41	1.86	-1.73	CT2-85	-0.70	-3.58
CT2-43	1.56	-2.26	CT2-86	-0.80	-3.25
CT2-44	2.19	-1.88	CT2-87	-1.79	-4.22
CT2-45	2.33	-2.03	CT2-88	-0.57	-3.25
CT2-46	2.17	-2.25	CT2-89	-0.91	-3.32
CT2-47	2.02	-2.30	CT2-90	-0.60	-3.09
CT2-48	1.90	-2.41	CT2-91	-0.79	-3.38
CT2-49	1.66	-2.52	CT2-92	-0.49	-3.07
CT2-50	1.83	-2.26	CT2-93	-0.86	-3.65
CT2-51	2.04	-2.17	CT2-94	-1.09	-3.59
CT2-52	1.96	-1.80	CT2-95	-0.72	-3.35
CT2-53	1.67	-2.61	CT2-96	-0.53	-2.74
CT2-54	1.44	-2.18			
CT2-55	1.80	-2.08			
CT2-57	1.78	-2.38			
CT2-58	0.98	-2.39			

is recorded in the interval of samples 18–26 (depths 169.90–152.60 m). The interval of samples 27–35 is characterised by a rapid decrease of the $\delta^{13}\text{C}$ values (2.15–0.65‰). The upper part of the Isfiye Fm. and the lower part of the Arqan Fm. (samples 36–57) are characterised by almost constant $\delta^{13}\text{C}$ values (1.43–1.78‰) with minor fluctuations. A

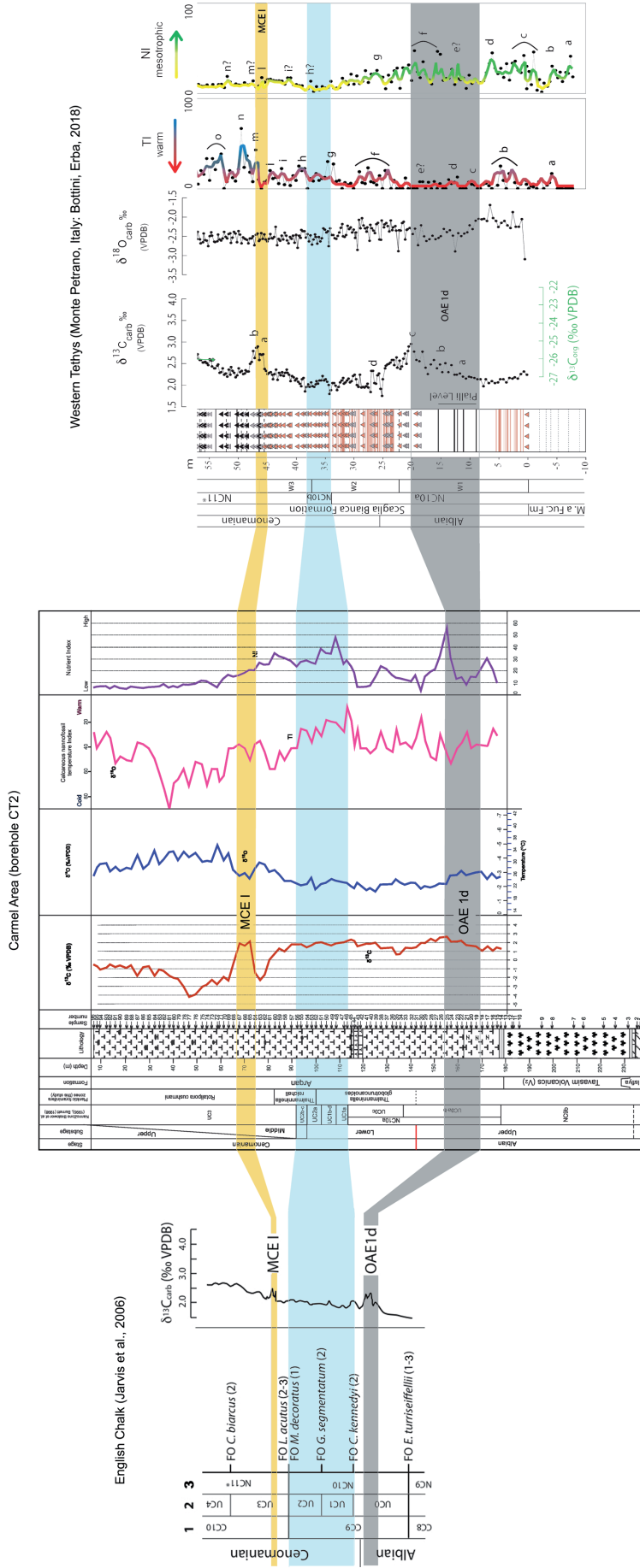


Figure 19. The correlation between the borehole CT2 (Carmel Region, NW Israel), English Chalk (Jarvis et al., 2006) and the western Tethys record (Bottini and Erba 2018). Blue: subzone NC10b (Bralower et al., 1995), which referred Zones UC1 and UC2 by Burnett (1998); grey: OAE 1d event, yellow: MCE 1 event.

very rapid drop of $\delta^{13}\text{C}$ values to ca. 3.28‰ (0.98 to -2.30‰) is detected in samples 58–63. Above this interval, a significant positive anomaly (-1.46 to -0.39‰) with increasing of the $\delta^{13}\text{C}$ values ca. $+3.6\text{‰}$ at 72.0 m (65 sample) are recorded in the interval of samples 64–68. The interval of samples 69–77 is characterised by a rapid decrease of $\delta^{13}\text{C}$ values from ca. 2‰ at 56.0 – 54.0 m. The upper part of the section (samples 78–96) is characterised by an increase of $\delta^{13}\text{C}$ values from -3.02 to -0.53‰ .

The $\delta^{13}\text{C}$ curve of the borehole CT2 is correlated fairly well with $\delta^{13}\text{C}$ records from other localities (e.g., Jarvis et al., 2006; Gambacorta et al., 2015; Giorgioni et al., 2015; Bornemann et al., 2017) (Fig. 19). The Upper Albian to the Lower Cenomanian $\delta^{13}\text{C}$ values detected throughout the CT2 section demonstrate significant positive shift ca. $+1.52\text{‰}$ at 169.90 – 152.60 m and negative anomaly of the $\delta^{13}\text{C}$ values (2.15 – 0.65‰) in the interval of 150.9 – 134.0 m. In the Middle–Upper Cenomanian (the lower part of *Rotalipora cushmani* Zone, depths 74.10 – 65.0 m), a significant positive anomaly (-1.46 to -0.39‰) with increasing of the $\delta^{13}\text{C}$ values ca. $+3.6\text{‰}$ at 72.0 m is recorded. These strong positive carbon isotopic values correspond to many records worldwide (e.g., English Chalk (Jarvis et al., 2006), Western Tethys (Italy) Giorgioni et al., 2015; Bottini & Erba, 2018). The $\delta^{18}\text{O}$ values grow more positive with depth (and not negative as expected from a strong impact of the diagenesis), and there is no correlation ($R^2=0.04$) between *W. barnesiae* abundance and the $\delta^{18}\text{O}$ record. This may imply the absence of a diagenetic imprint on both chemical and micropaleontological proxies, so the oxygen isotope data from borehole CT2 possibly preserve a primary isotopic signal.

5. DISCUSSION

5.1. Biostratigraphy

Carmel Area

Prior to the study of Shamrock and Watkins (2009), who first distinguished *E. casulus* from *E. turriseiffelii* sensu stricto (amended by Shamrock) based on their smaller size of coccoliths and the size of the central opening, the two species were diagnosed as *E. turriseiffelii* (sensu lato). Shamrock and Watkins (2009) further showed that their new species *E. casulus* first occurs slightly earlier (~ 600 kyr) than the amended *E. turriseiffelii* s. str. Therefore, the base of UC0 and NC10a as previously defined by Burnett (1998)

and Bralower et al. (1993, 1995) as the FO of *E. turriseiffelii* s.l., corresponds to the FO of the smaller *E. casulus*. In succession of the borehole CT8 the FO of *Eiffellithus turriseiffelii* s.str. is fixed higher in sample 17 (depth 190.7 m) than *E. casulus* which is recorded in sample 6 (depth 216.90 m). In borehole CT2, the FO of *Eiffellithus turriseiffelii* s.str. fs detected higher in sample 18 (depth 169.9 m) than *E. casulus* which is recorded in sample 14 (depth 177.90 m).

5.2. Age inferences for the Albian–Cenomanian interval of the Carmel Area (boreholes CT8 and CT2)

The identified calcareous nannofossil and planktic foraminiferal datums provide the basis for the NW Carmel region reference age–depth models i.e. a linear extrapolation of the age vs. depth (Fig. 20, borehole CT8; Fig. 21, borehole CT2). The Albian–

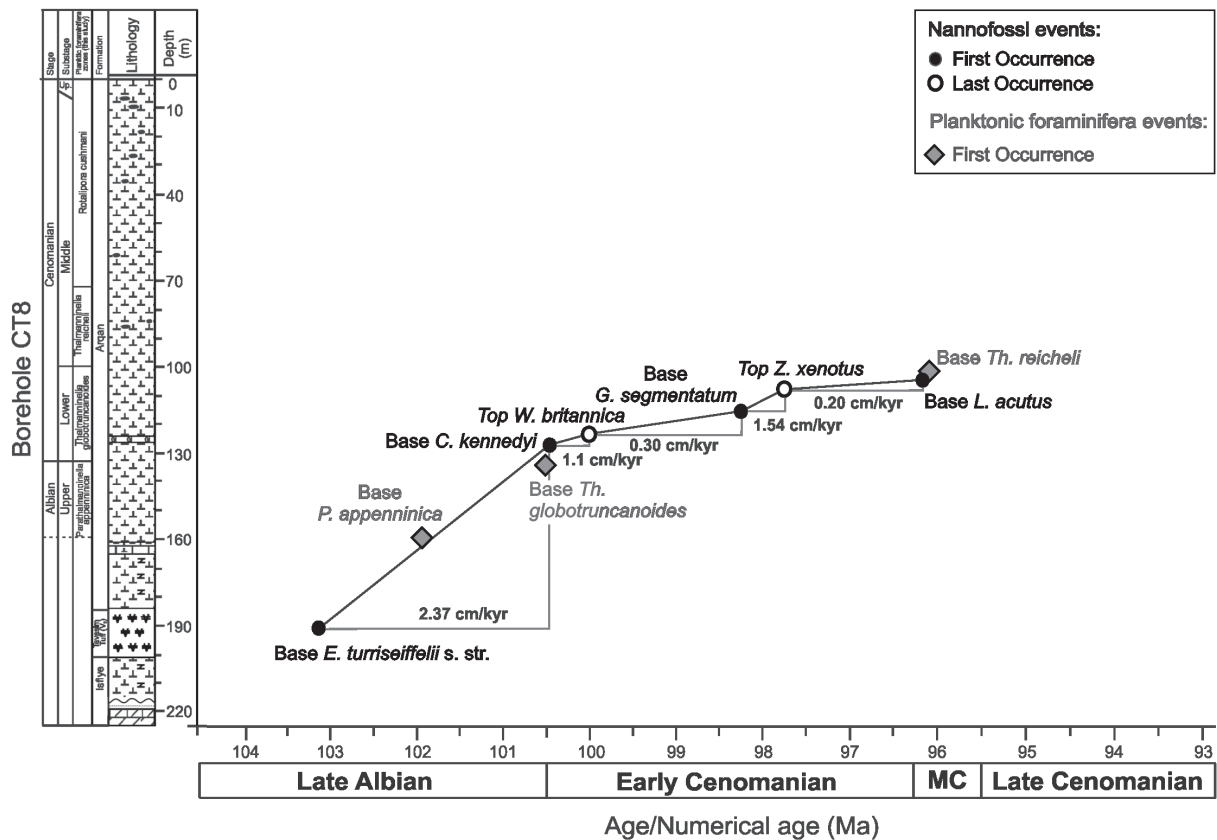


Figure 20. Age-depth model and derived sediment accumulation rates for the Albian – Cenomanian of the Carmel CT8 borehole, including events both nannofossil and planktonic foraminifera. Circles: nannofossil events, solid black – first occurrence, open – last occurrence; grey rhombs: first occurrences of planktonic foraminifera; MC – Middle Cenomanian.

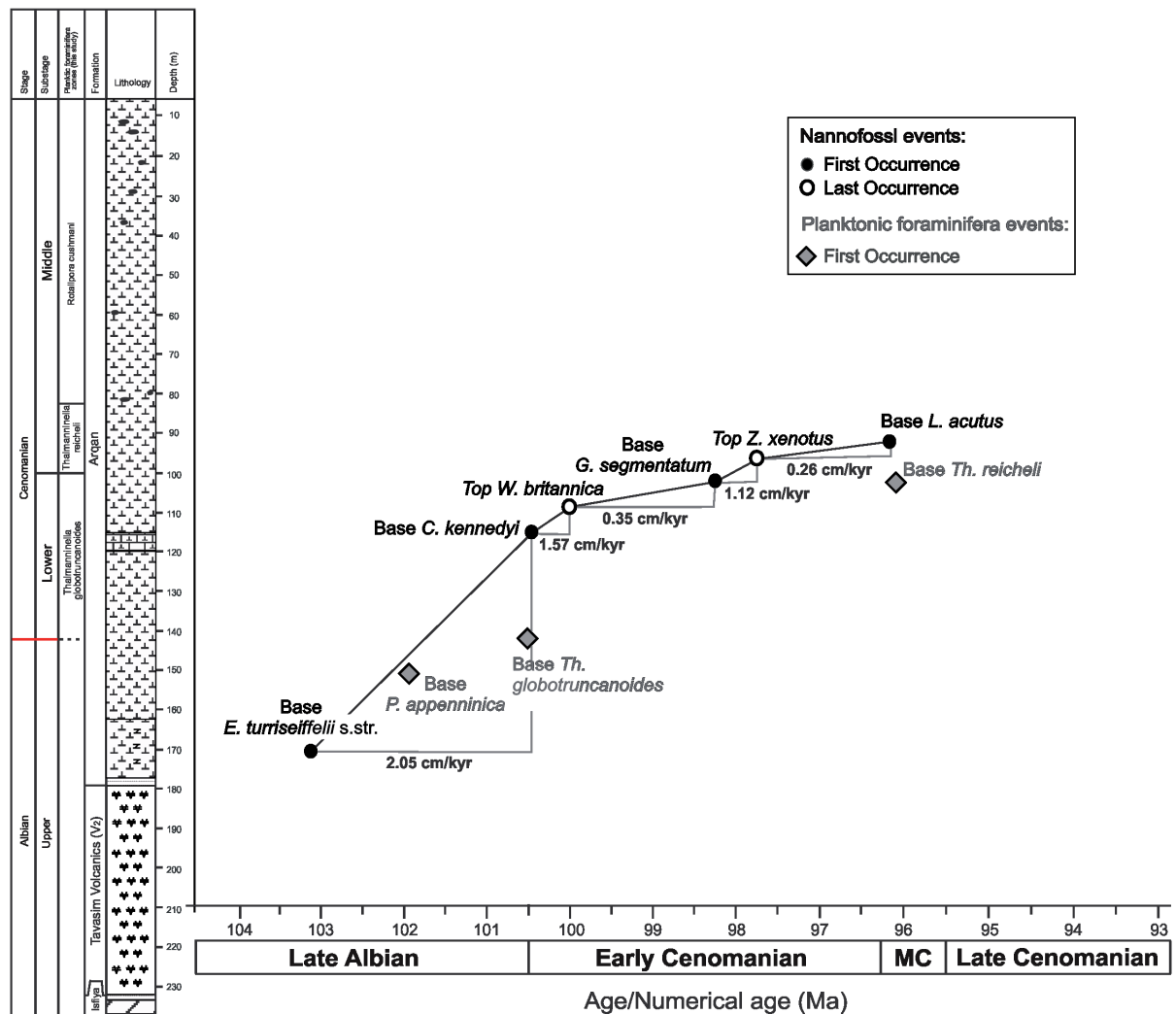


Figure 21. Age-depth model and derived sediment accumulation rates for the Albian – Cenomanian of the Carmel CT2 borehole, including events both nanofossil and planktonic foraminifera. Circles: nanofossil events, solid black – first occurrence, open – last occurrence; grey rhombs: first occurrences of planktonic foraminifera; MC – Middle Cenomanian.

Cenomanian chronostratigraphy of two boreholes is based on the Geologic Time Scale 2012 (Ogg & Hinnov, 2012).

Borehole CT8

This age model includes the following bioevents: FO of *E. turriseiffelii* s.l. (103.13 Ma) at 216.90 m, FO of *C. kennedyi* (100.45 Ma) at 127.15 m, LO of *W. britannica* (100.03 Ma) at 122.50 m, FO of *G. segmentatum* (98.26 Ma) at 116.50 m, LO of *Z. xenotus* (97.73 Ma) at 108.35 m, and FO of *L. acutus* (96.16 Ma) at 105.15 m. The model allows

estimation of sedimentation rates for the Albian–Cenomanian interval in borehole CT8 as varying between 0.20–2.37 cm/kyr.

Borehole CT2

This age model includes the following bioevents: FO of *E. turriseiffelli* s.l. (103.13 Ma) at 169.90 m, FO of *C. kennedyi* (100.45 Ma) at 115 m, LO of *W. britannica* (100.03 Ma) at 108.40 m, FO of *G. segmentatum* (98.26 Ma) at 102.10 m, LO of *Z. xenotus* (97.73 Ma) at 96.15 m, and FO of *L. acutus* (96.16 Ma) at 92.0 m. The model allows estimation of sedimentation rates for the Albian–Cenomanian interval in borehole CT2 as varying between 0.26–2.05 cm/kyr.

5.3. Integrated stratigraphy

Carmel Area

Borehole CT8

The upper part of the interval of subzones UC0a–b corresponds to the Upper Albian foraminiferal *P. appenninica* Zone (from the level of sample 32). Subzone UC0c correlates with the upper part of *P. appenninica* Zone and lowermost part of *Th. globotruncanoides* Zone of the Lower Cenomanian. The interval of samples 48–54 (127.15–118.55 m) (foraminiferal *Th. globotruncanoides* Zone) is assigned to the Lower Cenomanian UC1 Zone. The interval of samples 48–52 (127.15–122.50 m) (foraminiferal *Th. globotruncanoides* Zone) belongs to Subzone UC1a.

The interval of samples 55–60 (depths 116.50–106.45 m) (foraminiferal *Th. globotruncanoides* Zone) belongs to Zone UC2.

The upper part of the borehole (samples 61–108, depths 105.15–5.00 m) (uppermost part of *Th. globotruncanoides*, *Th. reicheli* and *R. cushmani* foraminiferal zones; Lower–Upper Cenomanian) is referred to the transitional basal Middle–Upper Cenomanian Zone UC3.

Borehole CT2

The upper part of the interval of subzones UC0a–b corresponds to the Upper Albian foraminiferal *P. appenninica* Zone (from the level of sample 27). Subzone UC0c and Zone UC1 of the Lower Cenomanian correlate with *Th. globotruncanoides* Zone of the Lower Cenomanian. Zone UC2 corresponds to the Middle Cenomanian *Th. reicheli*

foraminiferal zone. The transitional basal Middle–Upper Cenomanian Zone UC3 is assigned to the Middle Cenomanian *R. cushmani* foraminiferal Zone.

Since boreholes CT8 and CT2 are located very close to each other, the same sequences of appearance and disappearance levels of important markers of planktic foraminifera and calcareous nannoplankton are observed (Fig. 22). However, the correlation between foraminiferal zones and nannoplankton zone has following differences. The FO of *E. turriseiffelii* s.str. is recorded in the Tavasim Volcanics (sample 17) in borehole CT8, and slightly higher around 10 m tuff layer, in the lower part of the Arqan Fm. in borehole CT2. An undivided interval of Subzones UC0a–b is thicker and correlates with the lower part of *P. appenninica* Zone in CT8, whereas Subzones UC0a–b correspond

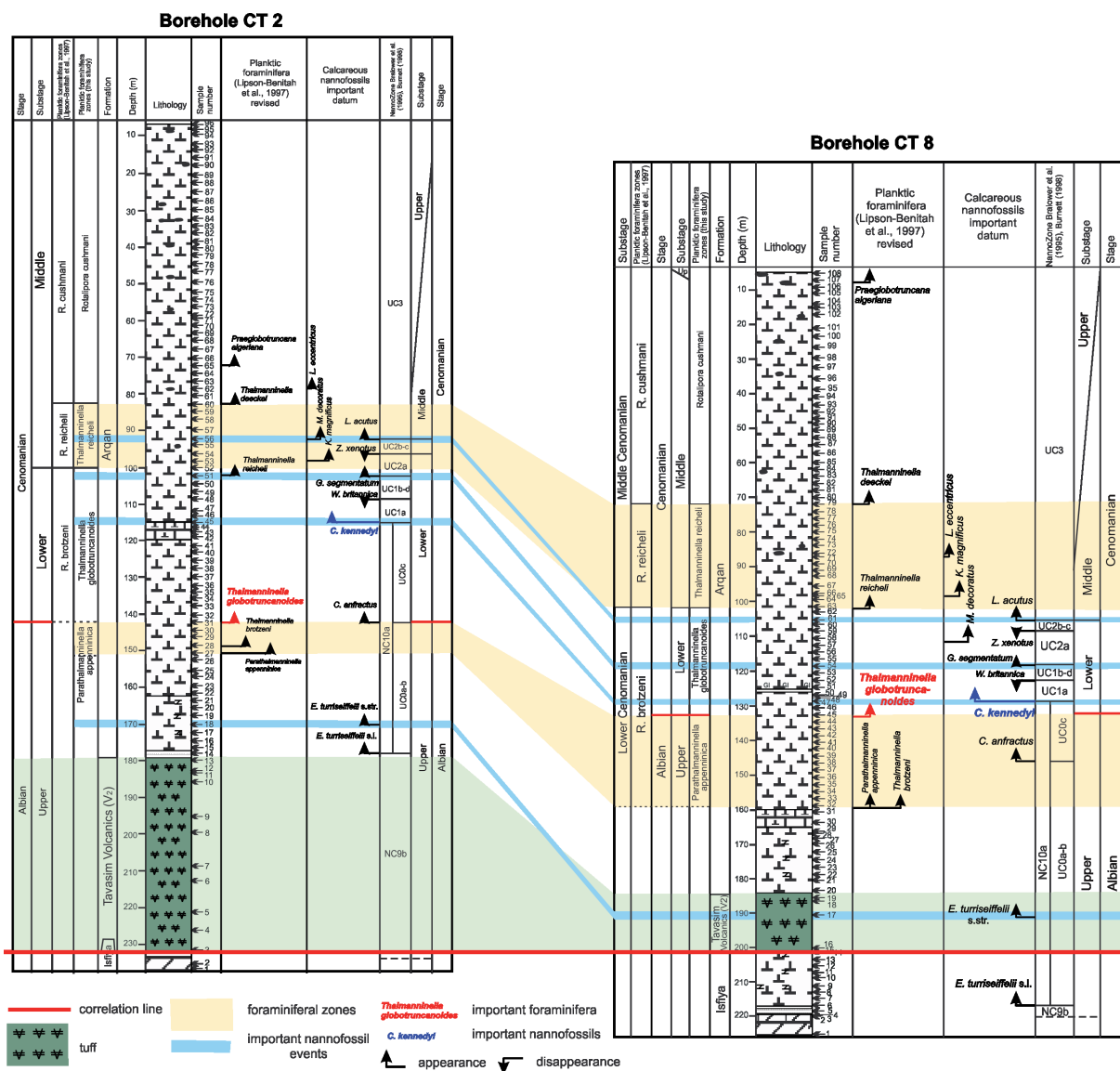


Figure 22. Biostratigraphical correlation of boreholes CT8 and CT2 (Carmel Area).

to the entire *P. appenninica* Zone in CT2. Subzone UC0c is assigned to the upper part of *P. appenninica* Zone and lowest part of *Th. globotruncanoides* Zone in CT8. In borehole CT2, the base of Subzone UC0c is fixed at the same level as the base of *Th. globotruncanoides* Zone (sample 31, depth 142.25 m) and UC0c correlates with the main part of *Th. globotruncanoides* Zone. Zones UC1 and UC2 correspond to *Th. globotruncanoides* Zone in the CT8, while in the CT2 only UC1 is assigned to *Th. globotruncanoides* Zone. Zone UC2 in borehole CT2 correlates with the lower part of *Th. reicheli* Zone. Zone UC3 in borehole CT8 corresponds to the uppermost part of *Th. globotruncanoides*, *Th. reicheli* and *R. cushmani* foraminiferal zones, while in borehole CT2 Zone UC3 correlates with the upper part of *Th. reicheli* and *R. cushmani* zones.

Coastal Plain

Negba 1

The Upper member of the Negba Fm. (depths 530–180 m) belongs to the Lower–Middle Campanian interval of planktic foraminifera *Thalmanninella globotruncanoides/Th. brotzeni* zones (Fig. 8). Noteworthy, the planktic foraminifera are very rare in the section and the boundaries are very conditional. Calcareous nannoplankton data indicate that the lower part of the Lower member of the Negba Fm. (depths 530–490 m) refers to the Aptian – Turonian; however, the nannofossil assemblage, which is determined in the underlying samples 14 and 15 (depths 608–603 m), belongs to the Upper Albian (BC26 Zone) – Lower Cenomanian. Therefore, assuming that the sequence of deposits is continuous, the interval of sediments (depths 530–490 m) is not older than Late Albian–Early Cenomanian.

The upper part (depths 375–250 m) belongs to the Upper Albian – Cenomanian. The benthic foraminifera data do not contradict this conclusion. The absence of planktic foraminifera *Praeglobotruncana algeriana*, *Marginotruncana hagni* (= *Dicarinella hagni*), *Marginotruncana imbricata* (= *Dicarinella imbricata*) do not allow to establish the Upper Cenomanian by these microfossils (Lipson-Benitah, 1994), but nannofossils allow to recognize the Upper Cenomanian due to the presence *M. decoratus* and *C. anfractus*.

5.4. Paleoenvironmental reconstructions

As one of the most abundant marine phytoplankton groups, calcareous nannoplankton is an important component of the marine ecosystem and it has been one of the primary

oceanic producers since the Triassic. The distribution of calcareous nanoplankton is strongly influenced by climatic and oceanographic conditions (e.g., Mutterlose et al., 2005). Quantitative studies of Cretaceous calcareous nannofossil assemblages have resulted in the identification of the paleoecological affinities of some taxa and the establishment of paleotemperature and paleofertility indices (Roth & Krumbach, 1986; Mutterlose & Wise, 1990; Mutterlose, 1991, 1996; Erba et al., 1992; Burnett et al., 2000; Mutterlose & Kessels, 2000; Street & Bown, 2000; Herrle, 2003; Herrle & Mutterlose, 2003; Lees et al., 2005; Tiraboschi et al., 2009; Bottini et al., 2015). Due to their sensitivity to temperature, nutrients, salinity and $p\text{CO}_2$, calcareous nanoplankton can be an excellent proxy of surface water conditions (Erba & Tremolada, 2004; Mutterlose et al., 2005; Tiraboschi et al., 2009; Erba et al., 2010).

The Early to Late Cretaceous transition was a time of global warming, when the Earth's climate was in an extreme greenhouse mode (e.g., Huber et al., 2002; Jenkyns, 2003, 2010; Hay, 2008; Ando et al., 2015; O'Brien et al., 2017). The northern and southern continents were separated by a wide eastern Tethys and narrow western Tethys and the Atlantic oceans. Starting from the late Albian, the Tethys and Atlantic oceans provided a circum-global connection at low latitudes probably with a stable, westward-flowing current throughout the Tethys (Roth, 1986; Barron, 1987; Hay et al., 1999; Giorgioni et al., 2015). Reconstruction of the surface-water paleotemperature, fertility, and chemistry dynamics in mid-Cretaceous oceans attract broad attention (Watkins et al., 2005; Forster et al., 2007; Ando et al., 2010; Gambacorta et al., 2016).

Over the last couple of decades, Cretaceous climate has been in the focus of several studies, which demonstrated the early Late Cretaceous – Early Turonian to be one of the warmest periods during the past 140 million years (e.g., Huber et al., 2002; Forster et al., 2007; Linnert et al., 2014; Ando et al., 2015). Tropical sea surface temperatures (over 35 °C) were estimated for the Late Cenomanian–Early Turonian with a strongly reduced latitudinal gradient (Linnert et al., 2014; O'Brien et al., 2017).

In this regard, the improved knowledge about the paleoecological affinity of some mid-Cretaceous nannofossil species (e.g., Roth & Krumbach, 1986; Watkins, 1989; Erba et al., 1992; Herrle & Mutterlose, 2003; Herrle et al., 2003; Erba, 2004; Tiraboschi et al., 2009) allows implementing the information about the evolution of paleoenvironments during the mid-Cretaceous. Further on, we discuss temperature and nutrient variations

reconstructed in the Carmel area on the basis of calcareous nannofossils and compare them with the results with the Late Albian–Late Cenomanian record of the western Tethys (Bottini & Erba, 2018).

Lipson-Benitah et al. (1995, 1997) recognises five ecostratigraphic intervals coinciding with sea-level changes (Fig. 23). Phase 1 of Lipson-Benitah et al. (1995, 1997) corresponds to shallow marine conditions (Isfye Fm.) reflected by low relative abundance of planktic foraminifera. Phase 2 (CT2 161.70–146.30 m and CT8 183.35–166.00 m) in the lowermost part of the Arqan Fm. is associated with a sea-level rise, which commenced earlier. A peak of planktic foraminifera composed of rotaliporids, and occasionally abundant *Hedbergella*, points to the open marine depositional environment during this phase (Lipson-Benitah et al., 1995, 1997). Phase 3 (CT2 144.70–113.10 m and CT8 163.7–128.5 m) is recorded in the lower part of the Arqan Fm. and it is characterised by a conspicuous sea-level drop inferred from an extremely low relative abundance of planktic foraminifera. In the western part of the Carmel region biomicrites with *Pycnodonte vesiculosa* (Sowerby) found in the growth position suggest the presence of a low-energy and more deep-water environment (Lipson-Benitah et al., 1995, 1997).

Phase 4 (CT2 110.90–82.50 m and CT8 127.15–97.50 m) characterises the middle part of the Arqan Fm. marked by a rich planktic foraminiferal assemblage, dominated by *Rotalipora brotzeni*, *R. globotruncanoides* and *R. greenhornensis*, and reflects a deeper oligotrophic environment (Lipson-Benitah et al., 1995, 1997). Species of *Hedbergella* or *Gubkinella* are occasionally numerous, and their abundance peaks may be associated with increased nutrient levels and/or a change in the stratification of the water column (Lipson-Benitah et al., 1995, 1997). Phase 5 (CT2 80.60–58.25 m and CT8 95.50–32.65 m) is recognised in the upper part of the Arqan Fm. and is characterised by a decrease in the relative abundance of planktic foraminifera, it may be connected to periodic sea-level drops (Lipson-Benitah et al., 1995, 1997).

The calcareous nannoplankton Temperature (TI) and Nutrient (NI) indices show some correspondence with quantitative data by planktic foraminifera and with cycles and sequences of Haq et al. (1988) and Robaszynski et al. (1993) (Fig. 23). The TI and NI are indicative of variations in surface water temperature and fertility throughout the succession, but temperature shows irregular fluctuations, which are not necessarily associated with changes in fertility, suggesting that temperature and fertility varied independently.

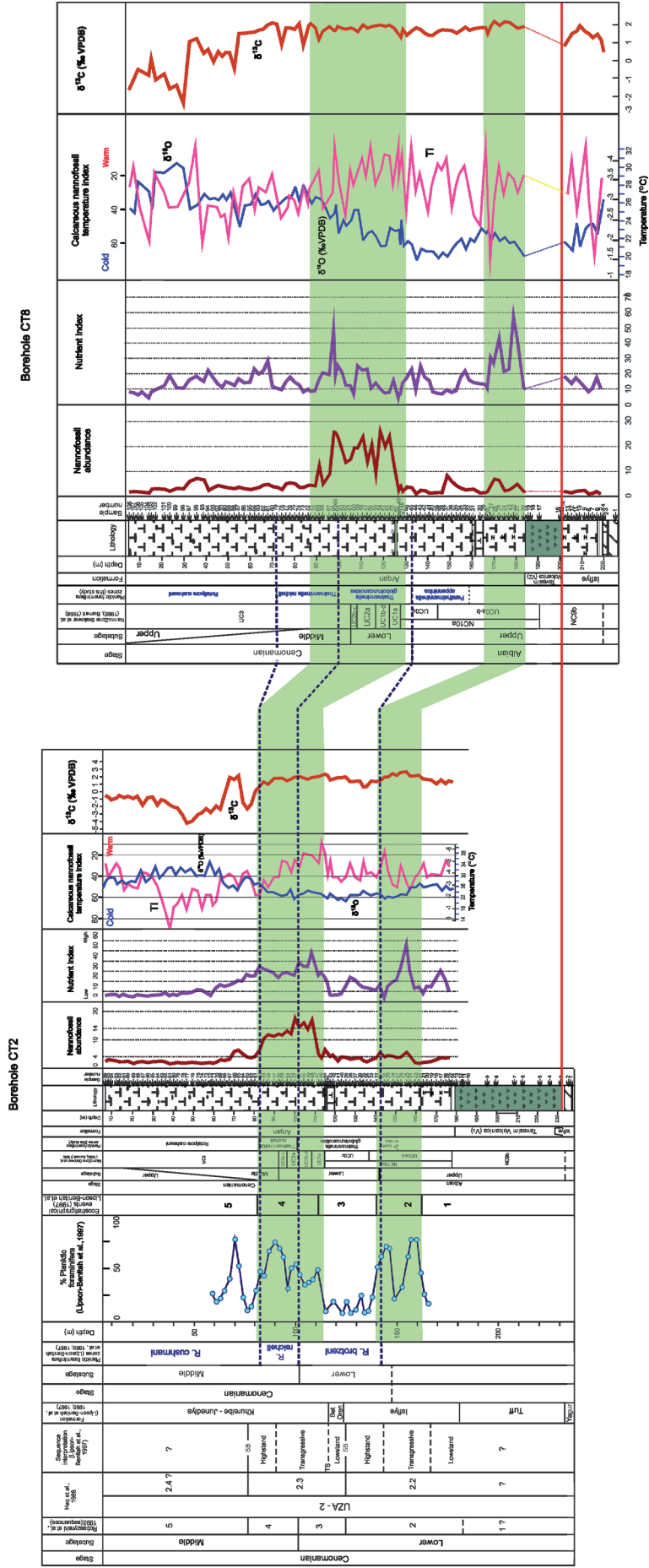


Figure 23. Comparison of quantitative data of planktic foraminifera (Lipson-Benitah et al., 1997) from borehole CT2 and borehole CT8 with total calcareous nannofossil abundance, calcareous nannofossil Nutrient and Temperature Indices and Temperature Indices. White – phases 1, 3, 5; green – phases 2, 4.

In the Late Albian (nannofossil Zone NC9b) temperatures were relatively cooler and surface water fertility was low. Fertility increased in the lower part of Subzone NC10a under intermediate temperatures. During the *P. appenninica* foraminiferal Zone, surface water conditions shifted towards warmer temperatures and lower fertility. A minor increase in fertility and a relative decrease in temperature marked the end of the *P. appenninica* Zone. The Lower Cenomanian (Subzone NC10b) was characterised by the warmest temperature of the studied interval and lower NI. In the Middle and Late Cenomanian (Zone NC11*) fertility was generally lower except for a peak in the middle part of Subzone NC10b (CT2) and at the base of Zone NC11* (CT8). The average temperature was cooler, although the TI shows alternating cooler and warmer phases.

In relation to the planktic foraminifera ecostratigraphic intervals in borehole CT2 (Lipson-Benitah et al., 1995, 1997), relatively higher total nannofossil abundance and peaks in the NI characterise the equivalent intervals of phases 2 and 4 of Lipson-Benitah et al. (1995, 1997). The correlation between higher surface water fertility conditions and transgressive phases is somehow contradictory. A possible explanation is that during a transgression phase, surface water fertility is reduced since phosphorous is extracted by sedimentation in the newly flooded shelf. Under such condition, the nitrogen-limited primary producers are favoured. Since coccolithophores are directly depending on nitrogen availability, the NI is shifted towards higher values.

Regarding the paleotemperature conditions of the Carmel area during the Late Albian–Cenomanian interval, there is a noticeable discrepancy between the two temperature proxies, for the TI and the $\delta^{18}\text{O}$ curves show opposite trends (Figs. 13 and 18). The oxygen isotopes suggest temperate conditions during the Late Albian–Early Cenomanian followed by a warming period in the late Early Cenomanian, with temperatures gradually increasing toward the Middle Cenomanian. Evidence for a gradual increase from $\sim 30^\circ\text{C}$ in the Albian to $\sim 31^\circ\text{C}$ during the Cenomanian were provided by oxygen isotope data on phosphatic fish remains from the Cretaceous to Eocene of Israel (Kolodny & Raab, 1988), but the low resolution of that dataset does not allow for a reliable comparison. The oxygen isotope record does not show any evidence for a diagenetic alteration of the primary signal, thus the differences between the TI and the oxygen isotopes may depend on the relatively low abundances of temperature indicative species used in the calculation of the TI. Compared to coeval sections in the Tethys (Bottini & Erba 2018),

E. floralis and *Z. diplogrammus* have similar average abundances and trends, while *Rh. asper* is less abundant. Despite this difference, the paleotemperature fluctuations indicated by the two TI records are comparable and, similarly to the Carmel area, the Cenomanian TI of the Tethys suggests cooler conditions with respect to the $\delta^{18}\text{O}$. In the following section we discuss two possible correlations between the Tethys and the Carmel area records.

5.5. Correlation with the western Tethys record

The studied sections are compared to the western Tethys (Bottini & Erba, 2018), which yields the only continuous record of the TI and NI through the Late Albian–Late Cenomanian interval (Figs. 19, 25). The nannofossil data take into account SSTs derived from TEX_{86} analyses (Forster et al., 2007; O'Brien et al., 2017) and are interpreted to trace supra-regional palaeoenvironmental conditions being similar to nannofossil datasets from other basins (e.g., Hardas et al., 2012; Kanungo et al., 2018). Possible correlations are suggested and discussed herein.

Correlation for the Borehole CT2 is based on nannofossil and foraminiferal biozones, and shows no evidence of missing biostratigraphic intervals, thus suggesting that the Late Albian–Late Cenomanian interval is complete in the studied section. The carbon signal in CT2 reflects quite well the globally recorded carbon isotopic anomalies (e.g., Jarvis et al., 2006; Gambacorta et al., 2015; Giorgioni et al., 2015; Bornemann et al., 2017) that mark the Oceanic Anoxic Event (OAE) 1d and Mid Cenomanian Event (MCE I) intervals. OAE 1d is fixed very clearly by the positive shift of 1.61‰ at 169.90–152.60 m and MCE I is recognised by the positive shift of 3.6‰ at 74.10–65.0 m. This general picture reflects the global carbon isotopic fluctuations (Fig. 19). It is therefore reasonable to assume that the isotopic signal is not diagenetically altered. It means that the $\delta^{18}\text{O}$ signal is not affected, and it can be used for paleotemperature reconstructions. The oxygen isotopes suggests temperate conditions during the Late Albian–Early Cenomanian (~26 °C) followed by a warming period in the late Early Cenomanian, with temperatures gradually increasing toward the Middle Cenomanian to ~32 °C. This scenario implies that there is no similar pattern of changes between the TI and NI compared to the western Tethys record (Bottini & Erba, 2018), and that the NI and TI of the Carmel area reflect very local fluctuations in this part of the Levant Basin.

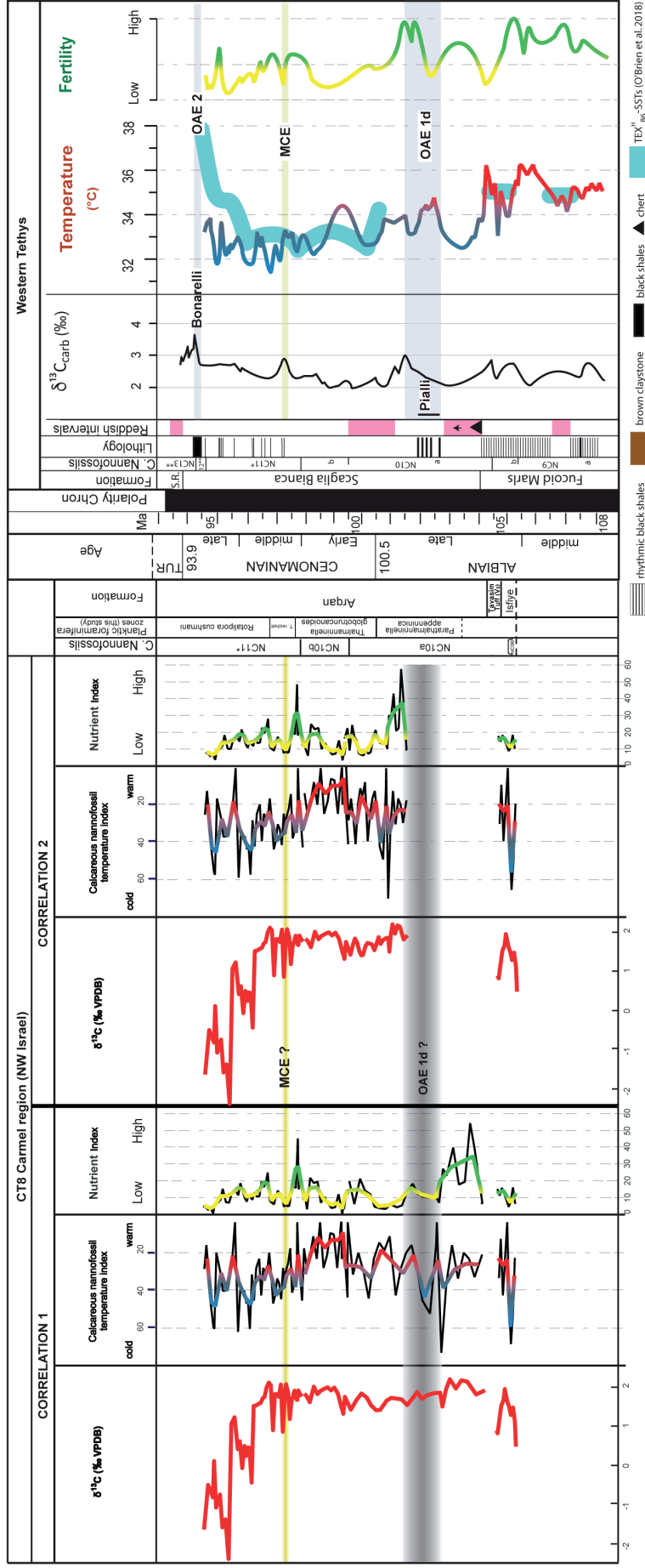


Figure 25. Proposed alternative correlations between borehole CT8 (Carmel Region, NW Israel) and the western Tethys record (Bottini and Erba 2018): Correlation 1 is based on calcareous nannofossil and foraminiferal biostratigraphy which indicate that the record is continuous in CT8 but marked by anomalous carbon isotope record and different Nannofossil Nutrient (NI) and Temperature (TI) indices trends compared to the Tethys; Correlation 2 takes into account calcareous nannofossil and foraminiferal biostratigraphy as well as chemostratigraphy and infers the presence of a hiatus eliding OAE 1d. The TI and NI trends are relatively similar to those traced in the Western Tethys but the carbon isotope record largely differs from the Tethys. Point by point TI and NI are reported together with the 3pt. moving average of the TI (blue-red line) and NI (yellow-green). Time scale is after Ogg and Hinnov (2012).

The possible correlation of two boreholes is presented in Fig. 24. Since the carbon isotope data in the borehole CT8 does not reflect the global carbon value fluctuations, there are two correlations (Fig. 25):

Correlation 1 is also based on nannofossil and foraminiferal biozones, and shows no evidence of missing biostratigraphic intervals, thus suggesting that the Late Albian–Late Cenomanian interval is complete in the studied section (Fig. 25). However, the carbon signal in borehole CT8 does not reflect the globally recorded carbon isotopic anomalies (e.g., Jarvis et al., 2006; Gambacorta et al., 2015; Giorgioni et al., 2015; Bornemann et al., 2017) that mark the Oceanic Anoxic Event (OAE) 1d and Mid Cenomanian Event (MCE) intervals. It is therefore plausible that the isotopic signal is diagenetically altered. It means that the $\delta^{18}\text{O}$ signal is affected too and, consequently, it cannot be used for palaeotemperature reconstructions. This scenario implies that there is no similar pattern of changes between the TI and NI compared to the western Tethys record (Bottini and Erba, 2018), and that the NI and TI of the Carmel area reflect very local fluctuations in this part of the Levant Basin.

Correlation 2 takes into account the biostratigraphic data as well as the $\delta^{13}\text{C}$ curve. The latter suggests that the OAE 1d interval is missing due to a hiatus coinciding with the lithostratigraphic boundary between the Tavasim Volcanics (V_2) of the Isfiye Fm. and the Arqan Fm. The $\delta^{13}\text{C}$ curve does not display any positive anomaly that can be correlated with the OAE 1d positive carbon isotopic shift elsewhere. The $\delta^{13}\text{C}$ curve shows instead a decreasing trend, which may represent the post-OAE 1d positive carbon isotopic anomaly starting around 101.5 Ma (Fig. 25). The absence of a positive carbon isotope anomaly in the Middle Cenomanian of the studied sections, does not allow identification of the MCE. However, neither the biostratigraphic data nor chemostratigraphy permit to state whether the MCE interval is recorded or elided. The carbon isotope curve across the Late Cenomanian is characterised by negative values, which do not find correspondence with other isotopic records worldwide and are interpreted to be diagenetically altered. Contrary to Correlation 1, in the second scenario the TI and NI of the CT8 section show main trends comparable to those in the western Tethys. In particular, the cooling spike identified in Subzone NC9b, at the base of the section, may correspond to similar cooler temperature registered in the Tethys in the same Subzone. The fertility spike detected in the middle of Subzone NC10a possibly corresponds to the fertility peak marking the end of OAE 1d. In both records a warm interlude is paralleled by low fertility around ca. 98 Ma, followed by a minor cooling and a fertility spike. Another similarity is identified in the progressive cooling trend of the Middle–Late Cenomanian, which is marked by

alternating phases of warming and cooling. The presence of relatively similar variations in the TI and NI suggest that Correlation 2 is more plausible compared to Correlation 1. On the basis of Correlation 2, the Carmel area appears to be characterised by paleoclimatic and paleoenvironmental conditions occurring during the Late Albian–Late Cenomanian at least at the supra-regional scale.

6. CONCLUSIONS

For the first time, the taxonomic composition and stratigraphic distribution of calcareous nannofossils from the sediments of the Judea Group (Albian–Cenomanian) of the Carmel area (NW Israel) and the Southern Coastal Plain were documented in detail. The identified assemblages in the Carmel Area are quite rich and consist of 113 taxa (borehole CT8) and 95 taxa (borehole CT2). On the Coastal Plain (borehole Negba 1) the impoverished assemblage of 24 taxa is recorded.

The detailed calcareous nannofossil biostratigraphy of the Carmel Area has been established and compared with planktic foraminiferal zones. In the Coastal Plain, different intervals are recorded and correlated with planktic foraminiferal zones.

The novel nannofossil data indicate that the Isfiye Fm. and the Tavasim Volcanics (V2), which is calculated as 98.2 Ma in the Carmel Area, are Late Albian, and the Arqan Fm. is Late Albian–Middle Cenomanian, not Cenomanian as it was considered prior to this study. The Albian–Cenomanian boundary in the Carmel Area is drawn at the first occurrence of *Thalmaninella globotruncanoides* (planktic foraminifera) in the lower part of the Arqan Fm. at ~52 m above the top Tavasim Volcanics in CT8 and at ~35.65 m above the Tavasim Volcanics in CT2. This is supported by the appearance of *Th. brotzeni* (planktic foraminifera) at 26 m (CT8) and 6.55 m (CT2) below, and *C. kennedyi* (nannofossils) above this level. Newly obtained stratigraphical data allow us to draw attention to the revision of the lithostratigraphic chart and, in particular, to updating the age of the Arqan Fm. On the Coastal Plain, rarity of nannofossils allows us to establish stratigraphic intervals only in broad terms: the upper part of the Yagur Fm. is Late Albian–Early Cenomanian, the Lower and Upper Members of the Negba Fm. is Albian–Late Cenomanian, the upper part of the Upper Member of the Negba Fm. is Late Cenomanian.

The quantitative analysis of the calcareous nannofossils suggests that the general dominance of *Watznaueria* spp. throughout the whole successions in the Carmel Area (boreholes CT8 and CT2) points to quite warm, open marine or coastal, generally oligotrophic conditions. Due to poor nutrient supply, the productivity of the calcareous nanoplankton was quite low except for two phases of higher fertility within Subzone

NC10a and Zone NC11*. Low values of the Shannon index, Evenness and Species richness can be interpreted as reflecting unstable environment. The Isfiye Fm. (Late Albian) accumulated in temperate, oligotrophic conditions. The lower part of the Arqan Fm. was deposited under temperate climate but mesotrophic conditions. The higher part of the Arqan Fm. (Early Cenomanian) was deposited in oligotrophic waters and relatively warm climate. The uppermost part of the Arqan Fm. (Middle–Late Cenomanian) was accumulated during a progressively cooling period, although characterized by alternating warming and cooling phases and oligotrophic conditions.

The calcareous nannoplankton quantitative data correlate very well with those obtained from planktic foraminifera (Lipson-Benitah et al., 1997) from the nearby area, and with cycles and sequences postulated by Haq et al. (1988), and suggest nutrification during phases of a risen sea level in the Late Albian and Early Cenomanian.

The biostratigraphy in the Carmel Area shows no hiatuses in the studied section, but carbon isotope data reflect different pictures. In borehole CT2 (Isfiye Fm., depths 169.90–152.60 m) the Oceanic Anoxic Event (OAE) 1d is recorded by the positive shift of 1.61‰ and MCE I by 3.6‰ (Arqan Fm., depths 74.10–65.0 m); these reflect well the globally recorded carbon isotopic anomalies (e.g., Jarvis et al., 2006; Gambacorta et al., 2015; Giorgioni et al., 2015; Bornemann et al., 2017). Considering that the isotopic signal is not diagenetically altered and the $\delta^{18}\text{O}$ signal is not affected in the CT2, the oxygen isotopes suggest temperate conditions during the Late Albian–Early Cenomanian (~26 °C) followed by a warming period in the late Early Cenomanian, with temperatures gradually increasing toward the Middle Cenomanian to ~32 °C. In borehole CT8 carbon isotope data seem to be affected by diagenetic alteration showing no evidence of the positive isotopic anomalies, which identify OAE 1d and MCE worldwide. A comparison with the western Tethys record suggests that OAE 1d is possibly missing in CT8 due to a hiatus at the Isfiye Fm. / Arqan Fm. boundary. Temperature and nutrient variations in CT8 correspond to the western Tethys record, thus suggesting that the detected paleoclimatic variations occurred at a supra-regional scale.

EXPECTED BENEFITS AND POTENTIAL CONTRIBUTION TO GOALS OF THE MINISTRY OF ENERGY AND WATER RESOURCES

Biostratigraphic and paleoecological outcomes of the present research will contribute to the robust definition of the stratigraphic tables of Israel, to the geologic knowledge

and paleoecological, the expansion of knowledge of the geological structure of Israel in the marine science field, as well as to exploration activity in the region.

POSSIBLE APPLICATIONS OF THE RESULTS

The current research endeavour contributes to improvement of the Cretaceous nannoplankton biostratigraphy in the Levant Basin and amends sequencing of deposits based on foraminifers. The newly generated biostratigraphic results can be incorporated in the next generation of geological maps of Israel.

The quantitative analysis of the calcareous nannoplankton combined with geochemical data contributes to understanding paleotemperature and depositional history of the Levant Basin during the mid and Late Cretaceous.

ACKNOWLEDGEMENTS

Thanks are due to Irit Gefen (GSI) for checking planktic foraminifera identification, Dr A. Ayalon (GSI) and T. Zilberman for analysis of stable isotopes, and Dr M.B. Mostovski (Tel Aviv University) for discussions, consultations at various stages of the manuscript preparation, editing text and typesetting the report. We are very grateful to Prof. D. Watkins for his help in clarifying taxonomical and biostratigraphical issues. Dr O. Varol, Dr J. Young, Dr J.A. Lees are thanked for valuable comments on the calcareous nannoplankton taxonomy. Dr O. Zlatkin (Ministry of National Infrastructures, Energy and Water Resources of Israel) is thanked for useful comments and suggestions on an earlier draft of the report. The project was supported by the Ministry of National Infrastructures, Energy and Water Resources of Israel, grant no. 217-17-023.

PUBLISHED RESULTS

Ovechkina, M. 2018. Palaeocological reconstructions of the Albian-Cenomanian in northwestern Israel (Mount Carmel) on basis of quantitative analysis of calcareous nannofossils. *Isr. Geol. Soc., Ann. Meeting, Israel – Cyprus, March 2018, Abstract Volume*, p. 38.

- Ovechkina, M. & Segev, A. 2018. An interdisciplinary insight into biostratigraphy and palaeoecology around the Albian–Cenomanian boundary in the Levant: A case study in the Mount Carmel Region. *International Journal of Earth Sci. Geol.* 2018, Abstracts Volume 1(2): 44.
- Ovechkina, M., Erba, E., Bottini, C., 2019. Calcareous nannoplankton proxies for palaeoenvironmental reconstruction of the Albian–Cenomanian succession in North-western Israel (Mount Carmel Region). *Marine Micropaleontology* 152, Art. 101742. <https://doi.org/10.1016/j.marmicro.2019.04.001>
- Ovechkina, M.N., Segev, A. Calibration of the Albian – Cenomanian boundary by microfossil biostratigraphy in Mount Carmel, Northwestern Israel. *Isr. Geol. Soc., Ann. Meeting, Israel, Abstract. Submitted.*
- Ovechkina, M.N., Segev, A. Calibration of the Albian / Cenomanian boundary by microfossils biostratigraphy (planktic foraminifera and calcareous nannofossils) in North-western Israel (Mount Carmel Region). *In preparation for Cretaceous Research.*

REFERENCES

- Ando, A., Huber, B.T., MacLeod, K.G., 2010. Depth-habitat reorganization of planktonic foraminifera across the Albian/Cenomanian boundary. *Paleobiology* 36(3), 357–373.
- Ando, A., Huber, B.T., MacLeod, K.G., Watkins D.K., 2015. Early Cenomanian “hot greenhouse” revealed by oxygen isotope record of exceptionally well preserved foraminifera from Tanzania. *Paleoceanography* 30(11), 1556–1572. <https://doi.org/10.1002/2015PA002854>
- Arkin, Y.; Braun, M., Starinsky, A. 1965. Type sections of Cretaceous Formations in Jerusalem - Bet-Shemesh Area. *Stratigraphic Sections No. 1, Part 1. Isr. Geol. Survey*, 42 p.
- Arkin, Y., Hamaoui, M., 1967. The Judea Group (Upper Cretaceous) in central and southern Israel. *Isr. Geol. Surv., Bull.* 42, 1–16.
- Avnimelech, M.A., 1965. Sur la presence de *Hyphoplites falcatus* (Mantell) (Ammonoïdes: Hoplitidae) dans le Cenomanien inferieur du Carmel (Israel). *Compte rendu sommaire des séances de la Soc. géol. France* 5, 160–161.

- Barron, E.J., 1987. Global Cretaceous Paleogeography. *Palaeogeogr. Palaeoclimatol. Palaeoecol.* 59, 207–214.
- Bartov, Y., 1990. Geological photomap of Israel and adjacent areas. Geological Survey of Israel, Jerusalem.
- Bein, A., 1976. Rudistid fringing reefs of Cretaceous shallow carbonate platform of Israel. *Bull. Am. Ass. Petroleum Geologists* 60, 258–272.
- Bein, A., Weiler, Y., 1976. The Cretaceous Talme Yafe Formation: a contour current shaped sedimentary prism of calcareous detritus at the continental margin of the Arabian Craton. *Sedimentology* 23, 511–532.
- Bornemann, A., Erbacher, J., Heldt, M., Kollaske, T., Wilmsen, M., Lübke, N., Huck, S., Vollmar, N.M., Wonik, T., 2017. The Albian–cenomanian transition and Oceanic Anoxic Event 1d—an example from the Boreal Realm. *Sedimentology* 64(1), 44–65.
- Bottini, C., Erba, E., Tiraboschi, D., Jenkyns, H.C., Schouten, S., Sinninghe Damste, J.S., 2015. Climate variability and ocean fertility during the Aptian Stage. *Clim. Past* 11, 383–402. <https://doi.org/10.13130/2039-4942/7726>
- Bottini, C., Erba, E. 2018. Mid-Cretaceous paleoenvironmental changes in the western Tethys. *Clim. Past* 14, 1147–1163. <https://doi.org/10.5194/cp-2018-34>
- Bown, P.R., Young, J.R., 1998. Techniques. In: Bown, P.R. (Ed.), *Calcareous Nannofossil Biostratigraphy*. British Micropaleontology Society Series. Chapman and Hall. Cambridge, London, pp. 16–28.
- Bralower, T.J., Leckie, R.M., Sliter, W.V., Thierstein, H.R., 1995. An integrated Cretaceous timescale. In Berggren, W.A., Kent, D.V., Aubry, M.-P., Hardenbol, J., (Eds.), *Geochronology Time Scales and Global Stratigraphic Correlation*. Soc. Econ. Paleontologists Mineralogists, Spec. Publ. 54, pp. 65–79.
- Bralower, T.J., Sliter, W.V., Arthur, M.A., Leckie, R.M., Allard, D.J., Schlanger, S.O., 1993. Dysoxic/anoxic episodes in the Aptian-Albian. In: Pringle, M.S., Sager, W.W., Sliter, W.V., Stein, S. (Eds.), *The Mesozoic Pacific: A volume in memory of Sy Schlanger*. Am. Geophys. Union Monogr. 73, pp. 5–37.
- Braun, M., Hirsch, F., 1994. Mid Cretaceous (Albian-Cenomanian) carbonate platforms in Israel. *Cuadernos de Geología Iberica* 18, 59–81.
- Burnett, J.A., 1998. Upper Cretaceous. In: Bown, P.R. (Ed.), *Calcareous nannofossil biostratigraphy*. Chapman and Hall, Cambridge, London, pp. 132–199.

- Burnett, J.A., Young, J.R., Bown, P.R., 2000. Calcareous nannoplankton and global climate change. In: Culver, S.J., Rawson, P.F. (Eds.), *Biotic Response to Global Change: the Last 145 Million Years*. The Nat. Hist. Mus., Cambridge University Press, London, pp. 35–50.
- Caron, M., Premoli Silva, I., 2007. New description of the Rotaliporid species *brotzeni* and *globotruncanoides* Sigal, 1948 based on re-examination of type material. *Riv. Ital. Paleont. Stratigr.* 113, 525–530.
- Chin, S.C., 2016. Upper Albian to Lower Cenomanian calcareous nannofossil biostratigraphy of the proto-North Atlantic. Unpublished MSc Thesis, The University of Nebraska-Lincoln, Lincoln, Nebraska, USA.
- Coccioni, R., Premoli Silva, E., 2015. Revised Upper Albian-Maastrichtian planktonic foraminifera biostratigraphy and magneto-stratigraphy of the classical Tethyan Gubbio section (Italy). *Newsl. Stratigr.* 48(1), 47–90.
- Conway, B.H., 1992. A palynological study of the Lower Cretaceous in Israel. Geological Survey of Israel, Technical Report, Negba-1 borehole, 24 p.
- Derin, B., 2016. The subsurface geology of Israel, Upper Paleozoic to Upper Cretaceous. 328 pp.
- Dodd, J.R., Stanton, R.J., Jr., 1981. *Palaeoecology, concepts and applications*. Wiley, New York, N.Y., 559 pp.
- Erba, E., 1992. Middle Cretaceous calcareous nannofossils from the western Pacific (Leg 129): Evidence for palaeoequatorial crossings. In: Larson, R.L., Lancelot, Y., et al. (Eds.), *Proc. Ocean Drilling Progr., Sci. Res.* 129, 189–201.
- Erba, E., 2004. Calcareous nannofossils and Mesozoic oceanic anoxic events. *Mar. Micropaleontol.* 52, 85–106.
- Erba, E., Bottini, C., Weissert, H.J., Keller, C.E., 2010. Calcareous nannoplankton response to surface-water acidification around Oceanic Anoxic Event 1a. *Science*, 329, 428–432.
- Erba, E., Castradori, D., Guasti, G., Ripepe, M., 1992. Calcareous nannofossils and Milankovitch cycles: the example of the Albian Gault Clay Formation (southern England). *Palaeogeogr. Palaeoclimatol. Palaeoecol.* 93, 47–69.

- Erba, E., Tremolada, F., 2004. Nannofossil carbonate fluxes during the Early Cretaceous: Phytoplankton response to nutrification episodes, atmospheric CO₂, and anoxia. *Paleoceanography* 19(1): Art. PA1008. <https://doi.org/10.1029/2003PA000884>
- Forster, A., Schouter, S., Bass, M., Sinninghe Damste, J.S., 2007. Mid-Cretaceous (Albian-Santonian) sea surface temperature record of the tropical Atlantic Ocean. *Geology* 35(10), 919–922.
- Gambacorta, G., Jenkyns, H. C., Russo, F., Tsikos, H., Wilson, P.A., Faucher, G., Erba, E., 2015. Carbon-and oxygen-isotope records of mid-Cretaceous Tethyan pelagic sequences from the Umbria–Marche and Belluno Basins (Italy). *Newsl. Stratigr.* 48(3), 299–323.
- Gambacorta, G., Bersezio, R., Weissert, H., Erba, E., 2016. Onset and demise of Cretaceous oceanic anoxic events: The coupling of surface and bottom oceanic processes in two pelagic basins of the western Tethys. *Paleoceanography* 31, 732–757.
- Giorgioni, M., Weissert, H., Bernasconi, S.M., Hochuli, P.A., Keller, C.E., Coccioni, R., Petrizzo, M.R., Lukeneder, A., Garcia, T.I., 2015. Paleoceanographic changes during the Albian–Cenomanian in the Tethys and North Atlantic and the onset of the Cretaceous chalk. *Glob and Planet. Change* 126, 46–61.
- Graden, P., Reiss, Z., Klug, K., 1960. Correlation of sub-surface Lower Cretaceous Units in the Southern Coastal Plain of Israel. *Geol. Survey of Israel, Bull.* 28 (8), 12 p.
- Gradstein, F.M., Ogg, J., Smith, A. 2004. *A Geologic Time Scale 2004*. Cambridge University Press, Cambridge.
- Grosheny, D., Tronchetti, G., Schaaf, A., 1992. Nouvelles données sur les foraminifères planctoniques et la biostratigraphie du Cénoomanien – Turonien dans le S. E. du bassin vocontien (S. E. France). *Comptes Rendus de l'Acad. Sci. Paris* 315, 773–776.
- Haq, B. U., Hardenbol, J., Vail, P. R., 1988. Mesozoic and Cenozoic chronostratigraphy and cycles of sea-level change. In: Wilgus, C.K. et al. (Ed.), *Sea-level changes — an integrated approach*, SEPM Spec. Publ. 42, pp. 71–108.
- Hammer, Ø., Harper, D.T., Ryan, P.D., 2001. Past: Paleontological Statistics Software Package for Education and Data Analysis. *Palaeontologia Electronica* 4(1): Art. 4. http://palaeo-electronica.org/2001_1/past/issue1_01.htm

- Hardas, P., Mutterlose, J., Friedrich, O., Erbacher, J., 2012. The Middle Cenomanian Event in the equatorial Atlantic: the calcareous nannofossil and benthic foraminiferal response. *Mar. Micropaleontol.* 96, 66–74.
- Hay, W.W., 2008. Evolving ideas about the Cretaceous climate and ocean circulation. *Cretac.Res.* 29, 725–753.
- Hay, W.W., DeConto, R.M., Wold, C.N., Wilson, K.M., Voigt, S., Schulz, M., Rossby Wold, A., Dullo, W.C., Ronov, A.B., Balukhovskiy, A.N., Söding, E., 1999. Alternative global Cretaceous paleogeography. In: Barrera, E., Johnson, C.C. (Eds.), *Evolution of the Cretaceous Ocean-Climate System*. Geol. Soc. Am. Spec. Paper 332, pp. 1–47.
- Hennhofer, D., Al Suwaidi, A., Bottini, C., Helja, E., Steuber, T. 2019. The Albian to Turonian carbon isotope record from the Shilaif Basin (United Arab Emirates) and its regional and intercontinental correlation. *Sedimentology* 66, 536–555.
<https://doi.org/10.1111/sed.12493>
- Herrle, J.O., 2003. Reconstructing nutricline dynamics of mid-Cretaceous oceans: evidence from calcareous nannofossils from the Niveau Paquier black shale (SE France). *Mar. Micropaleontol.* 47, 307–321.
- Herrle, J.O., Mutterlose, J., 2003. Calcareous nannofossils from the Aptian – early Albian of SE France: Paleoeological and biostratigraphic implications. *Cretac. Res.* 24, 1–22.
- Herrle, J.O., Pross, J., Friedrich, O., Kößler, P., Hemleben, C., 2003. Forcing mechanisms for mid-Cretaceous black shale formation: Evidence from the Upper Aptian and Lower Albian of the Vocontian Basin (SE France). *Palaeogeogr. Palaeoclimatol. Palaeoecol.* 190, 399–426.
- Huber, B.T., Norris, R.D., MacLeod, K.G., 2002. Deep-sea paleotemperature record of extreme warmth during the Cretaceous. *Geology* 30, 123–126.
- Jarvis, I.A.N., Gale, A.S., Jenkyns, H.C., Pearce, M.A., 2006. Secular variation in Late Cretaceous carbon isotopes: a new $\delta^{13}\text{C}$ carbonate reference curve for the Cenomanian–Campanian (99.6–70.6 Ma). *Geol. Mag.* 143(5), 561–608.
- Jenkyns, H.C., 2003. Evidence for rapid climate change in the Mesozoic–Paleogene greenhouse world. *Phil.Trans. Roy. Soc. Lond. A* 361, 1885–1916.
- Jenkyns, H.C., 2010. Geochemistry of oceanic anoxic events. *Geochem. Geophys. Geosyst.* 11, Q03004. <http://dx.doi.org/10.1029/2009GC002788>

- Kafri, U., 1972. Lithostratigraphy and environment of deposition Judea Group, Western and Central Galilee, Israel. *Bull. Geol. Surv. Isr.* 54, 1–56.
- Kanungo, S., Bown, P.R., Young, J.R., Gale, A.S., 2018. A brief warming event in the late Albian: evidence from calcareous nannofossils, macrofossils, and isotope geochemistry of the Gault Clay Formation, Folkestone, southeastern England. *J. Micro-palaeontol.* 37(1), 231–247.
- Karcz, I., Sneh, A., 2011. The geological map of Israel, scale 1:50,000, Hefa (Haifa). Jerusalem, Survey of Israel, Sheet 3-1.
- Kashai, E., 1966. The geology of the western and southwestern Carmel. Unpublished PhD thesis, The Hebrew University, Jerusalem, 115 pp. (In Hebrew, English abstract)
- Kennedy, W.J., Gale, A.S., Lees, J.A., Caron, M., 2004. The Global Boundary Stratotype Section and Point (GSSP) for the base of the Cenomanian Stage, Month To south, Hautes-Alpes, France. *Episodes* 27(1), 21–32.
- Kolodny, Y., Raab, M., 1988. Oxygen isotopes in phosphatic fish remains from Israel: Paleothermometry of tropical Cretaceous and Tertiary shelf waters, *Palaeogeogr. Palaeoclimatol. Palaeoecol.* 64, 59–67.
- Lees, J.A. Bown, P.R., Mattioli, E., 2005. Problems with proxies? Cautionary tales of calcareous nannofossil paleoenvironmental indicators. *Micropaleontology* 51(4), 333–343.
- Lewy, Z., Raab, M., 1978 [1976]. Mid-Cretaceous stratigraphy of the Middle East. *Ann. Mus. d'Hist. Natur. Nice* 4, 32.1–32.20.
- Lewy, Z., Kennedy, W.J., Chancelor, G., 1984. Cooccurrence of *Metoicoceras geslinianum* (d'Orbigny) and *Vascoceras cauvini* Chudeau (Cretaceous Ammonoidea) in the southern Negev (Israel) and its stratigraphical implications. *Newsl. Stratigr.* 13(2): 67–76.
- Linnert, Ch., Robinson, S.A., Lees, J.A., Bown, P.R., Pérez-Rodríguez, I., Petrizzo, M.R., Falzoni, F., Littler, K., Arz, J.A., Russell, E.E., 2014. Evidence for global cooling in the Late Cretaceous. *Nat. Comm.* 5, Art. 4194.
<https://doi.org/10.1038/ncomms5194>
- Lipson-Benitah, S., 1980. Albian to Coniacian zonation of the western coastal plain of Israel. *Cretac. Res.* 1, 3–12.

- Lipson-Benitah, S., 1994. Cenomanian stratigraphical micropaleontology of shelf deposits – Israel. *Rev. Esp. Microplaeontol.* 26, 83–100.
- Lipson-Benitah, S., Almogi-Labin, A., Sass, E., 1995. Microbiostratigraphy of Cenomanian strata of northwest Israel (mount Carmel). Ministry of Energy and Infrastructure, Earth Sci. Res. Administration, Final Rep. ES/44/95, 32 pp.
- Lipson-Benitah, S., Almogi-Labin, A., Sass, E., 1997. Cenomanian biostratigraphy and palaeoenvironments in the northwest Carmel Region, northern Israel. *Cretac. Res.* 18, 469–491.
- Makovsky, Y., Neuman, A., Surdyaev, A., Elad, M., 2018. General trends of the top-most sand unit along the coastline of Southern and Central Israel. Report submitted to Mediterranean Coastal Cliff Preservation Government Company Ltd., 32 p.
- Martinotti, G.M., 1993. Foraminiferal evidence of a hiatus between the Aptian and Albian offshore northern Israel. *J. Foram. Res.* 23, 66–75.
- Mutterlose, J., 1991. Das Verteilungs- und Migrationsmuster des kalkigen Nannoplanktons in der borealen Unterkreide (Valangin-Apt). *Palaeontographica* 221, 27–152.
- Mutterlose, J., 1996. Calcareous nannofossil palaeoceanography of the Early Cretaceous of NW Europe. *Mitt. Geol. Staatsinst. Hambg.* 77, 291–313.
- Mutterlose, J., Kessels, K., 2000. Early Cretaceous calcareous nannofossils from high latitudes: implications for palaeobiogeography and palaeoclimate. *Palaeogeogr. Palaeoclimatol. Palaeoecol.* 160, 347–372.
- Mutterlose, J., Wise, W., 1990. Lower Cretaceous nannofossil biostratigraphy of ODP Leg 113 holes 692B and 693A, continental slope of East Antarctica, Weddell Sea. *Proc. ODP 113*, 325–351.
- Mutterlose, J., Bornemann, A., Herrle, J.O., 2005. Mesozoic calcareous nannofossils — state of the art. *Palaontol. Zeitschrift* 79, 113–133.
- Müller, C., Higazi, F., Hamdan, W., 2010. Revised stratigraphy of the Upper Cretaceous and Cenozoic series of Lebanon based on nannofossils. Geological Society London, Special Publications 341(1), 287–303.
- O'Brien, C.L., Robinson, S.A., Pancost, R.D., Damsté, J.S.S., Schouten, S., Lunt, D.J., Alsenz, H., Bornemann, A., Bottini, C., Brassell, S.C., Farnsworth, A., Forster, A., Huber, B.T., Inglis, G.N., Jenkyns, H.C., Linnert, C., Littler, K., Markwick, P., McAnena, A., Mutterlose, J., Naafs, B.D.A., Püttmann, W., Sluijs, A., van Helmond, A.G.M., Vel-

- Ilecoop, J., Wagner, T., Wrobel, N.E., 2017. Cretaceous sea-surface temperature evolution. Constraints from TEX86 and planktonic foraminiferal oxygen isotopes. *Earth-Science Rev.* 172, 224–247.
- Ogg, J. G., Hinnov, L.A., 2012. Cretaceous. In: Gradstein, F.M. et al. (Eds.), *The Geologic Time Scale*. Elsevier, Amsterdam, pp. 793–853.
- Ovechkina, M., Erba, E., Bottini, C., 2019. Calcareous nannoplankton proxies for palaeoenvironmental reconstruction of the Albian–Cenomanian succession in North-western Israel (Mount Carmel Region). *Mar. Micropaleontol.* 152, Art. 101742.
<https://doi.org/10.1016/j.marmicro.2019.04.001>
- Perch-Nielsen, K., 1985. Cenozoic calcareous nannofossils. In: Bolli, H.M., Saunders, J.B., Perch-Nielsen, K. (Eds.), *Plankton Stratigraphy*. Cambridge University Press, Cambridge, UK, pp. 427–554.
- Picard, L., Kashai, E., 1958. On the lithostratigraphy and tectonics of the Carmel. *Bull. Res. Council Isr.* 7G, 1–19.
- Robaszynski, F., Caron, M., Dupuis, C., Amedro, F., Gonzalez Donoso, J. M., Linares, D., Hardenbol, J., Gartner, S., Calandra, F., Deloffre, R., 1990. A tentative integrated stratigraphy in the Turonian of central Tunisia: formations, zones and sequential stratigraphy in the Kalaat Senan area. *Bulletin des Centres de Recherches d'Exploration - Production Elf -Aquitaine* 14, 213–384.
- Robaszynski, F., Hardenbol, J., Caron, M., Amédro, F., Dupuis, C., González Donoso, J.M., Linares, D., Gartner, S., 1993. Sequence stratigraphy in a distal environment: the Cenomanian of the Kalaat Senan region (Central Tunisia). *Bull. Centres Rech. d'Exploration - Production Elf - Aquitaine* 17, 395–433.
- Rosenfeld, A., Hirsch, F., 2005. The Cretaceous of Israel. In: Hall, J.K. et al. (Eds.), *Geological Framework of the Levant. Vol. II: The Levantine Basin and Israel. Historical Production-Hall*, Jerusalem, Israel, 393–436.
- Rosenfeld, A., Raab, M., 1974. Cenomanian–Turonian ostracodes from the Judea Group in Israel. *Geol. Surv. Isr. Bull.* 62, 1–64.
- Rosenfeld A., Hirsch, F., Honigstein, A., 1995. Early Cretaceous ostracodes from the Levant. In: Riha, J. (Ed.), *Ostracoda and biostratigraphy. Proc. 12th Int. Symp. On Ostracoda*, Prague, July 1994, Rotterdam, Balkema, 111–121.

- Roth, P.H., 1978. Cretaceous nanoplankton biostratigraphy and oceanography of the northwestern Atlantic Ocean: Initial Reports of the Deep Sea Drilling Project, 44: 731–759.
- Roth, P.H., 1984. Preservation of calcareous nanofossils and fine-grained carbonate particles in mid-Cretaceous sediments from the southern Angola Basin. *Init. Rep. DSDP 75*, 651–655.
- Roth, P.H., 1986. Mesozoic palaeoceanography of the North Atlantic and Tethys Oceans. In: Summerhayes, C.P., Shackleton, N.J. (Eds.), *North Atlantic Palaeoceanography*. Geol. Soc. Lond. Spec. Publ. 21, pp. 299–320.
- Roth, P.H., Bowdler, J.L., 1981. Middle Cretaceous calcareous nanoplankton biogeography and oceanography of the Atlantic Ocean. *SEPM Spec. Publ.* 32, 517–546.
- Roth, P.H., Krumbach, K.R., 1986. Middle Cretaceous calcareous nanofossil biogeography and preservation in the Atlantic and Indian oceans: implications for paleoceanography. *Mar. Micropaleontol.* 10, 235–266.
- Sanders, H., L., 1968. Marine benthic diversity: a comparative study. *Am. Nat.*, 102, 243–282.
- Sass, E., 1980. Late Cretaceous volcanism in Mount Carmel. *Isr. J. Earth Sci.* 20, 8–24.
- Sass, E., Bein, A., 1978. Platform carbonates and reefs in the Judean Hills, Carmel and Galilee. *Tenth International Congress on Sedimentology, Guidebook 2*, 241–257.
- Sass, E., Bein, A., 1982. The Cretaceous carbonate platform in Israel. *Cret. Res.* 3, 135–144.
- Schroeder, R., Neumann, M. (coord.) 1985. Les grands foraminifères du Crétacé moyen de la région méditerranéenne. *Géobios, Mémoire Spécial 7*, 1–161.
- Schulze, F., Lewy, Z., Kuss, J. & Gharaibeh, A. 2003. Cenomanian–Turonian carbonate platform deposits in west central Jordan. *International Journal of Earth Sciences* 92: 641–660.
- Segev, A., 2009. $^{40}\text{Ar}/^{39}\text{Ar}$ and K–Ar geochronology of Berriasian–Hauterivian and Cenomanian tectonomagmatic events in northern Israel: implications for regional stratigraphy. *Cret. Res.* 30, 810–828.

- Segev, A., Sass, E., 2006. The geology of the central and southern Carmel. Field Excursion, Guide Book, Isr. Geological Soc. Annual Meeting, Bet Shean. pp. 69–88. (in Hebrew).
- Segev, A., Sass, E., 2014. Geology of Mount Carmel – Completion of the Haifa region. Isr. Geological Surv. Report, GSI/18/2014, 51 p. (in Hebrew, English abstract).
- Sissingh, W., 1977. Biostratigraphy of Cretaceous calcareous nannoplankton. *Geologie en Mijnbouw* 56, 37–65.
- Shamrock, J.L., Watkins, D.K., 2009. Evolution of the Cretaceous calcareous nannofossil genus *Eiffellithus* and its biostratigraphic significance. *Cretac. Res.* 30(5), 1083–1102.
- Sliter, W.V., Baker, R.A., 1972. Cretaceous bathymetric distribution of benthic foraminifera. *J. Foram. Res.* 2, 167–183.
- Sneh, A., 2008. The geological map of Israel, scale 1:50,000, Qiryat Gat. Jerusalem, Survey of Israel, Sheet 10-IV.
- Street, C., Bown, P., 2000. Palaeobiogeography of Early Cretaceous (Berriasian–Barremian) calcareous nannoplankton. *Mar. Micropaleontol.* 39, 265–291.
- Tiraboschi, D., Erba, E., Jenkyns, H.C., 2009. Origin of rhythmic Albian black shales (Piobbico core, central Italy) Calcareous nannofossil quantitative and statistical analysis and paleoceanographic reconstructions. *Paleoceanography* 24, PA2222. <https://doi.org/10.1029/2008PA001670>
- Thierstein, H.R., 1980. Selective dissolution of Late Cretaceous and Earliest Tertiary calcareous nannofossils: experimental evidence. *Cretac. Res.* 2, 165–176.
- Vahrenkamp, V.C., 2013. Carbon isotope signatures of Albian to Cenomanian (Cretaceous) shelf carbonates of the Natih Formation, Sultanate of Oman. *GeoArabia*, 18, 65–82.
- Watkins, D.K., 1989. Nannoplankton productivity fluctuations and rhythmically-bedded pelagic carbonates of the Greenhorn Limestone (Upper Cretaceous). *Palaeogeogr. Palaeoclimatol. Palaeoecol.* 74, 75–86.
- Watkins, D.K., 1992. Upper Cretaceous nannofossils from Leg 120, Kerguelen Plateau, Southern ocean. *Proc. Ocean Drilling Program, Sci. Results* 120, 343–370.

- Watkins, D.K., Bowdler, J.L., 1984. Cretaceous calcareous nannofossils from Deep Sea Drilling Project Leg 77, Southeast Gulf of Mexico. Initial Reports Deep Sea Drill. Project 77, 649–674.
- Watkins, D.K., Cooper, M.J., Wilson, P.A., 2005. Calcareous nannoplankton response to late Albian oceanic anoxic event 1d in the western North Atlantic. *Paleoceanography* 20(PA2010), 1–14.
- Wellings, F.E., 1944. Revision of south Palestine Stratigraphy Petral. Develop. (Palestine) Ltd. Geol. Dept. Rep. (unpublished).
- Williams, M.R., Bralower, T.J., 1995. Nannofossil assemblages, fine fraction stable isotopes, and palaeoceanography of the Valanginian–Barremian (Early Cretaceous) North Sea Basin. *Palaeoceanography* 10(4), 815–839.
- Wohlwend, S., Hart, M.B. and Weissert, H., 2016. Chemostratigraphy of the Upper Albian to mid-Turonian Natih Formation (Oman) – or: how authigenic carbonate changes a global pattern. *Depositional Rec.*, 2, 97–117.

APPENDIX A. TAXONOMIC APPENDIX

- Acuturris* Wind & Wise *in* Wise & Wind, 1977
- A. scotus* (Risatti, 1973) Wind & Wise *in* Wise & Wind, 1977
- Amphizygus* Bukry, 1969
- A. brooksii* Bukry, 1969
- Assipetra* Roth, 1973
- A. infracretacea* (Thierstein, 1973) Roth, 1973
- Axopodorhabdus* Wind & Wise *in* Wise, 1977
- A. biramiculatus* (Stover, 1966) Corbett & Watkins, 2014
- Biscutum* Black *in* Black & Barnes, 1959
- B. constans* (Górka, 1957) Black *in* Black & Barnes, 1959
- B. thurowii* Burnett, 1997
- Biscutum* sp.
- Braarudosphaera* Deflandre, 1947
- B. africana* Stradner, 1961
- B. bigelowii* (Gran & Braarud, 1935) Deflandre, 1947
- Broinsonia* Bukry, 1969
- B. cenomanica* (Black, 1973) Bown, 2001
- B. enormis* (Shumenko, 1968) Manivit, 1971
- B. matalosa* (Stover, 1966) Burnett *in* Gale et al., 1996
- Broinsonia* sp.
- Bukrylithus* Black, 1971
- B. ambiguus* Black, 1971
- Calcicalathina* Thierstein, 1971
- Calcicalathina* sp.
- Calciosolenia* Gran, 1912
- C. fossilis* (Deflandre *in* Deflandre & Fert, 1954) Bown *in* Kennedy et al., 2000
- Calculites* Prins & Sissingh *in* Sissingh, 1977
- C. anfractus* (Jakubowski, 1986) Varol & Jakubowski, 1989
- Calculites* sp.
- Chiastozygus* Gartner, 1968

Ch. amphipons (Bramlette & Martini, 1964) Gartner, 1968
Ch. litterarius (Górka, 1957) Manivit, 1971
Chiastozygus sp.
Corollithion Stradner, 1961
C. kennedyi Crux, 1981
Conusphaera Trejo, 1969
C. mexicana Trejo, 1969
Cretarhabdus Bramlette & Martini, 1964
C. conicus Bramlette & Martini, 1964
C. striatus (Stradner, 1963) Black, 1973
Cretarhabdus sp.
Cribrosphaerella Deflandre *in* Piveteau, 1952
C. circula (Risatti, 1973) Lees, 2007
C. ehrenbergii (Arkhangelsky, 1912) Deflandre *in* Piveteau, 1952
Crucibiscutum Jakubowski, 1986
Crucibiscutum sp.
Cyclagelosphaera Noël, 1965
C. margerelii Noël, 1965
C. rotaclypeata Bukry, 1969
Cylindralithus Bramlette & Martini, 1964
Cylindralithus sp.
Discorhabdus Noël, 1965
D. ignotus (Górka, 1957) Perch-Nielsen, 1968
Eiffellithus Reinhardt, 1965
E. casulus Shamrock & Watkins, 2009
E. gorkae Reinhardt, 1965
E. hancockii Burnett, 1997
E. monechiae Crux, 1991
E. turriseiffelli (Deflandre *in* Deflandre & Fert, 1954) Reinhardt, 1965
Eprolithus Stover, 1966
E. floralis (Stradner, 1962) Stover, 1966
Flabellites Thierstein, 1973

Fl. oblongus (Bukry, 1969) Crux in Crux et al., 1982
Gartnerago Bukry, 1969
G. segmentatum (Stover, 1966) Thierstein, 1974
Gartnerago sp.
Gorkaea Varol & Girgis, 1994
G. operio Varol & Girgis, 1994
G. pseudanthophorus (Bramlette & Martini, 1964) Varol & Girgis, 1994
Grantarhabdus Black, 1971
Gr. coronadventis (Reinhardt, 1966) Grün in Grün & Allemann, 1975
Haqius Roth, 1978
H. circumradiatus (Stover, 1966) Roth, 1978
Helenea Worsley, 1971
H. chiastia Worsley, 1971
Helicolithus Noël, 1970
Hc. compactus (Bukry, 1969) Varol & Girgis, 1994
Hc. trabeculatus (Górka, 1957) Verbeek, 1977
Isocrystallithus Verbeek 1976
Isocrystallithus sp.
Kamptnerius Deflandre, 1959
K. magnificus Deflandre, 1959
Lithraphidites Deflandre, 1963
L. acutus Verbeek & Manivit in Manivit et al., 1977
L. eccentricus Watkins in Watkins & Bowdler, 1984
L. alatus Thierstein in Roth & Thierstein, 1972
L. carniolensis Deflandre, 1963
L. houghtonii Jeremiah, 2001
Lithraphidites sp.
Loxolithus Noël, 1965
L. armilla (Black in Black & Barnes, 1959) Noël, 1965
Loxolithus sp.
Manivitella Thierstein, 1971
M. pemmatoidea (Deflandre in Manivit, 1965) Thierstein, 1971

Mennerius Luljeva, 1967
Mennerius sp.
Micrantholithus Deflandre *in* Deflandre & Fert, 1954
Micrantolithus sp.
Microrhabdulus Deflandre, 1959
M. decoratus Deflandre, 1959
Nannoconus Kamptner, 1931
N. bucheri Brönnimann, 1955
N. cornuta Deres & Acheriteguy (1980)
N. elongatus Brönnimann, 1955
N. fragilis Deres & Achéritéguy, 1980
N. scyphoides Kamptner, 1938
N. truittii frequens Deres & Achéritéguy, 1980
N. truittii truittii Brönnimann, 1955
Nannoconus sp. (view from above)
Nannoconus sp. 1
Nannoconus sp. 2
Placozygus Hoffman, 1970
P. fibuliformis (Reinhardt, 1964) Hoffmann, 1970
Prediscosphaera Vekshina, 1959
P. columnata (Stover, 1966) Perch-Nielsen, 1984
P. cretacea (Arkhangelsky, 1912) Gartner, 1968
P. grandis Perch-Nielsen, 1979
P. spinosa (Bramlette & Martini, 1964) Gartner, 1968
Radiolithus Stover, 1966
R. orbiculatus (Forchheimer, 1972) Varol, 1992
R. planus Stover, 1966
Repagulum Forchheimer, 1972
R. parvidentatum (Deflandre & Fert, 1954) Forchheimer, 1972
Retecapsa Black, 1971
R. angustiforata Black, 1971
R. crenulata (Bramlette & Martini, 1964) Grün *in* Grün & Allemann, 1975

R. ficula (Stover, 1966) Burnett, 1997
Retecapsa sp.
Rhagodiscus Reinhardt, 1967
Rh. achlyostaurion (Hill, 1976) Doeven, 1983
Rh. amplus Bown, 2005
Rh. angustus (Stradner, 1963) Reinhardt, 1971
Rh. asper (Stradner, 1963) Reinhardt, 1967
Rh. reniformis Perch-Nielsen, 1973
Rh. sageri Bown, 2005
Rh. splendens (Deflandre, 1953) Verbeek, 1977
Rhagodiscus sp.
Seribiscutum Filewicz et al. in Wise & Wind, 1977
Seribiscutum sp.
Sollasites Black, 1967
S. horticus (Stradner et al. in Stradner & Adamiker, 1966) Cepek & Hay, 1969
Staurolithites Caratini, 1963
Staurolithites sp.
Tetrapodorhabdus Black, 1971
T. decorus (Deflandre in Deflandre & Fert, 1954) Wind & Wise, 1983
Tranolithus Stover, 1966
T. gabalus Stover, 1966
T. orionatus (Reinhardt, 1966) Reinhardt, 1966
Watznaueria Reinhardt, 1964
W. barnesiae (Black, 1959) Perch-Nielsen, 1968
W. biporta Bukry, 1969
W. britannica (Stradner, 1963) Reinhardt, 1964
W. cf. W. bayackii Worsley, 1971
W. fossacincta (Black, 1971) Bown in Bown & Cooper, 1989
W. manivittiae Bukry, 1973
W. ovata Bukry, 1969
Zeugrhabdotus Reinhardt, 1965
Z. bicrescenticus (Stover, 1966) Burnett in Gale et al., 1996

- Z. clarus* Bown, 2005
- Z. diplogrammus* (Deflandre *in* Deflandre & Fert, 1954) Burnett *in* Gale et al., 1996
- Z. embergeri* (Noël, 1958) Perch-Nielsen, 1984
- Z. howei* Bown *in* Kennedy et al., 2000
- Z. moulladei* Bergen, 1998
- Z. noeliae* Rood et al., 1971
- Z. scutula* (Bergen, 1994) Rutledge & Bown, 1996
- Z. xenotus* (Stover, 1966) Burnett *in* Gale et al., 1996

Appendix D. Raw data of calcareous nannofossil counting, borehole Negba 1 (Coastal Plain).

Samples	Species/Presentation	Weizsaueria barnesae	Eiffelithus cf. E. gorkae	Cycloecosphera sp.	Nannoconus sp.	Zeugrhabdotus sp.	Weizsaueria ovata	Weizsaueria fossarincta	Eiffelithus cf. E. monochiae	Retecapsa sp.	Weizsaueria cf. W. baykii	Radolithus orbiculatus	Zeugrhabdotus birescens	Eprolithus florealis	Lithraphidites cambiensis	Biscutum constans	Acopoderhabdus braniculatus	Giantirhabdus coronadentis	Tranolithus oronatus	Zeugrhabdotus moulladei	Citrosphaerella cf. Cr. Ehrenbergii	Tranolithus sp.	Discorhabdus ignotus	Braarudosphaera bigelowii	Microrhabdulus decoratus	Calculites anfractus
52																										
51	P	1																								
50	P(M)	2																						1	1	1
49	P	2																								
48	P	2																								
47		no nannofossils																								
46	P	1																								
45	P	1			1													1								
44		no nannofossils																								
43	P	1																								
42		no nannofossils																								
41	P	2																							1	
40	M	1					1														1		1			
39		no nannofossils																								
38		no nannofossils																								
37		no nannofossils																								
36	P	1																								
35		no nannofossils																								
34		no nannofossils																								
33	M(P)	1													1	1	1	1	1							
32		no nannofossils																								
31		no nannofossils																								
30		no nannofossils																								
29		no nannofossils																								
28		no nannofossils																								
27		no nannofossils																								
26		no nannofossils																								
25	M(P)	1													1	1										
24	M(P)	1		1									1													
23		no nannofossils																								
22		no nannofossils																								
21		no nannofossils																								
20	M	1				1					1	1														
19		no nannofossils																								
18		no nannofossils																								
17		no nannofossils																								
16		no nannofossils																								
15	P(M)	3				2		1																		
14	M	11				3	5	1	1	1																
13		no nannofossils																								
12	M	1																								
11		no nannofossils																								
10		no nannofossils																								
9		no nannofossils																								
8		no nannofossils																								
7		no nannofossils																								
6		no nannofossils																								
5		no nannofossils																								
4		no nannofossils																								
3		no nannofossils																								
2	P	1			1	1	1																			
1	M(P)	1	1	1																						

Appendix E. Nannofossils groups.

Broinsonia cenomanica	Broinsonia/Gartnerago	Rare taxa	Acutturis scotus	others taxa
Br. enormis			Amphizygus brooksii	
B. matalosa			Assipetra infracretacea	
Broinsonia sp.			Braarudosphaera africana	
Gartnerago segmentatus			Br. bigelowii	
Gartnerago sp.			Bukrylithus ambiguous	
Cyclagelosphaera margerelii	Cyclagelosphaera spp.		Calicalathina sp.	
Cycl. rotaclypeata			Calciosolenia fossilis	
Cribrosphaerella ehrenbergii			Calculites anfractus	
Crucibiscutum sp.			Calculites supracretaceous	
Nannoconus bucheri	Nannoconus spp.		Calculites sp.	
Nannoconus cornuta			Chiastozygus amphipons	
Nannoconus elongatus			Ch. litterarius	
Nannoconus fragilis			Chiastozygus sp.	
Nannoconus scyphoides			Corolithion kennedyi	
N. trutti frequens			Cornusphaera mexicana	
Nannoconus tutti trutti			Cylindralithus sp.	
Nannoconus sp. (view from above)			Flabellites oblongus	
Nannoconus sp. A			Gorkaea operio	
Nannoconus sp. B			Gorkaea pseudanthophorus	
Radiolithus orbiculatus	Radiolithus spp.	Haqius circumradiatus		
R. planus		Helenia chiasta		
Repagulum parvidentatum		Helicolithus compactus		
Serbiscutum sp.		H. trabeculatus		
		Isocrystalithus sp.		
		Kamptnerius magnificus		
		Loxolithus armila		
		Loxolithus sp.		
		Mennerius sp.		
		Micrantolithus sp.		
		Microrhabdulus decoratus		
		Placozygus fibuliformis		
		Sollasites horticus		
		Staurolithites sp.		
		Tetrapodorhabdus decorus		

PUBLICATION DOCUMENTATION PAGE

Item	Value
1. Publication No. MONI -	MNI – ES – 21 - 20
2. Additional No.	
3. Recipient Accession No.	
4. Title and subtitle	Nannofossil stratigraphy and paleoenvironments of Israel Judea Group
5. Publication Date	June, 2020
6. Performing Organization Project No.	Geological Survey of Israel 40754
7. Author(s)	Maria Ovechkina
8. Performing Organization Report No.	
9. Performing organization names and addresses	Geological Survey of Israel, Yesha'yahu Leibowitz 32, Jerusalem
10. Ministry of Energy & Water Resources Contract No.	217-17-023
11. Sponsoring organization(s) names and address(es)	(a) Ministry of National Infrastructures Division of Research and Development P.O. Box 36148, 9136002 Jerusalem
12. Type of report and period covered	Annual report, 2018–2019
13. Sponsoring Org. Code	
14. Supplementary Notes	

Item	Value
15. Abstract	<p>The calcareous nannoplankton from the sediments of the Judea Group (Albian–Cenomanian) of the Carmel area (NW Israel) and the Southern Coastal Plain has been studied. The identified rich assemblages in the Carmel area consist of 113 taxa (borehole CT8) and 95 taxa (borehole CT2). On the Coastal Plain (borehole Negba 1), the impoverished assemblage of 24 taxa is recorded.</p> <p>The detailed calcareous nannofossil biostratigraphy of the Carmel area has been established and compared with planktic foraminiferal zones. In the Coastal Plain, different stratigraphical intervals are recorded and correlated with planktic foraminiferal zones.</p> <p>The novel nannofossil data indicate that the Isfiye Formation and the Tavasim Volcanics (V2) calculated as 98.2 Ma in the Carmel area are Late Albian, and the Arqan Fm. is Late Albian–Middle Cenomanian.</p> <p>The Albian–Cenomanian boundary in the Carmel area is drawn at the level of the first occurrence of <i>Thalmanninella globotruncanoides</i> (planktic foraminifera) in the lower part of the Arqan Fm. at ~52 m above the top Tavasim Volcanics in CT8 and at ~35.65 m above the Tavasim Volcanics in CT2. This is supported by the appearance of <i>Th. brotzeni</i> (planktic foraminifera) at 26 m (CT8) and 6.55 m (CT2) below, and <i>C. kennedyi</i> (nannofossils) above this level. Our novel stratigraphical data prompt a revision of the revision of the litho-stratigraphic table and updating the Arqan Fm. age.</p> <p>On the Coastal Plain, only wide stratigraphic intervals can be recognized due to rarity of nannofossils: the upper part of the Yagur Fm is Late Albian–Early Cenomanian, the Lower and Upper Members of the Negba Fm is Albian–Late Cenomanian, and the upper part of the Upper Member of the Negba Fm is Late Cenomanian.</p> <p>The quantitative analysis of the calcareous nannoplankton suggests that the general dominance of <i>Watznaueria</i> spp. throughout the whole successions in the Carmel Area reflects the original signal and points to quite warm, open marine or coastal, generally oligotrophic conditions. Due to poor nutrient supply, the productivity of the calcareous nannoplankton was quite low except for two phases of higher fertility within Subzone NC10a and Zone NC11*. Low values of the Shannon index, Evenness and Species richness can be interpreted as reflecting unstable environment. The Isfiye Formation (Late Albian) accumulated in temperate, oligotrophic conditions. The lower part of the Arqan Formation was deposited under temperate climate but mesotrophic conditions. The higher part of the Arqan Formation (Early Cenomanian) was deposited in oligotrophic waters and relatively warm climate.</p>

Item	Value
15. Abstract	<p>The uppermost part of the Arqan Formation (Middle–Late Cenomanian) was accumulated during a progressively cooling period, although characterised by alternating warming and cooling phases and oligotrophic conditions.</p> <p>The calcareous nannoplankton quantitative data correlate very well with those obtained from planktic foraminifera (Lipson-Benitah et al., 1997) from the nearby area, and with cycles and sequences established by Haq et al. (1988), and suggest nutrification during phases of a risen sea level in the Late Albian and Early Cenomanian.</p> <p>The biostratigraphy in the Carmel Area shows no hiatuses in the studied section, but carbon isotope data reflect different pictures. In the borehole CT2 (Isfiye Fm., depths 169.90–152.60 m), the Oceanic Anoxic Event (OAE) 1d and Middle Cenomanian Event (MCE) I (Arqan Fm., depths 74.10–65.0 m) are detected; these reflect well the globally recorded carbon isotopic anomalies. Considering that the isotopic signal is not diagenetically altered and the $\delta^{18}\text{O}$ signal is not affected in the CT2, the oxygen isotopes suggest temperate conditions during the Late Albian–Early Cenomanian (~26°C) followed by a warming period in the late Early Cenomanian, with temperatures gradually increasing toward the Middle Cenomanian to ~32°C.</p> <p>In the borehole CT8, carbon isotope data seem to be affected by diagenetic alteration showing no evidence of the positive isotopic anomalies, which identify OAE 1d and MCE I worldwide. Temperature and nutrient variations in CT8 correspond to the western Tethys record, thus suggesting that the detected paleoclimatic variations occurred at a supra-regional scale.</p>
16. Identifiers/Keywords/ Descriptors	Judea Fm., Albian; Cenomanian; calcareous nannoplankton planktic foraminifera; biostratigraphy; palaeoenvironment; Carmel; Southern Coastal Plain; Northern Israel.
17. Publications and patents following the research	
18. Copies of this Report are available from:	
19. Security Class (this report)	
20. Security Class (this page)	
21. No. of pages	113
22. Price	